GFZ

Helmholtz-Zentrum
POTSDAM

HELMHOLTZ-ZENTRUM POTSDAM
DEUTSCHES
GEOFORSCHUNGSZENTRUM

S. Fuchs

Well-log based determination of rock thermal conductivity in the North German Basin

Scientific Technical Report STR13/11

www.gfz-potsdam.de

HELMHOLTZ
GEMEINSCHAFT

Recommended citation:

Fuchs, S. (2013), Well-log based determination of rock thermal conductivity in the North German Basin. *Scientific Technical Report 13/11, GFZ German Research Centre for Geosciences*.

Citation example for individual chapters:

Fuchs, S. (2013) Evaluation of common mixing models for calculating bulk thermal conductivity of sedimentary rocks: correction charts and new conversion equations. In: Fuchs, S., Well-log based determination of rock thermal conductivity in the North German Basin (pp.27-51). *Scientific Technical Report 13/11, GFZ German Research Centre for Geosciences*.

Imprint

Helmholtz Centre Potsdam
GFZ German Research Centre for Geosciences

Telegrafenberg
D-14473 Potsdam

Published in Potsdam, Germany
October 2013

ISSN 1610-0956

DOI: 10.2312/GFZ.b103-13111
URN: urn:nbn:de:kobv:b103-13111

This work is published in the GFZ series
Scientific Technical Report (STR)
and electronically available at GFZ website
www.gfz-potsdam.de

Institut für Erd- und Umweltwissenschaften
Mathematisch-Naturwissenschaftliche Fakultät
Universität Potsdam

Well-log based determination of rock thermal conductivity in the North German Basin

Kumulative Dissertation

zur Erlangung des akademischen Grades
"doctor rerum naturalium" (Dr. rer. nat.)

in der Wissenschaftsdisziplin „Allgemeine Geologie“

eingereicht an der
Mathematisch-Naturwissenschaftlichen Fakultät
der Universität Potsdam

vorgelegt von
Dipl.-Ing. Sven Fuchs
Potsdam, den 30. April 2013

Betreuer:
Prof. Dr. Manfred Strecker (Universität Potsdam)

Gutachter:
Prof. Dr. Manfred Strecker (Universität Potsdam)
Prof. Dr. Francis Lucazeau (Institut de Physique du Globe de Paris, Fankreich)
Prof. Dr. Jürgen Schön (Montanuniversität Leoben, Österreich)

Datum der Einreichung: 30. April 2013
Datum der Verteidigung: 18. Juli 2013

Published online at the
Institutional Repository of the University of Potsdam:
URL http://opus.kobv.de/ubp/volltexte/2013/6780/
URN urn:nbn:de:kobv:517-opus-67801
http://nbn-resolving.de/urn:nbn:de:kobv:517-opus-67801

Meiner Familie.

DOI: 10.2312/GFZ.b103-13111

Abstract

In sedimentary basins, rock thermal conductivity can vary both laterally and vertically, thus altering the basin's thermal structure locally and regionally. Knowledge of the thermal conductivity of geological formations and its spatial variations is essential, not only for quantifying basin evolution and hydrocarbon maturation processes, but also for understanding geothermal conditions in a geological setting. In conjunction with the temperature gradient, thermal conductivity represents the basic input parameter for the determination of the heat-flow density; which, in turn, is applied as a major input parameter in thermal modeling at different scales. Drill-core samples, which are necessary to determine thermal properties by laboratory measurements, are rarely available and often limited to previously explored reservoir formations. Thus, thermal conductivities of Mesozoic rocks in the North German Basin (NGB) are largely unknown. In contrast, geophysical borehole measurements are often available for the entire drilled sequence. Therefore, prediction equations to determine thermal conductivity based on well-log data are desirable. In this study rock thermal conductivity was investigated on different scales by (1) providing thermal-conductivity measurements on Mesozoic rocks, (2) evaluating and improving commonly applied mixing models which were used to estimate matrix and pore-filled rock thermal conductivities, and (3) developing new well-log based equations to predict thermal conductivity in boreholes without core control.

Laboratory measurements are performed on sedimentary rock of major geothermal reservoirs in the Northeast German Basin (NEGB) (*Aalenian sandstone, Rhaethian-Liassic Complex, Stuttgart Fm., and Middle Buntsandstein*). Samples are obtained from eight deep geothermal wells that approach depths of up to 2,500 m. Bulk thermal conductivities of Mesozoic sandstones range between 2.1 and 3.9 W/(m·K), while matrix thermal conductivity ranges between 3.4 and 7.4 W/(m·K). Local heat flow for the Stralsund location averages 76 mW/m², which is in good agreement to values reported previously for the NEGB. For the first time, *in-situ* bulk thermal conductivity is indirectly calculated for entire borehole profiles in the NEGB using the determined surface heat flow and measured temperature data. Average bulk thermal conductivity, derived for geological formations within the Mesozoic section, ranges between 1.5 and 3.1 W/(m·K).

The measurement of both dry- and water-saturated thermal conductivities allow further evaluation of different two-component mixing models which are often applied in geothermal calculations (*e.g.*, *arithmetic mean, geometric mean, harmonic mean, Hashin-Shtrikman mean, and effective-medium theory mean*). It is found that the geometric-mean model shows the best correlation between calculated and measured bulk thermal conductivity. However, by applying new model-dependent correction, equations the quality of fit could be significantly improved and the error diffusion of each model reduced. The 'corrected' geometric mean provides the most satisfying results and constitutes a universally applicable model for sedimentary rocks. Furthermore, lithotype-specific and model-independent conversion equations are developed permitting a calculation of water-saturated thermal conductivity from dry-measured thermal conductivity and porosity within an error range of 5 to 10%.

The limited availability of core samples and the expensive core-based laboratory measurements make it worthwhile to use petrophysical well logs to determine thermal conductivity for sedimentary rocks. In

DOI: 10.2312/GFZ.b103-13111

literature, several formulations are given to estimate thermal conductivity based on well-log data. However, they all show the typical limitations of statistically derived empirical prediction equations that limit such application to specific geological formations (represented by specific rock compositions) from which rock samples are implemented in the analysis. The approach followed in this study is based on the detailed analyses of the relationships between thermal conductivity of rock-forming minerals, which are most abundant in sedimentary rocks, and the properties measured by standard logging tools (i.e., *gamma ray, density, sonic interval transit time, hydrogen index, and photoelectric factor*). By using multivariate statistics separately for clastic, carbonate and evaporite rocks, the findings from these analyses allow the development of prediction equations from large artificial data sets that predict matrix thermal conductivity within an error of 4 to 11%, without being affected by the limitations mentioned above. These equations are validated successfully on a comprehensive subsurface data set from the NGB. In comparison to the application of earlier published approaches formation-dependent developed for certain areas, the new developed equations show a significant error reduction of up to 50%. These results are used to infer rock thermal conductivity for entire borehole profiles. By inversion of corrected *in-situ* thermal-conductivity profiles, temperature profiles are calculated and compared to measured high-precision temperature logs. The resulting uncertainty in temperature prediction averages < 5%, which reveals the excellent temperature prediction capabilities using the presented approach.

In conclusion, data and methods are provided to achieve a much more detailed parameterization of thermal models, helping to understand the thermal structure of sedimentary basins in general and of the North German Basin in particular.

Keywords:

Thermal conductivity, Prediction equation, Well-log analysis, Northeast German Basin, temperature field, Heat-flow density, Multivariate statistical analysis, Sedimentary basin

Zusammenfassung

Die thermische Modellierung des geologischen Untergrundes ist ein wichtiges Werkzeug bei der Erkundung und Bewertung tiefliegender Ressourcen sedimentärer Becken (*e.g.*, Kohlenwasserstoffe, Wärme). Die laterale und vertikale Temperaturverteilung im Untergrund wird, neben der Wärmestromdichte und der radiogenen Wärmeproduktion, hauptsächlich durch die Wärmeleitfähigkeit (WLF) der abgelagerten Gesteinsschichten bestimmt. Diese Parameter stellen die wesentlichen Eingangsgrößen für thermische Modelle dar. Bohrkerne, welche zur laborativen Bestimmung der WLF genutzt werden können, sind selten und häufig nur für potentielle Reservoirhorizonte vorhanden. Die Kenntnisse zur WLF mesozoisch-känozoischer Sedimentgesteine des Norddeutschen Beckens (NDB) waren bisher dementsprechend lückenhaft. Thermische Modelstudien, regionaler oder lokaler Art, stützten sich daher bis Mitte der 2000er Jahre im Wesentlichen auf die Nutzung von Literaturdaten und, soweit vorhanden, auf bekannte Analogdaten anderer Sedimentbecken. Im Gegensatz zu Bohrkernen sind geophysikalische Bohrlochmessungen für nahezu jede Tiefbohrung vorhanden, was die Entwicklung empirischer Gleichungen zur Bestimmung der WLF anhand dieser Messungen zu einer interessanten Alternative macht. Die vorliegende Dissertation befasst sich mit der Bestimmung der Gesteins-WLF auf verschiedenen Skalen. Dies umfasst (1) laborative WLF-Messungen an mesozoischen Bohrkernproben, (2) die Evaluierung und Verbesserung der Prognosefähigkeit von Mischgesetzten zur Berechnung von Matrix- und Gesamt-WLF sedimentärer Gesteine, sowie (3) die Entwicklung neuer Prognosegleichungen unter Nutzung bohrlochgeophysikalischer Messungen und multivariater Analysemethoden im NGB.

Im Nordostdeutschen Becken (NEGB) wurden für die wichtigsten geothermischen Reservoire des Mesozoikums (*Aalen, Rhät-Lias-Komplex, Stuttgart Formation, Mittlerer Buntsandstein*) Bohrkerne geothermischer Tiefbohrungen (bis 2.500 m Tiefe) auf Ihre thermischen und petrophysikalischen Eigenschaften hin untersucht. Die WLF mesozoischer Sandsteine schwankt im Mittel zwischen 2,1 und 3,9 W/(m·K), die WLF der Gesteinsmatrix hingegen im Mittel zwischen 3,4 und 7,4 W/(m·K). Effektive Porositäten liegen für die meisten Sandsteinproben im Bereich zwischen 20% und 35%. Neu berechnete Werte zur Oberflächenwärmestromdichte (*e.g.*, 76 mW/m², Stralsund) stehen im Einklang mit den Ergebnissen früherer Studien im NEGB. Basierend auf diesen Daten wurde für das mesozoisch/känozoischen Intervall am Standort Stralsund erstmals im NGB, ein *in-situ* WLF-Profil berechnet. *In-situ* Formations-WLF, für als potentielle Modelschichten interessante, stratigraphische Intervalle, variieren im Mittel zwischen 1,5 und 3,1 W/(m·K) und bilden eine gute Grundlage für kleinskalige (lokale) thermische Modelle. Um die beobachtete WLF-Variabilität jedoch abbilden zu können, besteht für die Parametrisierung regionaler Modelle weiterhin ein hoher Bedarf an neuen WLF-Messungen.

Auf Grund der in aller Regel nur eingeschränkt verfügbaren Bohrkernproben sowie des hohen laborativen Aufwandes zur Bestimmung der WLF waren alternative Methoden gesucht. Die Auswertung petrophysikalischer Standardbohrlochmessungen (*e.g.*, Gamma-Log, Dichte-Log, Neutronen-Porosität, Akustik-Log) mittels mathematischer-statistischer Methoden (*Regressionstechniken, Künstliche Neuronal Netze, Varianzanalyse, etc.)* stellt einen lang genutzten und erprobten Ansatz dar. Die Anwendbarkeit in der Literatur beschriebener empirischer Gleichungen ist jedoch auf solche Bohrungsbereiche beschränkt, in welchen die aufgeschlossenen Gesteinsbereiche in Genese, Geologie, Stratigraphie,

Scientific Technical Report STR 13/11 Deutsches GeoForschungsZentrum GFZ
DOI: 10.2312/GFZ.b103-13111

Mineralogie, etc. dem ursprünglichen Probenmaterial hinreichend ähnlich sind. Um diese Einschränkungen aufzulösen, wurde ein leicht modifizierter Ansatz entwickelt. Dazu wurden die thermophysikalischen Eigenschaften der 15 wichtigsten gesteinsbildenden Minerale (in Sedimentgesteinen) statistisch analysiert. Aus variablen Mischungen dieser Basisminerale wurde ein umfangreicher, synthetischer Datensatz generiert, für welchen die theoretisch zu erwartenden physikalischen und thermischen Eigenschaften berechnet wurden. Dieser Datensatz wurde mittels multivariater statistischer Methoden bearbeitet, in dessen Ergebnis die Identifikation von drei Gesteinsgruppen (klastisch, karbonatisch, evaporitisch) gelang, für welche die Korrelationstrends zwischen WLF und anderen Logparametern nur geringe Schwankungen aufweisen. Für jedes dieser Cluster wurden Regressionsgleichungen abgeleitet, welche eine Prognose der Matrix-WLF erlauben. Die Validierung der prognostizierten Werte an Echtdaten zeigt, dass bei Anwendung dieser Gleichungen Fehler zwischen 4% und 11% zu erwarten sind. In einem zweiten Schritt wurden für dieses Echtdatenset (laborativ gemessene WLF und Standardbohrlochmessungen) empirische Prognosegleichungen für die Berechnung der Gesamt-WLF entwickelt. Die Daten entstammen vier tiefen Bohrungen im NDB mit Endteufen zwischen 700 und 4.000 m. Die berechneten WLF zeigen im Vergleich zu gemessenen WLF Fehler <15%. Die entsprechenden Gleichungen sind in Ihrer Anwendbarkeit jedoch auf die jeweiligen lithostratigraphischen Einheiten der getesteten Probengruppe beschränkt. Die Anwendung neu entwickelter, sowie in der Literatur publizierter Verfahren auf den NGB-Datensatz zeigt, dass mit den neu aufgestellten Gleichungen stets der geringste Prognosefehler erreicht wird. Die Inversion neu berechneter WLF-Profile erlaubt die Ableitung synthetischer Temperaturprofile, deren Vergleich zu gemessenen Gesteinstemperaturen in einen mittleren Fehler von < 5% resultiert.

Im Rahmen geothermischer Berechnungen werden zur Umrechnung zwischen Matrix- und Gesamt-WLF häufig Zwei-Komponenten-Mischmodelle genutzt (*Arithmetisches Mittel, Harmonische Mittel, Geometrisches Mittel, Hashin-Shtrikman Mittel, Effektives-Medium Mittel*). Ein umfangreicher Datensatz aus trocken- und gesättigt-gemessenen WLF und Porosität erlaubt die Evaluierung dieser Modelle hinsichtlich Ihrer Prognosefähigkeit. Diese variiert für die untersuchten Modelle stark (Fehler: 5 – 53%), wobei das geometrische Mittel die größte, quantitativ aber weiterhin unbefriedigende Übereinstimmungen zeigt. Die Entwicklung und Anwendung mischmodelspezifischer Korrekturgleichungen führt zu deutlich reduzierten Fehlern. Das korrigierte geometrische Mittel zeigt dabei, bei deutlich reduzierter Fehlerstreubreite, erneut die größte Übereinstimmung zwischen berechneten und gemessenen Werten und scheint ein universell anwendbares Mischmodel für sedimentäre Gesteine zu sein. Die Entwicklung modelunabhängiger, gesteinstypbezogener Konvertierungsgleichungen ermöglicht die Abschätzung der wassergesättigten Gesamt-WLF aus trocken-gemessener WLF und Porosität mit einem mittleren Fehler < 9%.

Die präsentierten Daten und die neu entwickelten Methoden erlauben künftig eine detailliertere und präzisere Parametrisierung thermischer Modelle sedimentärer Becken. Dies trägt zu einem verbesserten Verständnis der Temperaturverteilung des Untergrundes bei, eine Grundvoraussetzung zur effizienten Erkundung, Erschließung und Nutzung thermischer Ressourcen auch im Norddeutschen Becken.

DOI: 10.2312/GFZ.b103-13111

Schlagworte:

Wärmeleitfähigkeit, Temperaturfeld, Wärmestromdichte, Nordostdeutsches Becken, Bohrlochmessungen, Mischgesetze, Multivariate Analyse

DOI: 10.2312/GFZ.b103-13111

Table of contents

Scientific Technical Report STR 13/11
DOI: 10.2312/GFZ.b103-13111

DOI: 10.2312/GFZ.b103-13111

DOI: 10.2312/GFZ.b103-13111

Scientific Technical Report STR 13/11
DOI: 10.2312/GFZ.b103-13111

Acknowledgments

This dissertation would not have been possible without the support and help of numerous people to whom I would like to express my gratitude.

First, I am highly indebted to Dr. habil. Andrea Förster (GFZ Potsdam) for enrolling me in this scientific journey, for the opportunity to conduct this work under her supervision and for her constant support, whenever discussion or advice was needed. When I first came to Potsdam, having neither much knowledge nor experience in geothermal exploration, Andrea Förster believed in my pure enthusiasm and offered me this Ph.D. position. I appreciated her vast expertise and knowledge of heat-flow studies, thermal and petrophysical rock properties and exploration geology that she shared with me, adding considerably to my experience. All in all, I had a wonderful time and I could not imagine a better supervisor. Thanks a lot.

I thank Prof. Dr. Manfred Strecker (University of Potsdam) for guiding, supporting and reviewing this work. The two external reviewers of this dissertation, Prof. Dr. Francis Lucazeau and Prof. Dr. Jürgen Schön, are thanked for their help and willingness to evaluate and comment on my work within a very tight time frame.

Dr. John H. Doveton and Dr. Daniel F. Merriam (both from the Kansas Geological Survey), thank you for showing me how well logging and statistic works. I have learned a lot from you, and I am both lucky and happy that I had this chance. Furthermore, thank you for the opportunity to be a temporary member of the coffee brigade.

I would like to thank many unnamed members of the Section 4.1: Reservoir Technologies at the GFZ Potsdam for their support and encouragement. In particular, I like to express my gratitude to some members of the cluster 'exploration geology'. To Dr. Ben Norden for the fruitful discussions to well logging and the specificity and secrets of the Thermal Conductivity Scanner, my colleague Felina Schütz for the shared way through the 'doctoral thick and thin', and Dr. Hans-Jürgen Förster for the right pinch of distrust from time to time, I am especially grateful.

My project would not have been possible without the support of many people who helped me with the analytical work. I would like to thank Claudia-Tamara Rach, Christina Rudolph, David Goehring, Josephine Buhk, Marta Oldman and Christian Cunow (all from the GFZ Potsdam) for their excellent support during the laboratory measurements. Furthermore, Dr. Ben Norden performed the thermal conductivity measurements on the core samples of the Ketzin location, *in toto*.

My work benefited also from the support of the Geothermie Neubrandenburg Company (GTN), especially from the assistance of Dr. Markus Wolfgramm during my first Ph.D.-steps, who provided background data from boreholes.

I like to thank the state geological surveys 'Landesamt für Umwelt, Naturschutz und Geologie Mecklenburg Vorpommern' (LUNG), „Landesamt für Bergbau, Geologie und Rohstoffe Brandenburg' (LBGR), and the „Landesamt für Geologie und Bergwesen Sachsen-Anhalt' (LAGB) for providing remote sensing data, background data from boreholes and core material, respectively. I would like to

express my sincere thanks to Dr. Karsten Obst (LUNG) for his outstanding and full support, to Dirk Zorn and Michael Göthel (both LBGR) for the extensive library research and the warm welcome in the core depot and to Dr. Carl-Heinz Friedel and Thomas Koch (both LAGB) for their quick reactions on my information requests.

Dr. Thomas Wonik, Dr. Torsten Tischner and Judith Orilski (all LIAG) are greatly thanked for providing background data, especially the petrophysical measurements from the GeneSys project in Hannover. Without these data, the results of this work would be much less comprehensive.

In various stages of my thesis, I strongly appreciated constructive discussions with Torgny Sahlin (Baker Hughes, Norway), Prof. Niels Balling (Århus University, Denmark), and Prof. Willy Fjeldskaar (Tectonor, Stavanger, Norway).

My special thanks go to Julia Tetzner (University of Potsdam) for the fruitful and enlightening discussion on statistical stuff and to Ursula Loof and the staff of the library 'Wissenschaftspark Albert Einstein' for their productive help during three years of extensive literature research.

Last but not least I am very grateful to my family for their continuous support, understanding and encouragement during the last years. Thanks so much mum and dad. Finally, I am profoundly grateful to Anne for supporting me every single day. Thank you for our wonderful beloved kids – Arne, Adele and Tajo.

This Ph.D. project was performed in the framework of the German GeoEn project (Verbundvorhaben GeoEnergieforschung; Grant 03G0671A/B/C) funded by the Federal Ministry of Education and Research (BMBF) in the program 'Spitzenforschung und Innovation in den Neuen Ländern'.

Scientific Technical Report STR 13/11
DOI: 10.2312/GFZ.b103-13111

1 Introduction

1.1 Context and challenges

Thermal conductivity (TC) is an intrinsic physical rock property and a basic parameter required to determine the heat flow from the Earth's interior. Under stationary and conductive conditions, the heat-flow density (q) is defined as the product of the interval temperature gradient ($\Delta T/ \Delta z$) and its adjacent representative TC (Fourier's law). Adding the radiogenic heat production (a) of the overburden allows the terrestrial heat-flow (qs) to be calculated. Knowledge of qs provides insight into the heat potential at depth and allows the geothermal situation of an area, at depths beyond those encountered by boreholes to be inferred. Consequently, these thermal parameters are first-order controls on the thermal structure in sedimentary basins and thus are an important prerequisite for geothermal reservoir evaluation. Moreover, knowledge of the TC is an indispensable parameter in the understanding of basin evolution processes and thermal maturation modeling as well as for valid temperature models that are used for reliable resource evaluation or designation of concession areas.

Since decades, the determination of TC has been the target of numerous geoscientific studies. Even today, the most common method of determining TC is to measure it on rock samples under laboratory conditions (*e.g.*, von Herzen and Maxwell, 1959; Beck, 1965; Sass et al., 1971; Vacquier, 1985; Popov et al., 1999). The complexity of such laboratory work and the quality of the outcome depends on the chosen measurement technique (*e.g.*, steady-state or transient techniques), the sample type (*e.g.*, drill core or drill cutting), sample preparation, rock type and the saturation state (*e.g.*, air, gas, oil or water-saturated pore space). However, intact drill-core samples are scarce. Measurements on cutting samples are an alternative, but are much more demanding than state-of-the-art optical-scanning methods used on intact drill-core samples (Popov et al., 1999) and, hence, cause additional errors (*e.g.*, Sass et al., 1971).

Although several geothermal studies were performed in the North German Basin (NGB), the state of knowledge of these parameters is highly variable. Amongst other reasons, this is due to the different databases between eastern and western parts of the basin. In the Northwest German Basin (NWGB) TC was rarely measured and further petrophysical analyses were predominantly performed on cutting samples. Only a few regional studies on facies, hydraulic and hydrochemical properties, and reservoir temperature conditions of geothermal reservoir formations are published, *e.g.* for sandstones from the Lower Cretaceous (Beutler et al., 1994; Schulz and Röhling, 2000) Reliable information about the surface heat flow, based on unperturbed temperature-gradient and valid measured TC data, is largely unavailable. Information about borehole temperatures is mostly obtained from bottom-hole-temperature measurements (BHT), which may suffer large errors (Deming et al., 1990). In the Northeast German Basin (NEGB), petrophysical, chemical and hydraulic properties of potential target formations have been investigated in much more detail than in the NWGB. Drill-core samples and continuous temperature logs are available to a depth of 7,000 m. The sedimentology, petrology, facies and hydraulic properties of major geothermal Mesozoic aquifers (*e.g.*, Aalenian, Rhaethian-Liassic com-

DOI: 10.2312/GFZ.b103-13111

plex, Stuttgart Formation, Middle Buntsandstein) are well known (*e.g.*, Feldrappe et al., 2007, 2008; Franz, 2008; Franz and Wolfgramm, 2008; Rauppach et al., 2008; Wolfgramm et al., 2008; Förster et al., 2010) and are the object of recent and future studies (*e.g.*, Wolfgramm et al., 2011; Barth et al., 2012; Franz et al., 2012). Deeper aquifers, *i.e.* Upper Rotliegend sandstones, were mainly targeted in the course of oil and gas exploration until the 1990s.

Preliminary work toward determining the TC of rocks composing the sedimentary cover of the NEGB was initiated by Hurtig and Schlosser in the 1970s. The methodology applied by these authors, however, shows some weaknesses. For example, the dependency of TC from *in-situ* pressure and temperature conditions and the *in-situ* pore fluid composition was not considered. Additionally, the respective sample depths and borehole locations were not published, and the TC values presented by Hurtig (1968), Hurtig and Schlosser (1975), and Hurtig and Schlosser (1976) are often mean values for lithotypes of investigated stratigraphic units. Therefore, only a poor database of thermal rock properties was available for the first thermal-modeling studies in the NGB (*e.g.*, NEGB: Bayer et al., 1997; Ondrak et al., 1998; Vosteen et al., 2004; NWGB: Fromm et al., 2010).

The first extensive and systematical research on thermal rock properties in the NGB was published by Lotz (2004), Norden and Förster (2006) and Norden et al. (2008). In these studies, laboratory-derived TC was determined on hundreds of mainly Permo-Carboniferous drill-core samples in dry and saturated conditions, sampled from deep boreholes in the NEGB. The authors used unperturbed, continuous temperature logs to calculate *qs* at 13 locations. The radiogenic heat production was determined both by direct measurements of uranium, thorium, and potassium and by evaluating borehole measurements following the approaches of Rybach (1986) and used to determine the heat production of the sedimentary cover, to enable the calculation of *qs sensu stricto*. All in all, this work significantly improved the available knowledge about the major thermal rock properties in the Permo-Carboniferous strata of the NEGB.

Although the overlaying Mesozoic part of the sedimentary succession is of paramount importance for hydrogeothermal use, especially for heating purposes, it was not investigated systematically until today (only single TC values are known, *e.g.*, from scientific reports from the Rheinsberg borehole; Brandt et al., 1995).

Beyond the heat-flow determination, TC is frequently used as key parameter for numerical modeling of the thermal history of sedimentary basins. Thermal history is a main control on generation of oil and gas in source rocks and is especially used in maturation modeling of petroleum systems. Therefore, modeling of TC changes in depth over time and the accompanying changes in porosity is essential for this issue. The combination of dependable matrix TC values and porosity is, therefore, crucial. Due to laboratory determinations of dry or saturated TC, two-component mixing models are used to derive the matrix TC from both, measured bulk TC and effective porosity. Conversely, bulk TC can be inferred from the matrix TC and known porosity for different saturating fluids (*e.g.*, oil, gas, salty water, fresh water). Several mixing models are documented (*e.g.*, Wiener, 1912; Lichtenecker, 1924; Voigt, 1928; Reuss, 1929; Bruggeman, 1935; Hanai, 1960; Sugawara and Yoshizawa, 1961; Hashin and Shtrikman, 1962; Sen et al., 1981; Zimmerman, 1989; Schopper, 1991; Popov et al., 2003), some with a well-defined structural (physical) and some with a theoretical basis (*e.g.*, layered or inclusion models). Other mod-

DOI: 10.2312/GFZ.b103-13111

els use purely empirical or semi-empirical approaches (*e.g.*, geometric-mean model). Physical models generally may have a wider applicability than empirical models (depending on the degree of simplification to obtain a solution), but their usability is often limited by the inclusion of empirically determined parameters, compositional variations, or structural aspects. Empirical models have the drawback that they are strictly valid for the particular rock suite being used for model development. Extensive overviews of TC models are provided by Tinga et al. (1973), Progelhof et al. (1976) (for two-component mixtures) and Abdulagatova et al. (2009).

Many mixing-models were established in the past, but statistical verification by comparison with real data has not yet been comprehensively performed. Most studies that compared measured and calculated bulk TC values involved crystalline rocks (*e.g.*, Robertson and Peck, 1974; reevaluated by Horai, 1991; Pribnow, 1994). Only a few small studies are relevant for sedimentary rocks (*e.g.*, Woodside and Messmer, 1961 [n=6]; Hutt and Berg, 1968 [n=28]; Buntebarth and Schopper, 1998 [n=11]). Beyond this, Clauser (2006) compared TC data of various sedimentary lithotypes (n=1088, data collected from several studies of the working group of Yuri Popov) with theoretical mixing-model curves. These authors graphically identified the best fitting model. However, they did not show the statistical validity of their comparisons.

Due to the limited availability of drill-core samples, TC values derived with state-of-the-art TC analytics are scarce. If physical material for laboratory studies is not available, other methods for TC determination are required to overcome such limitations. Several approaches were developed in the past, such as (1) *in-situ* probes, the (2) inversion of high-precision equilibrium temperature logs, and the use of (3) conventional petrophysical well-logs.

The first two methods mentioned above were successfully realized. *In-situ* measurements were continuously developed using special probes (*e.g.*, Beck, 1965; Oelsner et al., 1968; Beck et al., 1971; Hyndman et al., 1979; Villinger, 1983; Kuriyagawa et al., 1983; Erbaş, 1988; Hornamand, 1993; Burkhardt et al., 1995; Burkhardt and Troschke, 1998). High-precision equilibrium temperature logs were employed originally by Blackwell and Steele (1989) and are applied to the NEGB in the first part of this thesis (Section 2). However, the available *in-situ* techniques work discontinuously, are too time-consuming and are not cost-efficient. Equilibrium temperature logs, which are measured years after the last circulation within the borehole, are rarely available, even for scientific purposes. Hence, other approaches are needed.

During the last five decades, numerous studies related to (3) were performed to determine TC based on petrophysical well logging data (*e.g.*, Thornton, 1919; Dachnov and Djakonov, 1952; Zierfuss and Van der Vliet, 1956; Bullard and Day, 1961; Karl, 1965; Tikhomirov, 1968; Moiseyenko et al., 1970; Anand et al., 1973; Goss et al., 1975; Goss and Combs, 1976; Evans, 1977; Houbolt and Wells, 1980; Balling et al., 1981; Molnar and Hodge, 1982; Lovell and Ogden, 1984; Lovell, 1985; Della Vedova et al., 1987; Vacquier et al., 1988; Griffith et al., 1992; Zamora et al., 1993; Sahlin and Middleton, 1997; Doveton et al., 1997; Popov et al., 2003; Özkahraman et al., 2004; Hartmann et al., 2005; Goutorbe, et al., 2006; Singh et al., 2007; Khandelwal, 2010; Popov et al., 2011; Singh et al., 2011; Gegenhuber and Schön, 2012). Due to the limitations of linear-statistical approaches a lot of recent studies used inversion techniques or nonlinear statistical methods (nonlinear regression, artificial neural networks) to achieve reliable and more

DOI: 10.2312/GFZ.b103-13111

generally valid TC predictions. Although provision of TC profiles would be a major step forward, no universally valid, well-log based TC prediction equation was developed until today.

1.2 Structure of the thesis

The results of the present thesis are distributed into three distinct manuscripts that have been submitted and accepted (the first two) for publication in peer-reviewed journals.

In the first part (Chapter 2), new laboratory measurements of petrophysical rock properties of Mesozoic rocks from the Northeast German Basin (NEGB) including TC, porosity and density are presented. This section presents, for the first time, a large compilation of measured TC data of sandstone aquifers that are interesting for hydro-geothermal use. Continuous high-precision equilibrium temperature logs are used for the calculation of the heat-flow density, which, in turn, is used to indirectly compute continuous *in-situ* bulk TC profiles for complete borehole sections. Based on these profiles, *in-situ* bulk TC values for different stratigraphic stages and formations are determined.

Chapter 2 -originally published in:

Fuchs, S.[1], Förster, A.[1] (2010): Rock *thermal conductivity of Mesozoic geothermal aquifers in the Northeast German Basin*. Chemie der Erde – Geochemistry 70(S3), 13-22.

DOI: *http://dx.doi.org/10.1016/j.chemer.2010.05.010*

GFZ: *http://edoc.gfz-potsdam.de/gfz/display.epl?mode=docandid=15306*

[1] *GFZ German Research Centre for Geosciences, Reservoir Technologies, Telegrafenberg, 14473 Potsdam, Germany*

In the second part (Chapter 3), statistical techniques are used to predict the validity of different two-component mixing models (*i.e.* arithmetic mean, harmonic mean, geometric mean, Hashin-Shtrikman mean, effective medium mean) on a large compilation of TC data, obtained by different authors (including the data presented in chapter 2, data from Norden and Förster (2006), Clauser et al. (2007), Schütz et al. (2013) and, more recently, unpublished TC measurements from the NEGB). Those models are commonly used to calculate the matrix TC of a rock from the measured bulk TC, if the effective porosity of the rock sample is known. Conversely, using these parameters, the bulk TC can be determined for pore fluids of different TC (*e.g.*, air, fresh water, salty water, oil, gas). The quality of fit between measured and calculated saturated bulk TC is studied separately for the influence of lithotype (sandstone, mudstone, limestone, and dolomite), saturation fluid (water and isooctane) and rock anisotropy (parallel and perpendicular to bedding). Correction equations are established that allow for a significant improvement of the accuracy of bulk TC data calculated on the basis of the discussed mixing models. Furthermore, lithotype-specific conversion equations are provided, permitting a calculation of the water-saturated bulk TC from data of dry-measured bulk TC and porosity (*e.g.*, well log derived porosity). This latter process does not require the use of a mixing model.

Chapter 3 - originally published in:

Fuchs, S.[1], Schütz, F.[1], Förster, H.-J.[1], Förster, A.[1] (2013): *Evaluation of common mixing models for calculating bulk thermal conductivity of sedimentary rocks: correction charts and new conversion equations*. Geothermics 47, 40-52.

DOI: http://dx.doi.org/10.1016/j.geothermics.2013.02.002

GFZ: http://edoc.gfz-potsdam.de/gfz/display.epl?mode=doc&id=20276

[1] *GFZ German Research Centre for Geosciences, Reservoir Technologies, Telegrafenberg, 14473 Potsdam, Germany*

The third part (Chapter 4) introduces both a novel approach to infer matrix TC from commonly logged geophysical well-log data and newly derived empirical prediction equations for bulk TC. The first approach is based on a detailed theoretical analysis of the relationships between TC and other petrophysical rock properties performed on large artificial data sets of varying rock compositions. The empirical equations are derived from new TC data from two locations in the North German Basin (Ketzin and Hannover). These developments are accompanied by a review of all well-log based TC prediction methods from the literature, including a comprehensive comparative study of all methods on the same data set. A workflow is presented to compute bulk TC profiles for full borehole sections, independent of the sedimentary rock type. These continuous TC profiles are converted to temperature gradient profiles using the methods proposed in chapter 2. Finally, the predictive quality of the newly developed prediction methods are validated by comparing TC-log derived data with TC values measured on drill-core samples and with *in-situ* measured temperature gradient profiles.

Chapter 4 - originally submitted in:

Fuchs, S.[1], Förster, A.[2] (2013): *Well-log based prediction of thermal conductivity of sedimentary successions: a case study from the North German Basin*. Geophysical Journal International, *accepted for publication: 17.09.2013*.

DOI: http://dx.doi.org/10.1093/gji/ggt382

[1] *Aarhus University, Department of Geoscience, Høegh-Guldbergs Gade 2, 8000 Aarhus C, Denmark*

[2] *GFZ German Research Centre for Geosciences, Reservoir Technologies, Telegrafenberg, 14473 Potsdam, Germany*

2 Rock thermal conductivity of Mesozoic geothermal aquifers in the Northeast German Basin

Abstract

This study reports laboratory-measured thermal-conductivity (TC) values of Mesozoic sandstones from eight wells (predominantly geothermal boreholes) of the Northeast German Basin (NEGB). The measurements were made on drill core using the optical scanning method. Bulk thermal conductivities of sandstones corrected for *in-situ* thermal conditions range between 2.1 and 3.9 W/(m·K). In general, the Mesozoic sandstones show a large effective porosity typically ranging between 16% and 30%. Matrix TC ranges from 3.4 to 7.4 W/(m·K). The higher values reflect the large quartz content in sandstone. Based on the *in-situ* bulk TC and corresponding interval temperature gradient, obtained from high-precision temperature logs measured under thermal borehole equilibrium, interval heat-flow values were computed in the Middle Buntsandstein section (between 1,400 and 1,500 m) of two boreholes located in the Stralsund area. The heat flow averages to 74 mW/m² (Gt Ss 1/85 borehole) and 78 mW/m² (Gt Ss 2/85 borehole) and, by adding a heat-flow component of 1.8 mW/m² for the heat production in the overburden, are in good correspondence with previously reported surface heat flow of 77 mW/m². Based on these values and the temperature log information, bulk TC was indirectly calculated for the entire borehole profiles. The discrepancy between laboratory-measured and computed bulk TC in the two boreholes is in the order of 0.24 and 0.56 W/(m·K). Formation *in-situ* bulk TC of the Mesozoic section ranges between 1.5 and 3.1 W/(m·K).

Keywords

Thermal conductivity, Porosity, Heat flow, Geothermal aquifers, North German Basin

DOI: 10.2312/GFZ.b103-13111

2.1 Introduction

The thermal conductivity (TC) of rocks is a major physical property for the study of the Earth's thermal field. It is a basic parameter required to determine heat flow (q), which, according to Fourier's law of heat conduction (Eq. 2-1), is given by the product of temperature gradient ($\delta T/\delta z$) and the apparent TC (λ) in a depth interval (z).

$$q = - \lambda \, \delta T/\delta z \qquad (2\text{-}1)$$

Knowledge of the surface heat-flow (q_s) value provides insight into the heat potential from depth and allows inferences for the deep geothermal situation of an area beyond depths encountered by boreholes. Additionally, the thermal properties of sedimentary formations are first-order controls on the thermal structure of basins and can be used to determine geothermal targets on regional and local scale. In areas previously explored for geo-resources such as the Northeast German Basin (NEGB), numerous boreholes provide essential data sources for thermal field exploration. Borehole temperature measurements, either as single-point temperature recordings or as continuous temperature logs (Förster, 2001), form basic data on the subsurface temperature conditions. In contrast, borehole core samples, on which TC could be measured, are scarce and limited to the targets of specialized exploration. For example, previous studies in the NEGB on TC concentrated on the measurement of core from Permian and Permo-Carboniferous formations (Norden and Förster, 2006) forming the basis for a study on surface heat flow (Norden et al., 2008). For the Mesozoic and Cenozoic sections practically no data are available up to now.

Research conducted in the framework of the GeoEnergy Program (this issue) fills this gap by providing new TC data for the Mesozoic sections. These sections host important geothermal aquifers recently explored by core and modern well-log analysis allowing the development of a combined use of these data. Thus a method is sought, which overcomes the limiting factor of point information on TC from core measurement alone and provides continuous TC-profiles for large depth sections using standard geophysical wireline logs.

The expected results are important influential parameters for other GeoEnergy research (this issue), for example in the modeling of thermal maturation of organic matter implemented in time-temperature basin modeling for hydrocarbon research or in combining geological structure and thermal properties for a quantification of the subsurface thermal structure on which the future utilization of geothermal energy is based.

The approach being developed and applied to the NEGB data uses multivariate statistics to determine TC based on a statistical function employing data from gamma-ray, neutron, density, and temperature logs. Additionally, TC will be determined indirectly from the major mineral constituents (derived from XRD analyses) and their thermal-conductivity values using different approaches described in the international literature. Comparing the results of these different approaches will provide an important insight into the potential error made by indirectly determining TC in basin analysis.

DOI: 10.2312/GFZ.b103-13111

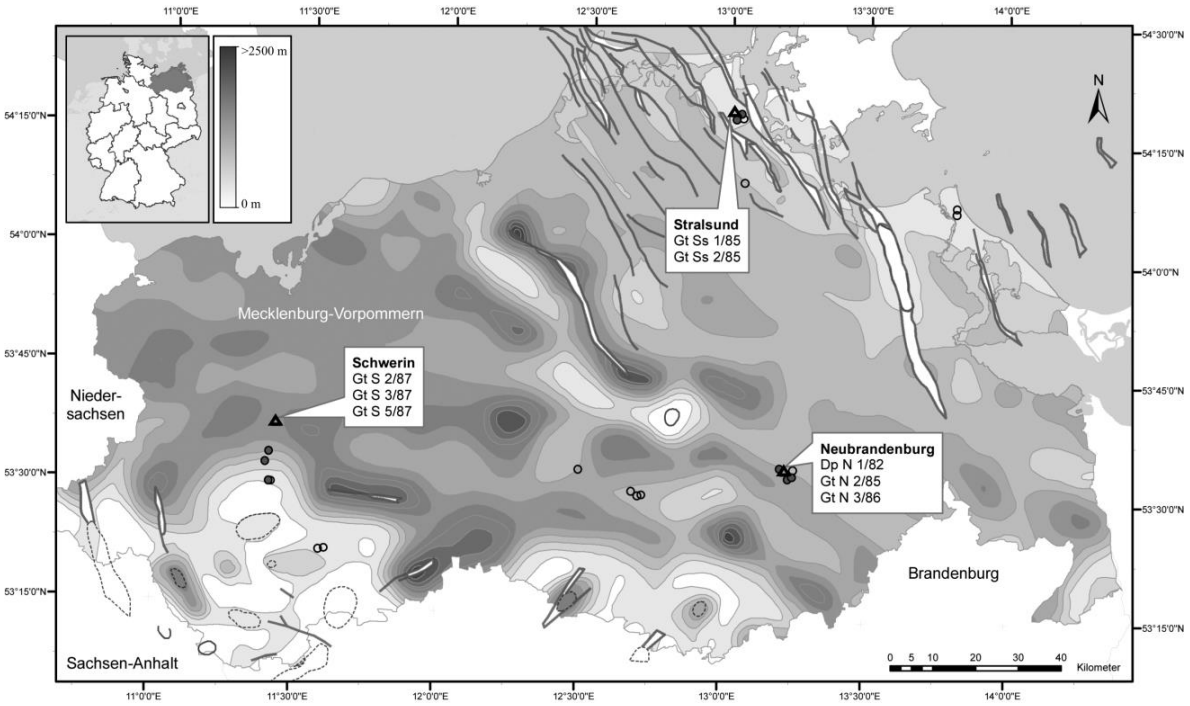

Figure 2-1 Study area in the NEGB. The thickness of the Permian Zechstein formation (after LUNG, 1997) is shaded grey (CI: 250 m). Grey solid circles show boreholes of this study selected from a pool of geothermal exploration wells (open circles) available in the area. Bold lines show major faults of Mesozoic age; broken line is the 500-m-depth isoline of top Zechstein; open triangles denotes the location of cities.

In this paper, a first set of laboratory measurements of TC is reported, which, later on, will be used to verify the statistical approach being part of ongoing research. The paper also contains for a subset of measured laboratory data a comparison with TC values calculated from mineral constituents and rock porosity. In addition, the laboratory data for different depth intervals are related to the respective interval temperature gradient, calculated from high-resolution, continuous temperature logs, allowing the calculation of an average heat flow for a borehole location. In turn, the this heat-flow value and the interval temperature gradient then are used to indirectly determine TC for those formations for which there is no drill core control.

Figure 2-1 shows the study area in Mecklenburg-Vorpommern, in which eight wells are investigated: the Gt Ss 1/85 and Gt Ss 2/85 boreholes located near the city of Stralsund at the northern margin of the NEGB; the Dp N 1/82, Gt N 2/85, and Gt N 3/86 boreholes near the city of Neubrandenburg and the Gt S 2/87, Gt S 3/87 and Gt S 5/87) boreholes near the city of Schwerin in the western part of the NEGB.

2.2 *Geological background*

The NEGB is a sub-basin of the Central European Basin system containing Cenozoic, Mesozoic, and Upper Paleozoic (Permian and Carboniferous) sediments that are up to 12 km thick (Hoth et al., 1993). Since the 1960s, a large number of wells were drilled in the sedimentary succession of the NEGB as part of an exploration for oil and gas and geothermal energy. Analyses of drill cores, geophysical well logs,

DOI: 10.2312/GFZ.b103-13111

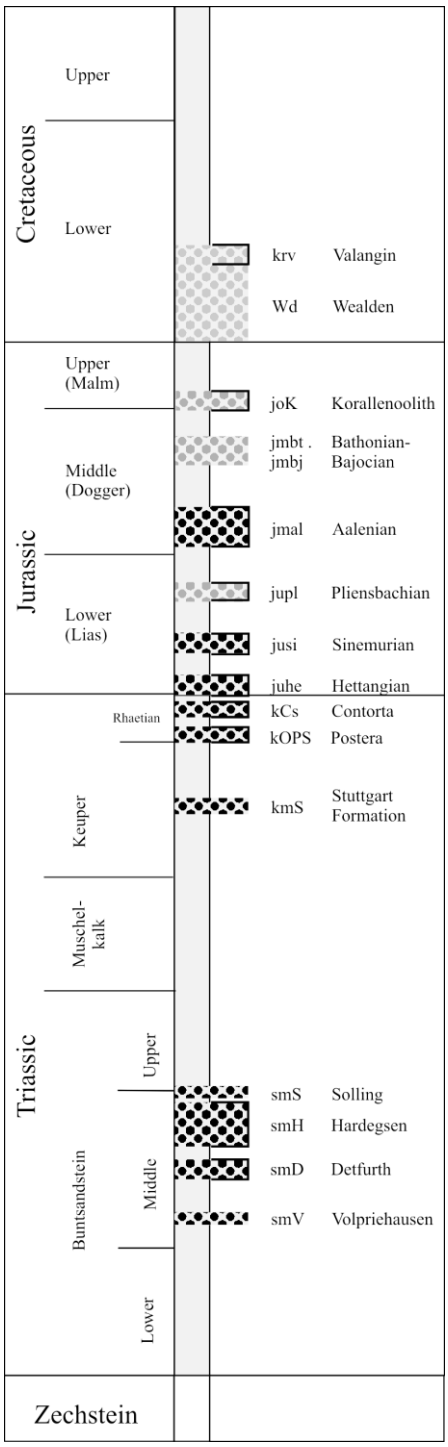

Figure 2-2 Generalized stratigraphic column of the Mesozoic with major geothermal sandstone aquifers (dotted pattern; modified after Feldrappe et al., 2008). Black-dotted intervals are the studied aquifers.

and hydraulic tests, performed in many of these wells formed the basis for a sound understanding of the geology and physical properties of the major reservoirs in this region. In recent years, the Mesozoic aquifers, predominantly made up of sandstones (Fig. 2-2), were studied for their lithological, mineralogical, petrophysical, and hydrogeological signatures (Feldrappe et al., 2008; Wolfgramm et al., 2008).

In this paper, the TC of the Mesozoic sandstone aquifer section is investigated, comprising the Aalenian (Dogger-β) (youngest) and the Detfurth Formation (Middle Buntsandstein) (oldest) (*cf.* Fig. 2-2).

The occurrence of the Aalenian (Dogger-β, Altmark) sandstone is limited to the southwestern area of Mecklenburg-Vorpommern. Its thickness is variable (15 – 92 m; Wolfgramm et al., 2008). Greatest thick-ness of about 80 m is observed in a well in the Schwerin area; the sandstone thins out farther to the north and the northeast. The base of the sandstone formation rests at depths between 100 m near the margins and 2,400 m in some rim synclines in the center of the NEGB (Feldrappe et al., 2008). The sandstone is medium to fine-grained, and typical porosities are in the range of 21 – 28% (Wolfgramm et al., 2008).

The poorly cemented sandstones of the Rhaethian-Liassic aquifer complex occur in most parts of Mecklenburg-Vorpommern (except of the northern Rügen area) and show maximum thicknesses in the south, near to the center of the NEGB.

The thickness of the Lias is in the range of 270 – 400 m. The base of the Lias rests between depths of 100 – 2,800 m (Feldrappe et al., 2008). The Lias is subdivided into three formations: the Pliensbachian (fine-grained sandstones), Sinemurian (fine-grained sandstones) and Hettangian consisting of sandstones, siltstones, and claystones. The Hettangian shows thicknesses ranging from 6–95 m (average 46 m) and porosities between 19 – 36% (average 26%; Wolfgramm et al., 2008). The Rhaethian

is between 50 and 250 m thick (Feldrappe et al., 2008). It is subdivided into the Triletes, the Contorta, and the Postera consisting of mature sandstones and claystones. The Postera is made up predominantly of sandstone and has a thickness of 12 – 40 m (average of 30 m), whereas the Contorta is pelitic and has thicknesses between 6 and 54 m (average of 12 m) (Wolfgramm et al., 2008). For both formations typical porosities are in the range of 20 – 25% (Feldrappe et al., 2008).

The fine to medium-grained sandstone of the Stuttgart Formation occurs in most parts of the NEGB (except of Rügen and Altmark areas) and shows a laterally and vertically alternating facies. Mudstones of the flood-plain facies alternate with fluvial channel deposits of variable thickness (Förster et al., 2006 and references therein). The base of the formation lies between depths of 400 and 2,500 m in Mecklenburg-Vorpommern; the thickness of the formation varies between 80 and 100 m (Feldrappe et al., 2008). Typical porosities of the channel sandstones are 20 – 36% (Wolfgramm et al., 2008 and references therein).

The limnic and marine sediments of the Middle Buntsandstein are widespread in the northern part of the NEGB. They are medium-grained and have a thickness of about 180 m near the city of Stralsund and a maximum thickness of about 500 m in the basin center. The base of the Middle Buntsandstein rests at a depth of about 1,000 m near the Baltic coast and at about 3,500 m in the basin center (Feldrappe et al., 2008). The Middle Buntsandstein group is subdivided into four formations. The Solling Formation on top is mostly composed of two 12 – 20-m-thick sandstone layers, separated by a 20-m-thick claystone. The Hardegsen Formation consists of basal sandstone (20 –50 m thick) and is overlain by siltstones and claystones, with some anhydrite. The Detfurth Formation is made up of sandstones (5 – 40 m thick) interbedded by siltstones and claystones. The Volpriehausen Formation consists of only poorly cemented sandstone (2 – 10 m thick). The Middle Buntsandstein shows an average sandstone porosity of about 20 – 30% (Feldrappe et al., 2008).

2.3 *Methods*

Typical techniques for the measurement of rock TC include the divided-bar steady-state technique, the needle-probe transient method (Sass et al., 1971; Sass et al., 1984), and the optical scanning method (Popov et al., 1999). We employed the latter one because of its ease in use allowing a study of large suites of samples in a short time. The optical scanning method is based on scanning a primed and black colored sample surface with a focused and continuously operated mobile heat source. The heat source and two infrared temperature sensors (measurement of initial and maximum sample temperature) move with a fixed distance between each other and with the same speed relative to the core sample. The temperature sensor behind the heat source continuously registers the value of the maximum temperature increase along the heating line and yields a continuous conductivity profile. With knowledge of the maximum temperature rise Θ, the heat source power Q, the distance x between heat source and temperature sensors and the measurement of a reference standard (Θ_S) with a known TC (λ_s), it is possible to determine the TC (λ) of each sample along the scanning line. This relation is described by equation (2-2):

DOI: 10.2312/GFZ.b103-13111

$$\lambda = \lambda_S \cdot \left(\frac{\Theta_S}{\Theta} \right) \qquad (2 - 2)$$

Bulk thermal conductivity (bulk TC) was measured on core samples both under dry and saturated conditions. For each sample, an average value was computed from at least three scan cycles. First, the rock samples were dried to constant weight at 60 °C in a vacuum oven. Later on, the dehydrated samples were saturated by submerging them in distilled water inside of a sealed vacuum exsiccator. Measurements were performed on both a sawed plane ($\lambda_\perp$); perpendicular to the bedding and in the direction of the vertical heat flow) and on the core mantle ($\lambda_{||}$) along the core axis, perpendicular to the principal heat-flow direction. A total of 75 core samples were analyzed. The core diameters varied between 45 and 90 mm, the sample length from 50 mm to 350 mm. For most of the investigated Mesozoic sediments the bedding was (nearly) parallel to the disk plane.

The effective porosity (Φ) was determined after the Archimedes method by the mass change between dry (dehydrated at 60 °C) and saturated sample. Bulk TC values, measured on saturated samples (λ_{satM}) were converted into the matrix thermal conductivity (matrix TC, λ_{matrix}) using the effective porosity Φ and the pore medium ($\lambda_{pore} = \lambda_{water}$ of 0.6 W/(m·K) according to the geometric-mean model (Eq. 2-3):

$$\lambda_{matrix}^{1-\phi} = \frac{\lambda_{satM}}{\lambda_{pore}^{\phi}} \qquad (2 - 3)$$

Matrix TC also was determined from the TC values of the mineral constituents of a particular rock type using the geometric-mean model (*e.g.*, Brigaud et al., 1990) as a mixing law (Eq. 2-4)

$$\lambda_{matrix} = \prod_{i=1}^{n} \lambda_i^{vol_i} \qquad (2 - 4)$$

where λ_i is the TC of the *i*th mineral constituent and vol_i is the fractional volume of the mineral constituents. The volumetric fractions of major minerals are obtained from XRD analyses (GTN, 2009, personal communication). The TC values of individual minerals are literature values (Horai, 1971; Schön, 1996; *cf.* Table 2 - 2).

High-precision temperature logs (LIAG, 2006) recorded in cm-intervals in borehole thermal equilibrium, were processed for temperature gradients. The temperature gradients were calculated as 1-m running averages and smoothed with an 11-point-mean filter.

2.4 Results

2.4.1 Laboratory-measured thermal conductivity

Table 2-1 shows the bulk TC measured in the direction of principal heat flow on saturated sandstone samples (λ_{satM}). Values in bold are average values for the different formations. Matrix values were corrected for *in-situ* temperature conditions using borehole temperature data. The correction applied is

DOI: 10.2312/GFZ.b103-13111

small [max. = 0.4 W/(m·K)]. The lowest TC value of 2.1 ± 0.11 (1-SD) W/(m·K) is observed in the Stuttgart Formation sandstones (kmS, Keuper) and the highest value of 3.9 ± 0.27 W/(m·K) in the Postera sandstone (kOPS, Rhaethian), respectively. The average TC values for the Contorta and the Postera sandstones are higher in the Schwerin boreholes [3.8 ± 0.18 W/(m·K) (kCs) and 3.9 ± 0.08 W/(m·K) (kOPS)] than in the Neubrandenburg boreholes [3.3 ± 0.27 W/(m·K) (kCs) and 3.4 ± 0.39 W/(m·K) (kOPS)].

The Middle Buntsandstein has the largest variation in bulk TC of all formations ranging from 2.7 ± 0.1 W/(m·K) (smH, Hardegsen, Gt Ss 1/85 borehole) to 3.5 ± 0.45 W/(m·K) (smS, Solling, Gt Ss 2/85 borehole) exhibiting a mean value of 3.2 ± 0.37 W/(m·K). The matrix TC (Table 2-1, column 6), calculated as an average of measurements under saturated and dry conditions, also is lowest for the Stuttgart Formation sandstones (kmS, Middle Keuper) [3.4 ± 0.8 W/(m·K)] and highest for the Postera (kOPS) sandstone [7.4 ± 0.5 W/(m·K)].

The regionally different bulk TC observed for the Contorta and the Postera sandstones also is reflected in matrix TC. Similarly, the large variation in bulk TC of the Middle Buntsandstein also is reflected in its matrix conductivity values, ranging from 4.2 ± 0.8 W/(m·K) (smH, Hardegsen, Gt Ss 1/85 borehole) to 5.5 ± 0.66 W/(m·K) (smH, Hardegsen, Gt Ss 2/85 borehole).

The average anisotropy ratio, as a ratio between measured maximum TC and minimum TC, is small (0.83 – 1.31; mean: 1.02 ± 0.08). No trend of higher values parallel to bedding ($TC_{||}$) compared to values perpendicular to bedding ($TC_{\perp}$) is observed.

2.4.2 *Thermal conductivity calculated from mineral constituents*

Table 2-2 shows a comparison between measured (A) and calculated (B) saturated formation bulk TC and their respective matrix values for a subset of geological formations for which XRD analyses were available. The values are not corrected for *in-situ* temperature.

The difference between measured and calculated bulk values is on average 0.37 ± 0.23 W/(m·K), ranging from 0.1 W/(m·K) (smD, Detfurth) to 0.7 W/(m·K) (kOPS, Postera). For matrix values, the average discrepancy is 1.13 ± 0.62 W/(m·K), ranging between 0.1 and 1.9 W/(m·K). The largest differences were observed in the Hardegsen (smH) and Stuttgart (kmS) Formations. Trends of increasing or decreasing discrepancy is related to mineralogy, however, this observation needs a further verification using a larger database.

DOI: 10.2312/GFZ.b103-13111

Table 2-1 TC of water saturated samples corrected for *in-situ* temperature.

Stratigraphic Unit	Borehole	Depth (MD)	Bulk TC		Average matrix TC	Effective Porosity
			meas.	corrected [a]	calculated	
		m	W/(m·K)		W/(m·K)	%
(jupl)	Dp N 1/82	991.2	3.6	3.5	5.5 ± 0.3	21.4
(jupl)	Dp N 1/82	1017.0	3.1	3.0	6.1 ± 1.1	26.1
			3.4	**3.3**	**5.8**	**23.8**
(jusi)	Dp N 1/82	1134.6	3.2	3.1	5.6 ± 1	28.4
(jusi)	Dp N 1/82	1136.0	3.2	3.0	5.6 ± 0.8	28.2
			3.2	**3.1**	**5.6**	**28.3**
(juhe)	Gt N 3/86	1120.5	3.3	3.2	5.2 ± 0	22.4
(juhe)	Gt N 3/86	1122.6	3.6	3.5	6.7 ± 0.6	24.8
(juhe)	Gt N 3/86	1124.3	3.5	3.3	5.1 ± 0.3	21.1
(juhe)	Gt N 3/86	1125.7	4.0	3.8	4.5 ± 1.7	16.5
(juhe)	Gt N 3/86	1144.2	3.0	2.9	7.6 ± 1.3	32.4
(juhe)	Gt N 3/86	1145.9	3.4	3.3	6.2 ± 0.1	26.9
(juhe)	Gt N 3/86	1150.7	3.2	3.1	6.1 ± 0.1	27.4
(juhe)	Gt N 3/86	1153.1	3.3	3.2	7.4 ± 0.2	31.5
(juhe)	Gt N 3/86	1154.0	3.2	3.1	5.5 ± 0.2	25.7
(juhe)	Gt N 3/86	1157.5	3.3	3.1	5.5 ± 0.9	26.7
(juhe)	Gt N 3/86	1159.3	3.3	3.2	6.9 ± 0.3	29.6
			3.4	**3.2**	**6.1**	**25.9**
(kCs)	Gt N 2/85	1222.1	3.4	3.2	5.2 ± 0.3	20.0
(kCs)	Gt N 2/85	1225.3	3.2	3.1	6.3 ± 1.1	25.3
(kCs)	Gt N 2/85	1229.4	3.8	3.6	5.5 ± 0.1	18.7
			3.5	**3.3**	**6.2**	**21.3**
(kCs)	Dp N 1/82	1252.0	3.5	3.3	4.7 ± 1.3	21.9
			3.5	**3.3**	**5.9**	**21.9**
(kCs)	Gt S 5/87	2063.2	4.0	3.7	6.8 ± 0.5	25.5
(kCs)	Gt S 5/87	2072.1	4.2	3.8	6.7 ± 0.1	22.8
(kCs)	Gt S 5/87	2072.7	4.1	3.7	7.4 ± 1.4	23.7
(kCs)	Gt S 5/87	2072.9	4.5	4.0	6.1 ± 0.4	20.0
(kCs)	Gt S 5/87	2109.5	4.4	4.0	6.5 ± 0.3	20.1
(kCs)	Gt S 5/87	2110.5	4.2	3.8	6.1 ± 0.1	20.5
(kCs)	Gt S 5/87	2112.4	3.7	3.4	6.2 ± 0.9	22.3
(kCs)	Gt S 5/87	2113.1	4.0	3.6	5.5 ± 0	18.8
(kCs)	Gt S 5/87	2114.2	4.2	3.8	7.2 ± 0.9	23.0
(kCs)	Gt S 5/87	2115.2	4.1	3.7	8 ± 2.8	22.6
			4.1	**3.8**	**6.6**	**21.9**
(kOPS)	Gt S 5/87	2136.5	4.5	4.1	7.7 ± 1.2	22.0
(kOPS)	Gt S 5/87	2136.9	4.1	3.7	7.1 ± 1.3	22.1
			4.3	**3.9**	**7.4**	**22.0**
(kOPS)	Dp N 1/82	1274.6	3.8	3.6	5.2 ± 0.3	22.4
(kOPS)	Dp N 1/82	1275.0	3.7	3.5	6.3 ± 1.1	26.3
(kOPS)	Dp N 1/82	1281.8	3.3	3.2	5.5 ± 0.1	25.2
			3.6	**3.4**	**5.7**	**24.7**
(kOPS)	Gt N 2/85	1255.5	3.6	3.5	7.8 ± 0.1	30.5
(kOPS)	Gt N 2/85	1261.0	3.1	3.0	7.1 ± 1.2	30.0
			3.4	**3.2**	**7.4**	**30.3**

DOI: 10.2312/GFZ.b103-13111

Table continue

(kmS)	Gt N 2/85	1517.5	1.9	1.9	2.4 ± 0.2	11.0
(kmS)	Gt N 2/85	1525.4	2.1	2.1	2.7 ± 0.2	13.7
(kmS)	Gt N 2/85	1528.0	2.0	2.0	3.2 ± 0.9	17.0
(kmS)	Gt N 2/85	1537.7	2.1	2.1	4.3 ± 0.8	26.3
(kmS)	Gt N 2/85	1541.7	2.2	2.2	4.2 ± 0.2	25.8
			2.1	**2.1**	**3.4**	**18.8**
(smS)	Gt Ss 1/85	1404.6	2.6	2.5	4.1 ± 0.9	19.0
(smS)	Gt Ss 1/85	1406.6	3.2	3.1	4.5 ± 0.1	18.8
(smS)	Gt Ss 1/85	1408.2	3.2	3.1	5.3 ± 0	23.2
(smS)	Gt Ss 1/85	1412.3	4.2	3.9	5.3 ± 1.2	18.5
			3.3	**3.2**	**4.8**	**19.9**
(smS)	Gt Ss 2/85	1448.1	3.4	3.3	5.3 ± 0.4	19.8
(smS)	Gt Ss 2/85	1452.3	3.9	3.7	5.6 ± 0.9	21.5
(smS)	Gt Ss 2/85	1454.3	3.2	3.0	4.5 ± 0.4	16.9
(smS)	Gt Ss 2/85	1463.0	4.3	4.0	3.9 ± 0.9	6.0
			3.7	**3.5**	**4.8**	**16.1**
(smH)	Gt Ss 1/85	1424.0	2.8	2.7	4.7 ± 0.2	24.0
(smH)	Gt Ss 1/85	1426.0	2.6	2.5	2.8 ± 0.1	22.0
(smH)	Gt Ss 1/85	1430.4	2.8	2.7	4.4 ± 0.6	25.0
(smH)	Gt Ss 1/85	1434.7	2.7	2.7	4.5 ± 0.5	22.0
(smH)	Gt Ss 1/85	1435.6	2.9	2.8	4.4 ± 0.7	24.0
			2.8	**2.7**	**4.2**	**23.4**
(smH)	Gt Ss 2/85	1485.5	3.3	3.1	5.5 ± 0.2	23.5
(smH)	Gt Ss 2/85	1489.5	3.6	3.5	6.2 ± 0	24.1
(smH)	Gt Ss 2/85	1496.2	3.4	3.3	5 ± 0.3	21.0
(smH)	Gt Ss 2/85	1504.9	3.1	2.9	4.6 ± 0.8	23.5
(smH)	Gt Ss 2/85	1514.1	3.6	3.4	5.7 ± 0.2	21.7
(smH)	Gt Ss 2/85	1518.7	3.3	3.2	6.5 ± 0.7	26.4
(smH)	Gt Ss 2/85	1519.3	3.5	3.3	5.3 ± 0.2	21.4
			3.4	**3.2**	**5.5**	**23.1**
(smD)	Gt Ss 1/85	1467.4	3.8	3.6	4.8 ± 1.2	19.1
(smD)	Gt Ss 1/85	1491.2	3.5	3.3	4.9 ± 1	22.5
(smD)	Gt Ss 1/85	1530.3	3.0	2.9	4.6 ± 0.6	19.1
(smD)	Gt Ss 1/85	1540.9	3.1	3.0	4.5 ± 1.3	18.0
			3.3	**3.2**	**4.7**	**19.7**
(smD)	Gt Ss 2/85	1533.9	3.7	3.5	5.1 ± 0.2	17.1
(smD)	Gt Ss 2/85	1540.6	3.3	3.1	5 ± 0	21.7
(smD)	Gt Ss 2/85	1545.2	3.0	2.9	4.2 ± 0.4	21.0
(smD)	Gt Ss 2/85	1547.6	3.2	3.0	5 ± 0.2	23.0
(smD)	Gt Ss 2/85	1560.1	3.5	3.3	5.5 ± 0.1	21.6
(smD)	Gt Ss 2/85	1562.2	3.3	3.1	4.8 ± 0.2	20.4
(smD)	Gt Ss 2/85	1568.9	3.8	3.6	6.6 ± 0.6	23.7
(smD)	Gt Ss 2/85	1577.6	3.6	3.4	6.4 ± 0	25.7
(smD)	Gt Ss 2/85	1602.1	3.5	3.4	3.8 ± 0.3	9.6
			3.4	**3.3**	**5.1**	**20.4**

[a] Correction after Sass et al. (1992)

2.4.3 *Interval heat flow*

Temperature logs and measured bulk TC values were used in the Gt Ss 1/85 borehole and Gt Ss 2/85 borehole (Stralsund area) to indirectly compute TC profiles (Fig. 2-3) using interval (index *i*) temperature gradients (∇T) and a conductive heat-flow value (q) according to equation (2-5).

$$q_i = -\lambda_i \cdot \nabla T_i \qquad (2\text{-}5)$$

This approach follows a concept originally employed by Blackwell and Steele (1989) to indirectly determine a TC value for shale imbedded in carbonates.

The temperature logs used in both wells are semi-linear showing only minor breaks correlated to changes in lithology (Fig. 2-3). No fluid-flow signatures are observed in the log, so that heat-conduction conditions are assumed. This is supported by the good correlation between temperature gradient changes and lithological heterogeneity reflected by the gamma-log.

Temperature conditions are not affected by heat refraction effects of nearby major salt structures. The heat flow was computed in four Middle Buntsandstein sandstone intervals of homogeneous temperature gradients (Fig. 2-4). For each single interval, an average temperature gradient and an average bulk TC value was calculated from the laboratory-measured values. The bulk TC values were used as temperature-corrected values. The calculated interval heat-flow values vary between 68.4 mW/m² and 79.3 mW/m² (averaging to 74.2 ± 4.6 mW/m²; Gt Ss 1/85 borehole) and between 75.2 mW/m² and 81.9 mW/m² (averaging to 78.5 ± 4.8 mW/m²; Gt Ss 2/85 borehole) (Table 2-3). The heat-flow interval values are within 8% and 4% of the mean value, respectively.

Table 2-2 Comparison of (A) saturated measured bulk TC and respective matrix TC (uncorrected values) and (B) bulk TC for saturated samples based on *in-situ* matrix TC, calculated from mineral constituents and porosity. Pore fill is water.

Location	Stratigraphy	(A) No. Sample	(A) Bulk TC mean	(A) Matrix TC mean	(B) No. Sample	(B) Mineral composition[a] Quartz	Alkali feldspar	Plagio-clase	Others	(B) Bulk TC mean	(B) Matrix TC mean
			W/(m·K)			%	%	%	%	W/(m·K)	
N	(juhe)	11	3.4	5.8	6	85	3	3	10	2.97	5.84
	(kCs)	1	3.5	4.5	3	64	5	7	24	2.79	4.06
	(kOPS)	3	3.6	6.5	2	82	2	2	14	2.86	5.41
	(kmS)	5	2.1	3.1	8	48	5	26	21	2.51	3.84
S	(smS)	4	3.3	4.8	6	78	9	4	10	3.13	5.36
	(smH)	5	2.8	3.9	7	80	9	3	8	3.13	5.42
	(smD)	4	3.3	4.3	4	83	6	2	9	3.25	5.65

[a] *TC of minerals: quartz: 6.5 W/(m·K), alkali feldspar: 2.3 W/(m·K), plagioclase: 1.9 W/(m·K), Others: 3.0 - 5.6 W/(m·K).*

Table 2-3 Heat flow calculated for the Stralsund area.

Interval	Depth interval	Stratigraphic unit	No. TC values	Equilibrium temperature	Corrected average bulk TC		Calculated heat flow
	m			°C/km	W/(m·K)	1-σ	mW/m²
Gt Ss 1/85 borehole							
I	1405.90 - 1415.95	(smS)	3	23.5 ± 3.4	3.37	0.40	79.3
II	1421.30 - 1434.30	(smH)	3	27.3 ± 3.1	2.69	0.03	73.3
III	1434.00 - 1475.30	(smH, smD)	3	22.7 ± 3.5	3.02	0.42	68.4
IV	1483.80 - 1498.10	(smD)	1	23.1 ± 2.9	3.29	0.00	75.9
						average:	**74.2 ± 4.6**
Gt Ss 2/85 borehole							
I	1446.70 - 1456.40	(smS)	4	23.3 ± 5.5	3.52	0.45	81.9
II	1484.85 - 1521.10	(smH)	7	23.2 ± 5.0	3.24	0.18	75.2
						average:	**78.5 ± 4.8**

Considering an overburden of the heat-flow interval in this study of about 1,400 m and radiogenic heat-production values for this section as determined by Norden and Förster (2006), a heat-flow component on the order of 1.8 mW/m² has to be added to the calculated heat flow for a surface heat flow *sensu stricto*. This value is within the error range of heat-flow determination in this study.

2.4.4 *Thermal-conductivity profiles*

Using the mean interval heat-flow values and the temperature gradient values versus depth in the two boreholes, *in-situ* bulk TC was determined (see Eq. 2-4) for the Mesozoic section with a 0.1-m depth resolution. As expected, in the Buntsandstein section the calculated TC differs only slightly from the measured values (about 0.24 ± 0.20 W/(m·K); Gt Ss 1/85 borehole and 0.56 ± 0.51 W/(m·K); Gt Ss 2/85 borehole) (Fig. 2-4). Table 2-4 lists the formation TC values, calculated on the basis of a stratigraphic profile (Gt Ss 1/85 borehole), in conjunction with the formation temperature gradients. The lowest TC [1.5 W/(m·K)] is observed in the Toarcian (mostly claystones) and the highest [3.1 W/(m·K)] in the Hardegsen Formation (mostly sandstones), respectively. In general, however, the formation TC values are < 3.0 W/(m·K), which for sandy/silty rocks is a reflection of a relatively high porosity.

The impact of lithological heterogeneity on the formation TC is reflected in the 1-σ standard deviation (Table 2-4). A high variability is observed in the Upper Jurassic and the Lower Cretaceous. In these formations, claystones of low TC alternate with carbonates and sandstones, both of higher TC. Resulting from the variability of temperature gradients, the error of a calculated formation TC is assumed to be between 0.1 and 1.1 W/(m·K).

DOI: 10.2312/GFZ.b103-13111

Table 2-4 Average bulk TC calculated for Mesozoic formations in conjunction with formation temperature gradients (Gt Ss 1/85 borehole).

MD		Stratigraphy		Temperature gradient	Calculated average bulk TC[a]
m				°C	W/(m·K)
57		(qp)	Pleistocene	-	-
223	Cretaceous	(krt)	Turonian	26.3 ± 4.7	2.8 ± 0.4
250	Cretaceous	(krc)	Cenomanian	26.6 ± 16.1	2.8 ± 1.1
261	Cretaceous	(krl)	Albian	24.7 ± 12.6	3.0 ± 1.0
282	Cretaceous	(krh)	Hauterivian	28.7 ± 12.4	2.6 ± 0.8
356	Jurassic	(jutc)	Toarcian	50.8 ± 10.6	1.5 ± 0.3
460	Jurassic	(juplo)	Domerian (Upper Pliensbachian)	33.8 ± 11.4	2.2 ± 0.6
481	Jurassic	(juplu)	Carixian (Lower Pliensbachian)	28.9 ± 4.2	2.6 ± 0.3
666	Jurassic	(jusiu+juhe)	Lower Sinemurian + Hettangian	25.7 ± 9.3	2.9 ± 0.8
690	Triassic	(kTs)	Triletes (Upper Keuper)	30.4 ± 3.6	2.4 ± 0.3
711	Triassic	(kCs)	Contorta	28.3 ± 3.1	2.6 ± 0.3
753	Triassic	(kOPS)	Upper Postera	29.2 ± 4.4	2.5 ± 0.3
783	Triassic	(kmSM2-3)	Lower Postera	33.7 ± 14.2	2.2 ± 0.7
800	Triassic	(kmSM1)	Basisdolomit	26.0 ± 9.6	2.9 ± 0.8
819	Triassic	(kmS)	Stuttgart Formation (Middle Keuper)	36.1 ± 3.3	2.1 ± 0.2
949	Triassic	(kmGu)	Lower Gipskeuper	40.0 ± 12.6	1.9 ± 0.4
1015	Triassic	(ku)	Lettenkeuper (Lower Keuper)	36.9 ± 11.6	2.0 ± 0.5
1093	Triassic	(mm)	Upper Muschelkalk	41.3 ± 12.4	1.8 ± 0.4
1173	Triassic	(mmAN)	Middle Muschelkalk / Anhydrite	35.6 ± 9.8	2.1 ± 0.5
1258	Triassic	(mu)	Lower Muschelkalk / Wellenkalk	35.2 ± 3.6	2.1 ± 0.2
1275	Triassic	(soMY)	Myophorien (Upper Buntsandstein)	40.4 ± 3.0	1.8 ± 0.1
1374	Triassic	(soPR)	Pelitröt	37.4 ± 9.7	2.0 ± 0.4
1393	Triassic	(soSR)	Salinarröt	34.1 ± 6.8	2.2 ± 0.4
1421	Triassic	(smS)	Solling (Middle Buntsandstein)	30.6 ± 8.9	2.4 ± 0.5
1463	Triassic	(smH)	Hardegsen	24.2 ± 4.1	3.1 ± 0.4
1510	Triassic	(smDW)	Detfurth alt. sequence	24.4 ± 3.5	3.0 ± 0.4
1542	Triassic	(smDS)	Detfurth	-	-
1600	Triassic	(smV)	Volpriehausen	-	-

[a] Calculation based on computed heat-flow value of 74.2 mW/m² (Gt Ss 1/85 borehole).

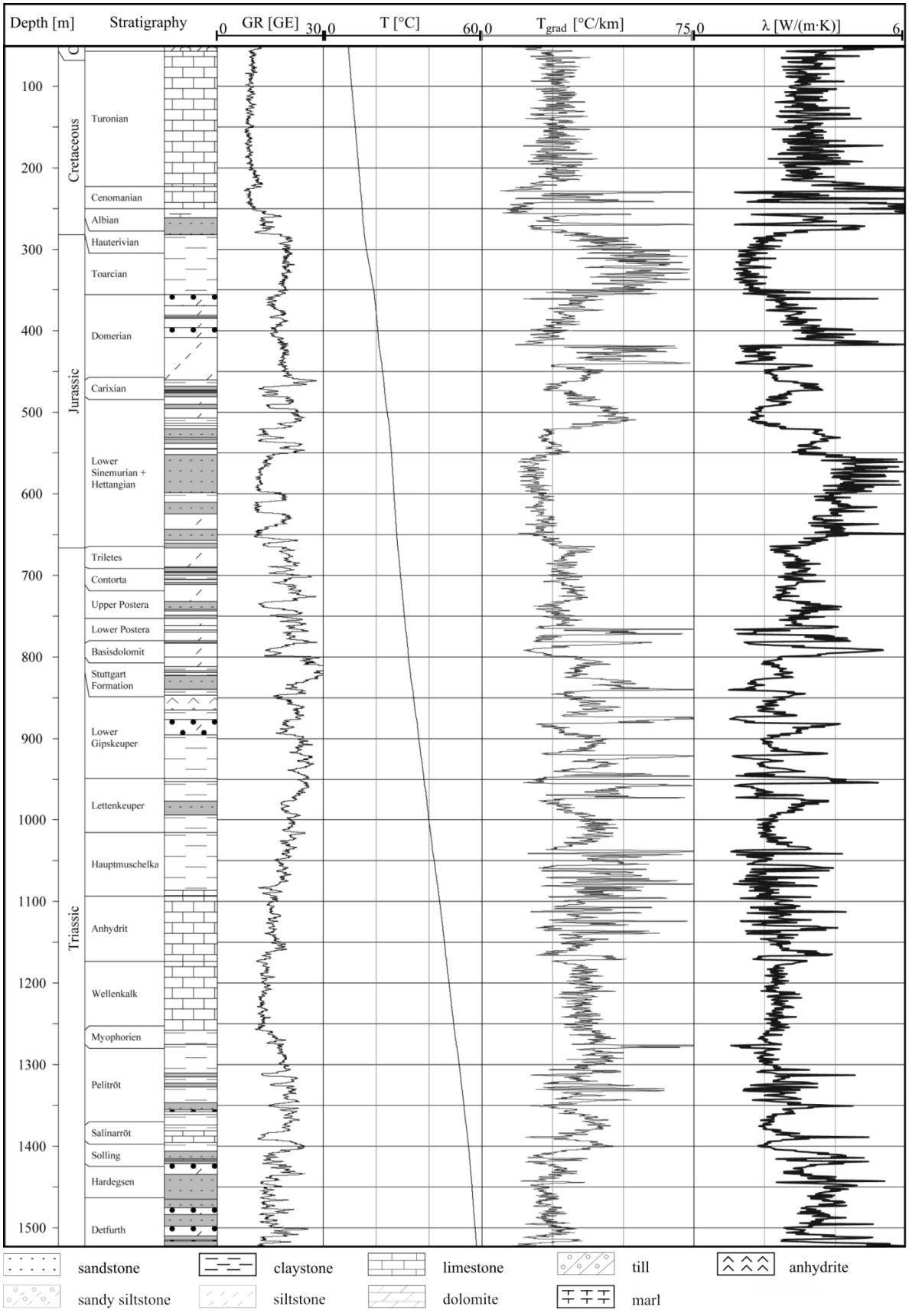

Figure 2-3 Bulk TC (λ), temperature (T), temperature gradient (T_{grad}) and gamma-ray (GR) profiles of the Mesozoic section (Gt Ss 1/85 borehole).

DOI: 10.2312/GFZ.b103-13111

2.5 Discussion

The average measured bulk TC values (2.1 – 3.8 W/(m·K), Table 2-1) of the Mesozoic sandstones are slightly lower than values published for the Permo-Carboniferous sandstones (2.3 – 4.8 W/(m·K); Norden and Förster, 2006). For example, the Permian Elbe and Havel Subgroup, comprised of quartz-cemented, fluvial-lacustrine siltstones and mudstones interbedded with pebbly sandstones has an average bulk TC of 4.6 ± 0.7 W/(m·K) (n = 54). However, the values for the Permo-Carboniferous are not corrected for *in-situ* temperature conditions. Correction would result in a decrease of about 0.5 W/(m·K) for saturated laboratory values (after Sass, 1992).

In general, the larger bulk values for the Permo-Carboniferous sandstones are related to lower porosity as a result of greater burial depth (3,000 – 5,000 m) compared to the Mesozoic formations, resting at present at 1,000 – 2,000 m. About 85% of the porosity values (n = 109) of the Permo-Carboniferous rocks are lower than 10% (Norden and Förster, 2006). In contrast, the porosity values of the Mesozoic sandstones range between 20 and 35%.

The observed dependence of bulk TC on matrix mineralogy is reflected in a strong correlation with calculated matrix TC (average values of 3.4 – 6.5 W/(m·K), Table 2-2). The strongest influence on matrix TC is the volume fraction of quartz (89 – 96%, except of the Stuttgart Formation of 48%). In general, the aquifer sandstones contain only minor amounts of feldspars and clasts (< 5.4% and 2.2 – 8.4%, respectively; Wolfgramm et al., 2008) classifying these rocks as sublitharenites or subarkoses (Pettijohn et al., 1987). An increase of TC with increasing quartz content also was described for example by Brigaud et al. (1990) for samples of the Tertiary sedimentary section in the Uinta Basin or by Norden and Förster (2006) for the Permian Rotliegend sandstones in the NEGB.

The TC measured in the laboratory has been corrected for *in-situ* temperature after Sass (1992). Due to the moderate burial depth of the samples, the corrected values differ only slightly from values under ambient laboratory conditions.

Thus, the maximum error introduced by not considering a correction for *in-situ* temperature is about 0.4 W/(m·K) [average value: 0.17 ± 0.1 W/(m·K)]. For 80% of the corrected values the error would be < 0.2 W/(m·K).

The interval heat flow determined in the Stralsund area (average 74.2 ± 4.6 mW/m²; Gt Ss 1/85 borehole and 78.5 ± 4.8 mW/m²; Gt Ss 2/85 borehole) in the Middle Buntsandstein section (Table 2-3) supports the surface heat-flow values of 68 – 91 mW/m² (Norden et al., 2008). Their values, determined on 13 locations in the NEGB at depths of 1,500 – 5,000 m, average to a surface heat flow of 77 mW/m². For wells in the particular Stralsund area, the surface heat flow is 76 and 80 mW/m² compared to the surface heat flow by Norden et al. (2008) of 74 mW/m² (Ba 1/63 borehole), 72 mW/m² (Sam 101/62 borehole), and 77 mW/m² (Binz 1/73 borehole). The strong similarity between the values indicates that there is no paleoclimatic effect on the interval heat flow, determined in the Middle Buntsandstein section (at 1,400 – 1,500 m).

DOI: 10.2312/GFZ.b103-13111

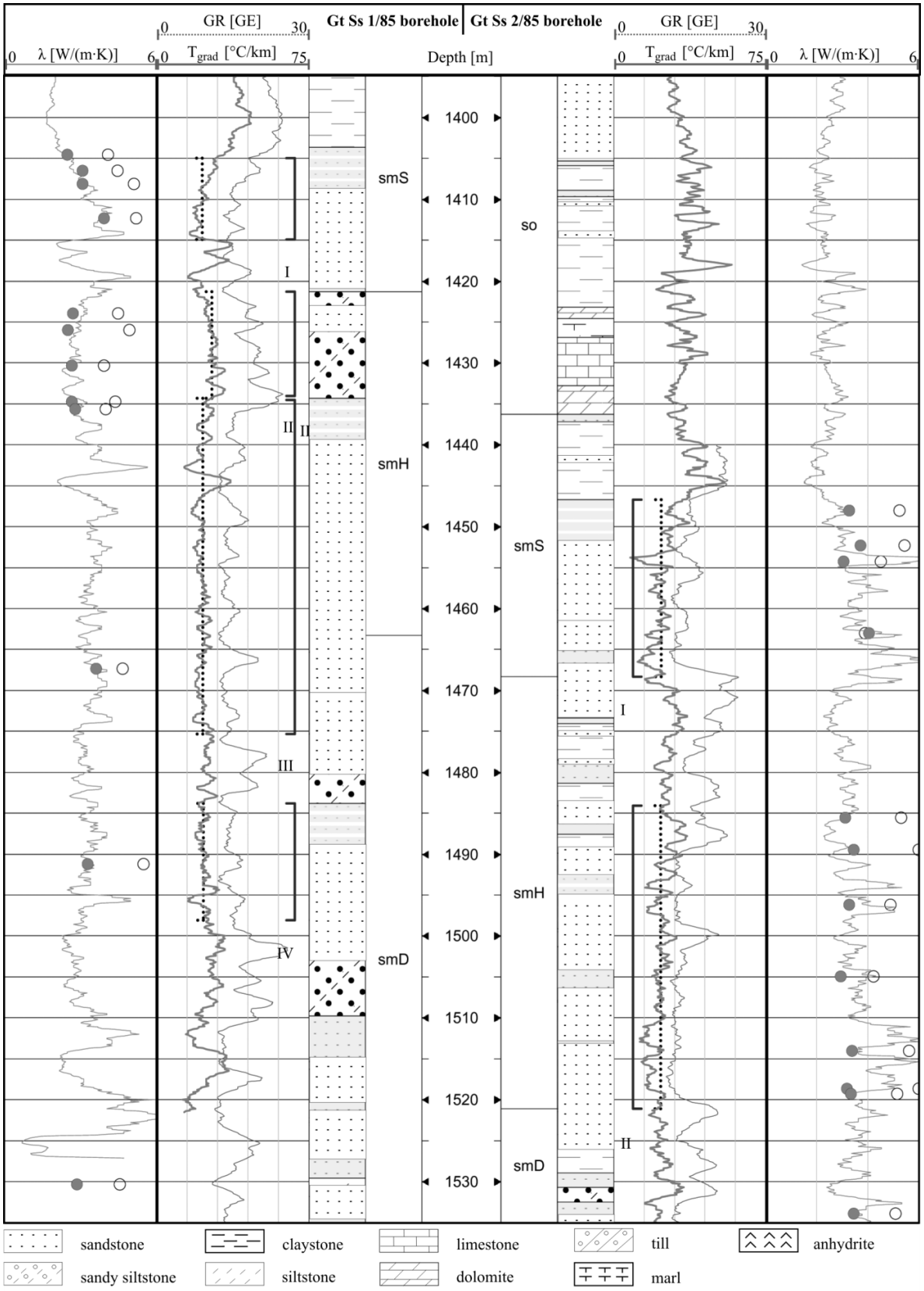

Figure 2-4 Thermal-conductivity profiles calculated for the Gt Ss 1/85 borehole and Gt Ss 2/85 borehole in the Stralsund area. Dots show bulk TC measured on saturated samples, open circles show average matrix TC calculated from dry rom dry and saturated measurements and porosity. Grey lines attached to the lithoprofile show the intervals for which mean temperature gradients were calculated; black bold dotted line indicates the average temperature gradient, thin dotted grey line show the gamma-ray.

DOI: 10.2312/GFZ.b103-13111

The calculated thermal-conductivity values based on these heat-flow values show some heterogeneity along the profile, which is a result of variable lithology. The strong negative correlation observed between the gamma-ray and TC values in general is indicative of the shale (clay) content. Thus, formations with the highest clay content exhibit the lowest TC and vice versa. For example, the Turonian limestones and limy marlstones as well as the Wellenkalk Formation (limestone), reflected as a very homogeneous sections, show a small bandwidth of high temperature gradients and of low gamma response exhibiting low clay content. In the Rhaethian, the interbedding of sandstone, siltstone and claystone also is well reflected in both the gamma and the gradient log. The Toarcian (claystones) shows the lowest formation TC in the borehole section. In contrast, the Sinemurian and Hettangian sandstones, well distinguishable in the gamma log by its clay content, are not well resolved in the gradient log,

The study performed in three areas of the NEGB reports for the first time laboratory-measured, *in-situ* TC for sandstones of different Mesozoic aquifers. Using some well-log approach, thermal-conductivity values for the entire Mesozoic succession are generated for the Stralsund area in the basin. Together with the thermal-conductivity values for the Permo-Carboniferous formations (Norden and Förster, 2006), a nearly complete geological section with thermal properties is now available to verify the calculated surface heat flow. Further work is planned to enlarge the database for Mesozoic rocks on other locations and further for Cenozoic formations. A larger database of the laboratory TC will also allow a validation of the indirectly determined values.

An envisioned systematic basin-wide approach of evaluating the variability of TC for key formations would be the basis for a comprehensive evaluation of the geothermal potential of the basin. Up to now, temperature maps are available in the NEGB for the base of the Detfurth Formation (Middle Buntsandstein/Keuper), the Stuttgart (Schilfsandstein) Formation (Keuper), the Jurassic, the Middle Jurassic, and the Lower Cretaceous (from oldest to youngest) (Feldrappe et al., 2008, and references therein). These formations comprise a depth range from about 400 – 2,000 m (with max. temperatures of 120 °C) in the northeastern part of the basin to about 1,600 – 3,000 m (with max. temperatures of 150 °C) in the southwestern part, respectively. The mapped temperatures are approximated from an isotherm map at 1,500 m by applying some average geothermal gradient for extrapolation of temperature to different depth. Also, 'expert knowledge' was applied to qualitatively correct temperature in the vicinity of major salt structure for heat refraction effects. Thus these maps show a highly resolved temperature pattern, strongly resembling the geological structure, but the pattern itself is not grounded in such a detail on measured borehole data nor on the petrophysical properties of the rocks. Future in-depth studies are needed to elaborate the value of these maps and to advance exploration techniques to revise the mapping. The approach used in this study builds a cornerstone to achieve this goal.

2.6 Acknowledgments

This study was performed in the framework of the GeoEN (www.geoen.de) project funded by the Federal Ministry of Education and Research (BMBF) in the program 'Spitzenforschung und Innovation in den Neuen Ländern'. We thank the Geothermie Neubrandenburg GmbH (GTN) and the geological survey 'Landesamt für Umwelt, Naturschutz und Geologie Mecklenburg Vorpommern' (LUNG) for

providing background data from boreholes and core material. Claudia Rach, David Goehring, and Christian Cunow (GFZ Potsdam) assisted in the laboratory measurements. The work benefited from a review by Niels Balling (Århus).

2.7 References

Blackwell, D. D., Steele, J. L. (1989). Heat flow and geothermal potential of Kansas. *In:* Steeples, D.W. (Ed.), Geophysics in Kansas, *Kansas Geological Survey Bulletin* 226, 267–295.

Brigaud, F., Chapman, D.S., Le Douaran, S. (1990). Estimating thermal conductivity in sedimentary basins using lithological data and geophysical well logs. *AAPG Bulletin* 74(9), 1459–1477.

Feldrappe, H., Obst, K., Wolfgramm, M. (2008). Mesozoic sandstone aquifers of the North German Basin and their potential for geothermal utilization. *Zeitschrift für geologische Wissenschaften* 36, 199–222.

Förster, A. (2001). Analysis of borehole temperature data in the Northeast German Basin: Continuous logs versus bottom-hole temperatures. *Petroleum Geoscience* 7(3), 241–254.

Förster, A., Norden, B., Zinck-Jørgensen, K., Frykman, P., Kulenkampff, J., Spangenberg, E., Erzinger, J., Zimmer, M., Kopp, J., Borm, G., Juhlin, C., Cosma, C.-G., Hurter, S. (2006). Baseline characterization of the CO2SINK geological storage site at Ketzin, Germany. *Environmental Geosciences* 13(3), 145–161.

Horai, K. (1971). Thermal conductivity of rock-forming minerals. *Journal of Geophysical Research* 76(5), 1278–1308.

Hoth, K., Rusbült, J., Zagora, K., Beer, H., Hartmann, O. (1993). Die tiefen Bohrungen im Zentralabschnitt der Mitteleuropäischen Senke – Dokumentation für den Zeitabschnitt 1962–1990. *Schriftenreihe für Geowissenschaften* 2, Gesellschaft für Geowissenschaften e.V., Berlin, Germany.

LIAG (2006). Geophysics Information System (FIS GP). URL: *https://www.fis-gp-appl.liag-hannover.de/app/fis_gp/index.php*, last accessed: 08.2010. See also: Kühne, K. (2006): Das Fachinformationssystem Geophysik und seine Nutzung über das Internet. *In: Merkel, B., Schäben, H., Wolkersdorfer, C., Hasche-Berger, A. (Eds.): GIS – Geowissenschaftliche Anwendungen und Entwicklungen, 57. Berg- und Hüttenmännischer Tag, 23.06.2006, Wissenschaftliche Mitteilungen des Instituts für Geologie 31, Freiberg, 227–231.*

LUNG (Geologisches Landesamt Mecklenburg – Vorpommern) (1997). Geologische Karte von Mecklenburg – Vorpommern: Übersichtskarte 1:500.000 – Strukturen im Untergrund nach oberflächengeophysikalischen Ergebnissen (Zechsteinsalzstrukturen), 1. Auflage.

Norden, B., Förster, A. (2006). Thermal conductivity and radiogenic heat production of sedimentary and magmatic rocks in the Northeast German Basin. *AAPG Bulletin* 90(6), 939–962.

Norden, B., Förster, A., Balling, N. (2008). Heat flow and lithospheric thermal regime in the Northeast German Basin. *Tectonophysics* 460(1–4), 215–229.

Pettijohn, F. J., Potter, P. E., Siever, R. (1987). Sand and Sandstone. Springer-Verlag, Berlin, 533 pp.

Popov, Y. A., Pribnow, D. F. C., Sass, J.H., Williams, C. F., Burkhardt, H. (1999). Characterization of rock thermal conductivity by high-resolution optical scanning. *Geothermics* 28(2), 253–276.

Sass, J. H., Lachenbruch, A. H., Moses, Jr. T. H., Morgan, P. (1992). Heat flow from a scientific research well at Cajon Pass, California. *Journal of Geophysical Research*, 97(B4), 5 017–5 030.

Sass, J. H., Lachenbruch, A. H., Munroe, R. J. (1971). Thermal conductivity of rocks from measurements on fragments and its application to heat-flow determinations. *Journal of Geophysical Research* 76(14), 3 391–3 401.

Sass, J. H., Stone, C., Munroe, R. J. (1984). Thermal conductivity determinations on solid rock – a comparison between steady-state divided bar apparatus and a commercial transient line-source device. *Journal of Volcanology and Geothermal Research*, 20(1–2), 145–153.

Schön, J.-H., 1996. Physical properties of rocks, fundamentals and principles of petrophysics. *In:* Treitel, S. and Helbig, K. (Eds.), Handbook of Geophysical Exploration: Seismic Exploration, vol. 18. Oxford, UK, Pergamon, p. 583.

Wolfgramm, M., Rauppach, K., Seibt, P. (2008). Reservoir-geological characterization of Mesozoic sandstones in the North German Basin by petrophysical and petrographical data. *Zeitschrift für geologische Wissenschaften* 36(4-5), 249–265.

3 Evaluation of common mixing models for calculating bulk thermal conductivity of sedimentary rocks: correction charts and new conversion equations

Abstract

Different numerical models can be deployed to calculate the matrix thermal conductivity of a rock from the bulk thermal conductivity (bulk TC), if the effective porosity of the rock is known. Vice versa, using these parameters, the bulk TC can be determined for saturation fluids of different thermal conductivity (TC). In this paper, the goodness-of-fit between measured and calculated bulk TC values of sedimentary rocks has been evaluated for two-component (rock matrix and pores) models that are used widely in geothermics: arithmetic mean, geometric mean, harmonic mean, Hashin-Shtrikman mean, and effective-medium theory mean. The examined set of samples consisted of 1147 TC data in the interval 1.0 to 6.5 W/(m·K). The quality of fit was studied separately for the influence of lithotype (sandstone, mudstone, limestone, dolomite), saturation fluid (water and isooctane), and rock anisotropy (parallel and perpendicular to bedding). From the studied models, the geometric mean displays the best, however not satisfying correspondence between calculated and measured bulk TC. To improve the fit of all models, respective correction equations are calculated. The 'corrected' geometric mean provides the most satisfying results and constitutes a universally applicable model for sedimentary rocks. In addition, the application of the herein presented correction equations allows a significant improvement of the accuracy of existing bulk TC data calculated on the basis of the other mean models. Finally, lithotype-specific conversion equations are provided permitting a calculation of the water-saturated bulk TC from data of dry-measured bulk TC and porosity (*e.g.*, well log derived porosity) with no use of any mixing model. For all studied lithotypes, these correction and conversion equations usually reproduce the bulk TC with an uncertainty < 10%.

Keywords

Sedimentary rock, Thermal conductivity, Porosity, Mixing model,

Geometric mean, Statistical analysis

DOI: 10.2312/GFZ.b103-13111

3.1 Introduction

In geothermal studies, the rock thermal conductivity (TC) constitutes an important parameter. It is essential for the determination of the heat flow from the Earth's interior and is indispensable in any thermal modeling. In sedimentary-basin research, large databases of TC are required to characterize the major lithotypes making up the different geological formations and hence entire sedimentary sections. The amount of data needed to characterize fully a sedimentary setting thereby depends on the geological history and associated facies changes and may be large.

The most reliable TC values originate from direct laboratory measurements. If core samples are not available, indirect methods are used to calculate TC from petrophysical properties, including porosity, a parameter provided through well logging (*e.g.*, Balling et al., 1981; Goss and Combs, 1976; Goutorbe et al., 2006; Hartmann et al., 2005). Another indirect approach of TC determination uses the abundance and composition of the rock-forming minerals and the porosity as a multi-component system (*e.g.*, Brailsford and Major, 1964; Brigaud et al., 1990; Demongodin et al., 1991, Vasseur et al., 1995). All these indirect methods have their shortcomings and restrictions.

Various laboratory methods for the measurement of TC are available comprising steady-state techniques (*e.g.*, divided bar technique, needle probe) and transient techniques (*e.g.*, line-source methods, ring-source methods, optical scanning). Comprehensive reviews on these techniques are provided by Kappelmeyer and Haenel (1974), Beck (1988), Blackwell and Steele (1989), and Somerton (1992). The less time-consuming optical scanning technique (OS) is, since introduced in the 1990s by Y. Popov, recently the most frequently used method to measure TC for large sample sets. This method was applied successfully to crystalline rocks (*e.g.*, He et al., 2008; Popov et al., 1999) as well as to sedimentary rocks (*e.g.*, Clauser, 2006; Fuchs and Förster, 2010; Hartmann et al., 2005, 2008; Homuth et al., 2008; Liu et al., 2011; Majorowicz et al., 2008; Mottaghy et al., 2005; Norden and Förster, 2006; Orilski et al., 2010; Popov et al., 1995, 2003, 2010, 2011; Schütz et al., 2012). It involved the measurement of TC under ambient temperature and pressure, which is in contrast to the other widely used method, the divided-bar technique (DB). This method obtains TC applying uniaxial pressure. Measurements under pressure have the advantage that micro cracks that may have originated from decompression and cooling as result of borehole drilling or rapid uplift, will get closed. The presence of micro cracks would cause underestimation of TC compared to an intact sample, whereby the rate of underestimation strongly depends on the type of saturation (air or water). Schärli and Rybach (1984) showed that because of micro cracks, the difference between dry and water-saturated TC in granitic rocks may be as high as 30%. For saturated metamorphic rocks (gneiss and amphibolite), the comparison of TC obtained by the DB and OS methods resulted in small discrepancies (AME: < 3%), although an axial load of 4 – 6 MPa was applied in the DB approach (Popov et al., 1999). An analog study for sedimentary rocks is missing. However, despite this circumstance we are confident that the approach of this paper, which is entirely based on OS results, is scientifically sound.

To perform the laboratory work economically, *i.e.*, studying large sample numbers in affordable time, measurements are usually performed in dry state, with air as the pore-saturating medium. Additional effort then is needed to convert these TCs to values typical for *e.g.*, aquifers with water as the pore-filling fluid or hydrocarbon reservoirs, in which the rock contains either water, oil, or gas, or a mixture

DOI: 10.2312/GFZ.b103-13111

of those. The calculation of the rock TC for different saturation fluids then requires the use of mixing models.

In general, those multi-component mixture models to describe the TC of a rock can be grouped in (1) well-defined physical (often referred as structural or theoretical) models and in (2) purely empirical or semi-empirical approaches. A third group of models is based on numerical simulations. Physical models may have a wider applicability (depending on the degree of simplification to obtain a solution), but their usability is often limited by the inclusion of empirically determined parameters, compositional variations, or structural aspects (*e.g.*, Popov et al., 2003; Schopper, 1991; Sugawara and Yoshizawa, 1961; Zimmerman, 1989; Schopper, 1991). Empirical models have the drawback that they are strictly valid for the particular rock suite being used for model development. Extensive overviews of TC models are provided by Tinga et al. (1973) and Progelhof et al. (1976) (for two-component mixtures) as well as by Abdulagatova et al. (2009).

Rather simple models, easily and comfortably applied, are based on a two-phase system of the rock comprising the solid mineral matrix and the pore space. Thus, if porosity and bulk TC of a sample are measured, a matrix TC can be inferred for the sample and in turn a bulk TC for another pore fluid with different TC calculated.

This paper provides a validity study of simple and usually used mixing models for a two-phase rock system involving (1) the layered medium model (series and parallel model corresponding to the arithmetic and harmonic means and the mean of both), (2) an empirical model not relying on any physical theory (the geometric mean), (3) the Hashin-Shtrikman mean, the upper and lower bounds of which provide tighter constraints than the arithmetic and harmonic means, and (4) the effective medium mean (based on the effective-medium theory). The selection of these models builds on results of Clauser (2009), who discussed the performance of these mixing models for a fixed matrix TC and a variable porosity, however without validating the results with measured laboratory TC.

It was examined, which of the selected mixing models best describes the TC of sedimentary rocks. The evaluation considers three different aspects: (1) lithotype, (2) pore content (air, water, or other saturating fluids), and (3) anisotropy. The statistical analysis of the deviations between laboratory-measured and calculated bulk TC data comprises 1147 single values obtained from 717 samples of sandstone, mudstone, limestone, and dolomite. As a result of this statistical analysis, the paper provides correction equations that yield an improved fit for some of the examined models. Finally, we present conversion equations that permit calculation of the water-saturated bulk TC from the dry-measured bulk TC for the case that porosity is known, *e.g.*, from petrophysical well logging. This approach has the advantage that a bulk TC could be inferred for a different saturating fluid without application of any mixing model.

3.2 *Previous comparison studies*

A verification of the different mathematical models, considering a solid and a pore volume, by comparison with real data has not yet been comprehensively performed. Most studies comparing between measured and calculated bulk TC values encompassed crystalline rocks.

Robertson and Peck (1974) compared bulk TC calculated from eleven theoretical mean models with TC values measured on 61 olivine-bearing basalt samples. None of the models showed a good agreement over the large range of porosity that the samples possessed (2–97%). The study showed on the one hand that a correction factor must be applied to the computed values to reduce the calculation error and on the other hand that the geometric-mean model belongs to those few approaches yielding the best, although unsatisfying, match. Horai (1991) reevaluated the data from Robertson and Peck (1974) and concluded that the mismatch in modeled and measured data is caused by errors introduced by the use of data from different measurement techniques.

More recently, Pribnow (1994) examined the four most widely used models (geometric mean, arithmetic mean, harmonic mean, and the Hashin-Shtrikman mean) for 85 water-saturated amphibolite and gneiss samples using the DB technique (Birch, 1950) and the line-source approach (Lewis et al., 1993). The geometric-mean model, together with the mean of the arithmetic and harmonic-mean models, provided the best fit.

Analog studies of the evaluated mean models focusing on sedimentary rocks are rare. Woodside and Messmer (1961*b*) used six sandstone samples to validate the geometric-mean model for consolidated rocks and recognized a good agreement between predicted and measured bulk TC. Hutt and Berg (1968) analyzed several mean models (arithmetic mean, harmonic mean, geometric mean, Bruggeman, Maxwell, Rayleigh, Archie) for 28 sandstone samples. They compared the calculated bulk TC (using the TC of minerals for calculating the matrix TC) with values measured with a needle probe. The harmonic mean showed a good fit, whereas the arithmetic and geometric-mean model overestimated the measured data. Buntebarth and Schopper (1998) explored various models for a suite of eleven sedimentary-rock samples saturated with different fluids (TC measurements with a needle probe). In their study, the application of the harmonic- and arithmetic-mean models resulted in a better fit relative to the geometric-mean model. Clauser (2006) compared TC data of various sedimentary lithotypes with theoretical model curves and graphically identified the closest approximation of measured (using the OS technique) and calculated values for the geometric-mean model, except for limy sandstones. Several authors (*e.g.*, Carson et al., 2005; Revil, 2000; Zimmerman, 1989) used the database of Woodside and Messmer (1961*b*) to test their own models for consolidated and unconsolidated rock. However, the number of data available for comparison was small and not comparable to the data set deployed in this study.

3.3 Methods applied

3.3.1 Models of two-phase systems

Calculation of the bulk TC (λ_b) of a two-component rock system involves the matrix TC (λ_m), the effective porosity (ϕ), and the TC of the pore content (λ_p).

DOI: 10.2312/GFZ.b103-13111

3.3.1.1 Geometric mean

The empirical geometric-mean model (GM), which went back to Lichtenecker (1924) and was evaluated first by Woodside and Messmer (1961*a*, 1961*b*) for consolidated sandstones and unconsolidated sands, represents the most usual approach. The empirical formula provides a relatively simple mathematical expression to calculate the bulk TC of a porous rock.

GM: $$\lambda_b = \lambda_m^{1-\phi} \cdot \lambda_p^{\phi} \tag{3-1}$$

3.3.1.2 Arithmetic and harmonic mean

Other frequently applied approaches comprise the arithmetic-mean (AM) and harmonic-mean (HM) models, which both are based on a sheet model representing a layered structure of phases, where the heat flow passes either parallel (AM) or perpendicular (HM) with respect to the plane boundaries. The two models are independent of the pore structure and constitute special cases (boundaries) of Wiener's mixing law (Wiener, 1912), which applies to both isotropic and anisotropic mixtures. The models were introduced by Voigt (1928) and Reuss (1929) to define the upper and lower TC boundaries.

AM: $$\lambda_b = (1-\phi) \cdot \lambda^m + \phi \cdot \lambda_p \tag{3-2}$$

HM: $$\lambda_b = \frac{1}{\frac{(1-\phi)}{\lambda_m} + \frac{\phi}{\lambda_p}} \tag{3-3}$$

3.3.1.3 Hashin-Shtrikman mean

The model of Hashin and Shtrikman (1962) (also referred as Maxwell–Eucken equations) is based on the theory of Maxwell (1892) and was extended by the work of Eucken (1940). It also uses upper (λ_{HS}^U; represents fluid − filled, spherical pores) and lower (λ_{HS}^L; represents grains suspended in a fluid) boundaries to calculate the TC of a two-phase system. The Hashin-Shtrikman bounds provide more restrictive narrower upper (Eq. 3-5) and lower bounds (Eq. 3-7) for isotropic mixtures, yet independent of the pore structure (Zimmerman, 1989). The mean of both bounds is often used as best approximation of rock bulk TC.

$$\lambda_{\mathrm{b}} = \frac{1}{2}\left(\lambda_{\mathrm{HS}}^{\mathrm{U}} + \lambda_{\mathrm{HS}}^{\mathrm{L}}\right) \tag{3-4}$$

$$\lambda_{HS}^U = \lambda_m + \phi \Big/ \left(\frac{1}{\lambda_p - \lambda_m} + \frac{1-\phi}{3\lambda_m}\right) \tag{3-5}$$

$$\lambda_{HS}^L = \lambda_p + (1-\phi) \Big/ \left(\frac{1}{\lambda_m - \lambda_p} + \frac{\phi}{3\lambda_p}\right) \tag{3-6}$$

Solving equation (3-5) for λ_m produces a quadratic equation requiring the quadratic formula for the solution, which leads to two results but only one produces the real value (Eq. 3-8).

$$\lambda_{\mathrm{m}} = \frac{1}{2}\left(\lambda_{m\,\mathrm{HS}}^{\mathrm{U}} + \lambda_{m\,\mathrm{HS}}^{\mathrm{L}}\right) \tag{3-7}$$

DOI: 10.2312/GFZ.b103-13111

$$\lambda_{m\,HS}^{U} = \frac{b+\sqrt{(b)^2+4\cdot ac}}{2\cdot a} \tag{3-8}$$

$$a = 2\cdot(\phi-1);\ b = \lambda_{HS}^{U}\cdot(2+\phi) - \lambda_p\cdot(1+2\phi);\ c = \lambda_{HS}^{U}\cdot\lambda_p\cdot(1-\phi)$$

$$\lambda_{m\,HS}^{L} = \frac{\lambda_p^2\cdot(2\phi)-\lambda_{HS}^{L}\cdot\lambda_p\cdot(3-\phi)}{\lambda_{HS}^{L}\cdot\phi+\lambda_p\cdot(2\phi-3)} \tag{3-9}$$

3.3.1.4 *Effective-medium theory mean*

To infer the TC for homogenous (isotropic) rocks, Bruggeman (1935) put forward the effective-medium theory (often referred as self-consistent medium approximation), which also uses the Lichtenecker (1924) formula. The effective-medium theory assumes different spherical inclusions embedded in a conducting host medium where all phases were mutually dispersed. This approach was further developed by Hanai (1968) and Sen et al. (1981) to the Bruggeman–Hanai–Sen equation for two-component systems. In this differential effective-medium theory the host phase percolates for the full range of fractions and the inclusions (second phase) may or may not conduct.

The effective-medium theory model is applicable to the determination of the TC of a multiphase system. Clauser (2009) transformed this equation to calculate the bulk TC for a two-component system (Eq. 3-10) consisting of pore fluid and rock matrix:

$$\lambda_b = \frac{1}{4}\left\{3\phi(\lambda_p-\lambda_m) + 2\lambda_m - \lambda_p + \sqrt{9\phi^2\lambda_m^2 + 18\phi\lambda_m\,\lambda_p - 18\phi^2\lambda_m\,\lambda_p - 12\phi\lambda_m^2 + \lambda_p^2 - 6\phi\lambda_p^2 + 4\lambda_m\,\lambda_p + 9\phi^2\lambda_p^2 + 4\lambda_m^2}\right\} \tag{3-10}$$

Equation (3-10) can be transposed to get matrix TC on its own (Eq. 3-11):

$$\lambda_m = \frac{\lambda_b\,(-2\cdot\lambda_b+3\cdot\phi\cdot\lambda_p-\lambda_p)}{\lambda_b(3\phi-2)-\lambda_p} \tag{3-11}$$

3.3.2 *Anisotropy of thermal conductivity*

The anisotropy of TC is a property that relates to the structure and texture of a rock, such as crystal anisotropy of the individual rock-forming minerals, intrinsic or structural anisotropy related to the shape of the grains and their textural arrangement, orientation and geometry of cracks, the spatial fracture distribution and other defects (Schön, 1996). For the quantification of anisotropy, TC is usually measured parallel ($\lambda_{||}$) and perpendicular ($\lambda_{\perp}$) to bedding or schistosity.

The anisotropy ratio (A) then is defined as:

$$A = \frac{\lambda_{||}}{\lambda_{\perp}} \tag{3-12}$$

3.3.3 *Methods of error calculation*

DOI: 10.2312/GFZ.b103-13111

To evaluate the reliability of the different mean models applied, the measured bulk TC is compared with the respective calculated bulk TC. For an individual sample, the deviation (E, in%) between calculated (λ_{cal}) and measured (λ_{mea}) TC is expressed as:

$$E = 100 \cdot \frac{|\lambda_{cal} - \lambda_{mea}|}{\lambda_{mea}} \tag{3-13}$$

For evaluating the different mean-model approaches, the arithmetic mean error (a) was used to compare the calculated and the measured bulk TC:

$$AME = \frac{1}{n}\sum_{i=1}^{n} E_i \tag{3-14}$$

where n is the number of samples in each lithotype group.

In the following, the error is noted as the AME complemented by the respective 1σ standard deviation (SD). The AME can be expressed also as root mean square error (RMS), which is a good measure of model accuracy, having the form:

$$RMS = \sqrt{\frac{\sum_{i=1}^{n} E_i^2}{n}} \tag{3-15}$$

The fit between predicted and measured data is statistically evaluated by regression analysis and the analysis of variances. The critical significance level α (mostly the statistical benchmark of 0.05), the observed significance level p, and the F-value constitute the key parameters for comparison (see Section 3.6.1).

3.4 *The database*

In total, 1147 TC measurements performed on 717 samples were evaluated. The database comprises four data sets from different sedimentary basins: (a) Mesozoic platform sediments of the northern Sinai Microplate in Israel (81 drillcore samples; Schütz et al., 2012), (b) the eastern part of the North German Basin [339 drillcore samples of the Mesozoic; Fuchs and Förster, 2010, 2013 (unpublished results); 129 drillcore samples of the Permo-Carboniferous; Norden and Förster, 2006]; and (c) the South German Scarplands and the Molasse Basin (168 drillcore and outcrop samples; Clauser et al., 2007). The studied samples encompass the following lithotypes: 137 limestone samples, 63 dolomite samples, 409 sandstone samples, and 108 mudstone (claystone + siltstone) samples. The TC data from these lithological subsets were scrutinized with respect to statistical distribution, and outliers (> 2σ SD) were omitted in additional analyses.

All these TC data have in common that they were obtained with the Thermal Conductivity Scanning (TCS) apparatus (Lippmann and Rauen, GbR Schaufling, Germany), which is based on the high-resolution OS method (Popov et al., 1999) The sample size correlated with the drill-core diameter, which varied between 5 and 10 cm. Sample thickness was variable, but exceeded the required minimal length of scanning lines of 4 cm. Measurements were performed on a flat sample surface displaying a roughness of < 1 mm. The error of determination was less than 3%.

DOI: 10.2312/GFZ.b103-13111

All samples were measured under ambient pressure and temperature, both dry (oven-dried at 60 °C) and water-saturated using distilled water. Determination of the anisotropy ratio of macroscopically isotropic samples involved TC measurement on the top/bottom of the cylindrical core and along the vertical core axis. For optically anisotropic samples, this ratio was calculated by measuring TC parallel and perpendicular to bedding (see Section 3.3.2). The effective porosity was quantified by the mass change between dry and water-saturated samples (Archimedes method). Because of clay-swelling effects, mudstones and argillaceous sandstones were saturated with isooctane (density: 0.698 x 10^3 kg m^{-3}; Budavari, 1989) instead of water to determine their porosity. TC values of 0.025 W/(m·K) for air (Gröber et al., 1955), 0.095 W/(m·K) for isooctane (Watanabe, 2003), and 0.604 W/(m·K) (Lemmon et al., 2005) for distilled water were used in the calculations.

Figure 3-1 provides a compilation of measured bulk TC and effective porosity for the four lithotypes. The rocks covered a large range in effective porosity, from almost zero to about 30%. The carbonate rocks are usually less porous relative to the clastic rocks. Eighty percent of the entire data population of carbonates fall in the porosity range 1–13%, in contrast to 3–28% encompassed by the clastic rocks. As to the measured bulk TC, the sample suite spans the interval between 1.0 and 6.5 W/(m·K). The larger variability in TC observed for sandstone [3.8 ± 0.7 W/(m·K)], mudstone [2.5 ± 0.7 W/(m·K)], and dolomite [3.3 ± 0.7 W/(m·K)] relative to limestone [2.6 ± 0.3 W/(m·K)] is a reflection of their greater heterogeneity in terms of modal mineralogy.

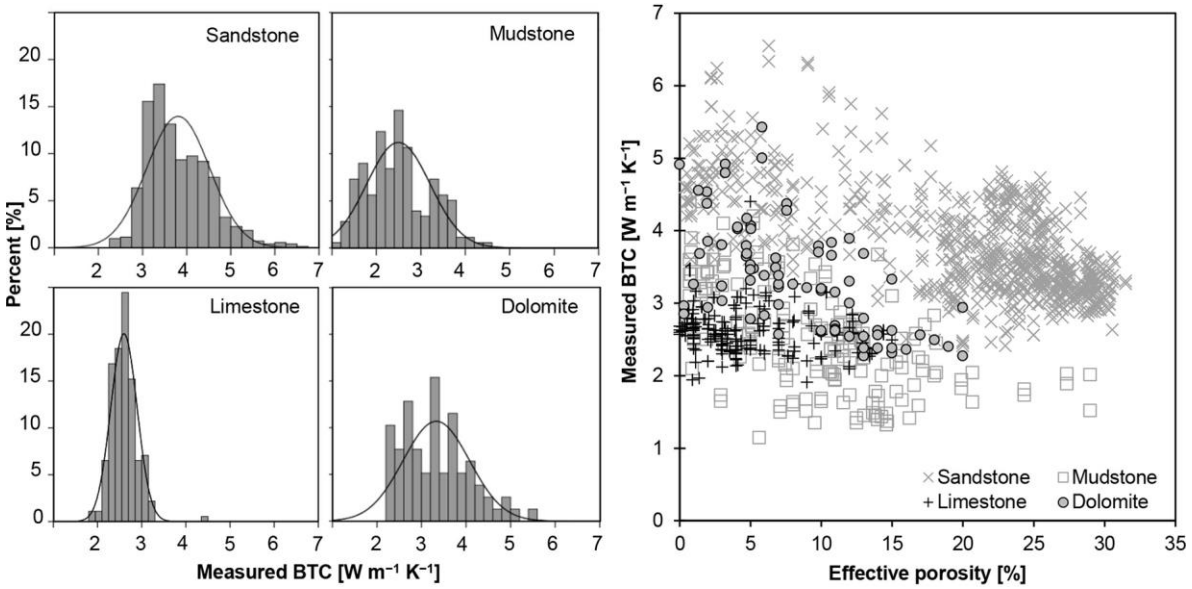

Figure 3-1 Left: Histograms of the measured bulk TC of different lithotypes. Right: Effective porosity vs. measured bulk TC (both water and isooctane-saturated) of the clastic and carbonate samples from this study.

3.5 *Results*

The matrix TC was calculated from measured dry and saturated values for arithmetic, harmonic, and geometric means using equations (3-1), (3-2) and (3-3) transposed to λ_m. Equations (3-7) and (3-11) were applied for the Hashin–Shtrikman and the effective medium means, respectively. Water-saturated

bulk TC for the various mixing models were subsequently calculated from equations (3-1) – (3-4) and (3-10). The bulk TC results are shown as scatter plots for the six models (Fig. 3-2). Figure 3-3 illustrates the influence of different saturation fluids (water and isooctane) on bulk TC.

3.5.1 *General model fit*

A regression analysis was performed to ascertain the model with the highest coefficient of determination (R^2). The results show that most of the evaluated mixing models predict the measured bulk TC unsatisfactorily. The highest value of R^2 is related to the geometric mean (R^2 = 0.62, F ~ 1348).

Significantly poorer fits are observed for the arithmetic mean (R^2 = 0.37, F ~ 600), followed by the effective medium mean (R^2 < 0.24, F ~ 321) and Hashin-Shtrikman mean (R^2 = 0.23, F ~ 298). The harmonic mean (R^2 < 0.01, F = 1.56) as well as the mean of arithmetic and harmonic mean (R^2 = 0.01, F = 9.01) show even lower coefficients of determination. If the value obtained for F is equal to or larger than the critical F-value, then the null hypothesis (H_0: $\mu_1 = \mu_2$) is rejected, and the result is significant at the chosen level of probability (α = 0.05). This critical value is assumed to be F_{crit} (1/1017) = 3.85.

Fig. 3-2 shows the comparison between measured and calculated bulk TC for the different models. The arithmetic mean (Fig. 3-2a) tends to underestimate bulk TC in particular for clastic sediments (AME: 33 ± 20%), but yields an acceptable fit for carbonate samples (deviation 11 ± 20%). The harmonic mean (Fig. 3-2b) consistently underestimates bulk TC and, with respect to the insignificant regression relation, is excluded from further discussion. This poor match also holds for the mean of arithmetic and harmonic means (Fig. 3-2c). The geometric mean (Fig. 3-2d) shows a reasonably good fit for both carbonate (AME: 6 ± 10%) and clastic (AME: 5 ± 17%) rocks. It tends to slightly overestimate bulk TC, but 80% of the samples show deviations ≤ 20%.

The Hashin-Shtrikman mean (Fig. 3-2e) shows an acceptable fit for carbonate (AME: 19 ± 13%), but a poor fit for clastic rocks (AME: 51 ± 18%).Its overall distribution pattern largely corresponds to those of the arithmetic and effective medium means (Fig. 3-2f). Because these three models provided virtually the same goodness-of-fit (ANOVA, Tukey's HSD, α = 0.05, n = 1,019), the effective medium mean could be eliminated from further analysis.

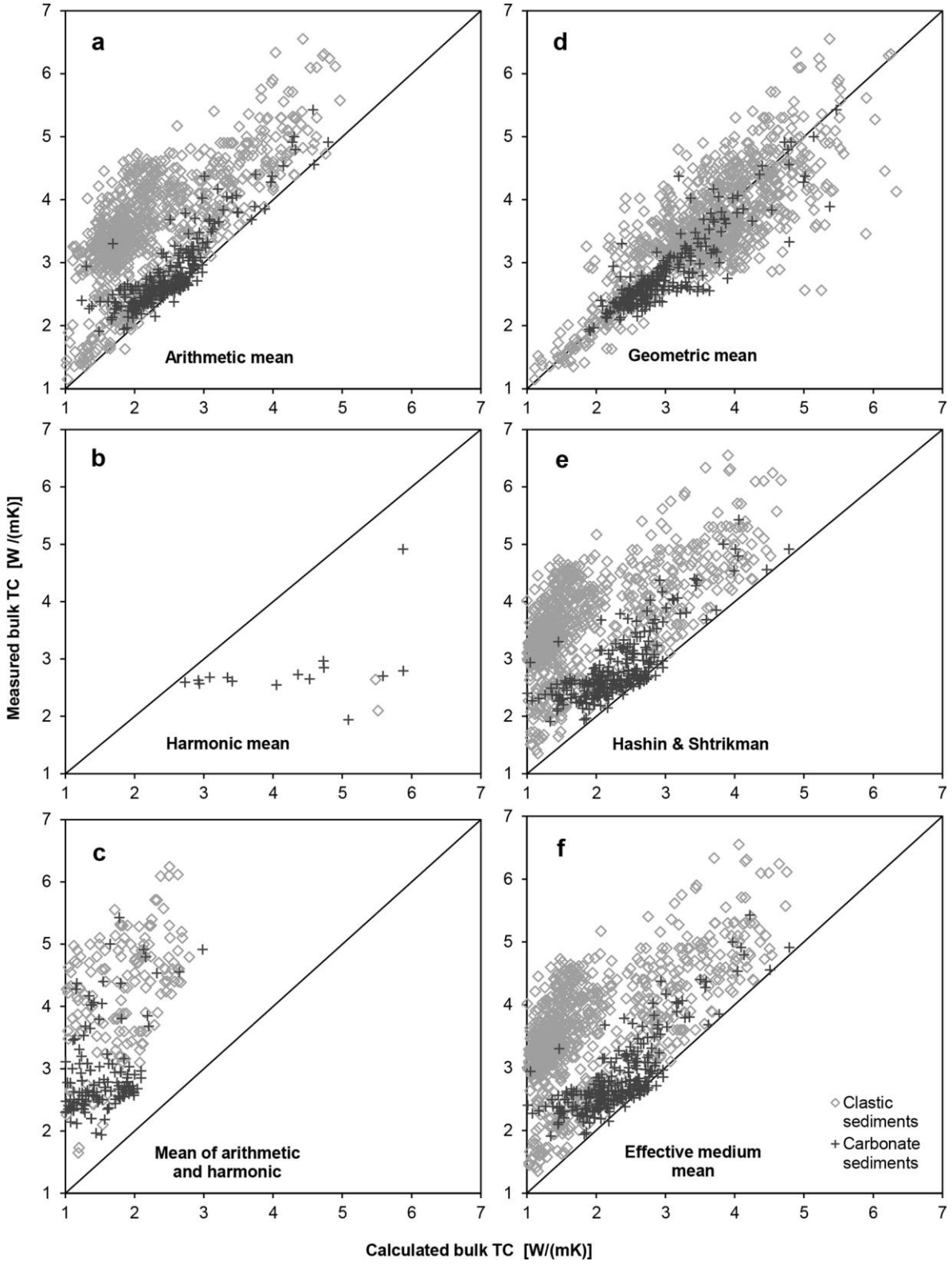

Figure 3-2 Scatter plots of measured vs. calculated water-saturated bulk TC for clastic (n = 885) and carbonate sediments (n = 262).

DOI: 10.2312/GFZ.b103-13111

3.5.2 *Anisotropy of thermal conductivity*

The vast majority of rock samples possess anisotropy ratios between 0.8 and 1.2 (Fig. 3-3). Whereas the carbonate rocks and most sandstone samples are largely isotropic (mean anisotropy ratio = 1.01 ± 0.05 and 0.97 ± 0.08, respectively), many mudstone samples are anisotropic, exposing a mean anisotropy ratio of 1.11 ± 0.19.

Rock samples showing an anisotropy > 5% (n = 424) are evaluated in terms of a possible impact that anisotropy has on the mixing model that should be selected for calculation. A paired *t*-test was made to compare the average deviations of the predicted bulk TC with the bulk TC measured parallel and perpendicular to bedding.

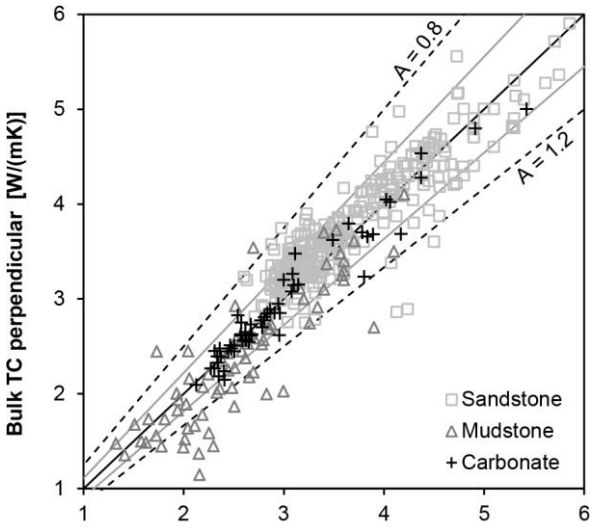

Figure 3-3 Scatter plot of measured water-saturated bulk TC parallel and perpendicular. See text for explanation.

Because the arithmetic-mean model is based on a sheet model with the heat flowing parallel to the components, it seemed reasonable to assume that this model will better fit the bulk TC parallel than perpendicular to bedding (harmonic mean) as well as those models that refer to isotropic media (the geometric and the Hashin-Shtrikman means).

However, the expectations are not met. For data referring to measurements parallel to bedding, the arithmetic-mean model provides the same poor fit as for data related to measurements performed in the opposite direction (paired *t*-test, n = 128, α = 0.01, p = 0.425). As to the geometric and Hashin-Shtrikman means, the results are in line with the theoretical background that the goodness-of-fit is basically the same for isotropic or anisotropic rocks.

3.5.3 *Saturating fluid*

The correlation between measured and calculated bulk TC of samples saturated with water or isooctane is displayed in Fig. 3-4. For the range where measured TC values are available, the goodness-of-fit for samples saturated with isooctane is basically the same as for samples saturated with water. Accordingly, both the arithmetic and Hashin-Shtrikman means seriously underestimate bulk TC also for samples saturated with isooctane. For this saturation fluid, the geometric mean again shows the best fit (AME: 6 ± 6%).

3.5.4 *Impact of lithotype*

Figure 3-5 shows the model-based relations between measured and calculated bulk TC for the different lithotype groups. For sandstones (Fig. 3-5a), only the geometric mean shows an acceptable fit (AME: 13 ± 11%), whereas the arithmetic and the Hashin-Shtrikman means strongly underestimate the bulk TC (AME: 41 ± 14% and 53 ± 16%, respectively). For limestones (Fig. 3-5b), the fit for the geometric and the arithmetic means is reasonably good (AME: 6 ± 5% and 8 ± 6%) and still acceptable for the Hashin-Shtrikman mean (AME: 12 ± 9%).

For mudstones (Fig. 3-5c), the geometric mean is the only approach resulting in a good fit. Both the arithmetic (AME: 14 ± 9%) and the Hashin-Shtrikman means (AME: 20 ± 12%) again underestimate the bulk TC, but less significantly. For dolomite, none of the models gave rise to a fit evaluated as good. An acceptable fit was obtained upon utilization of the geometric and arithmetic means (AME: 12 ± 11% and 16 ± 12%, respectively).

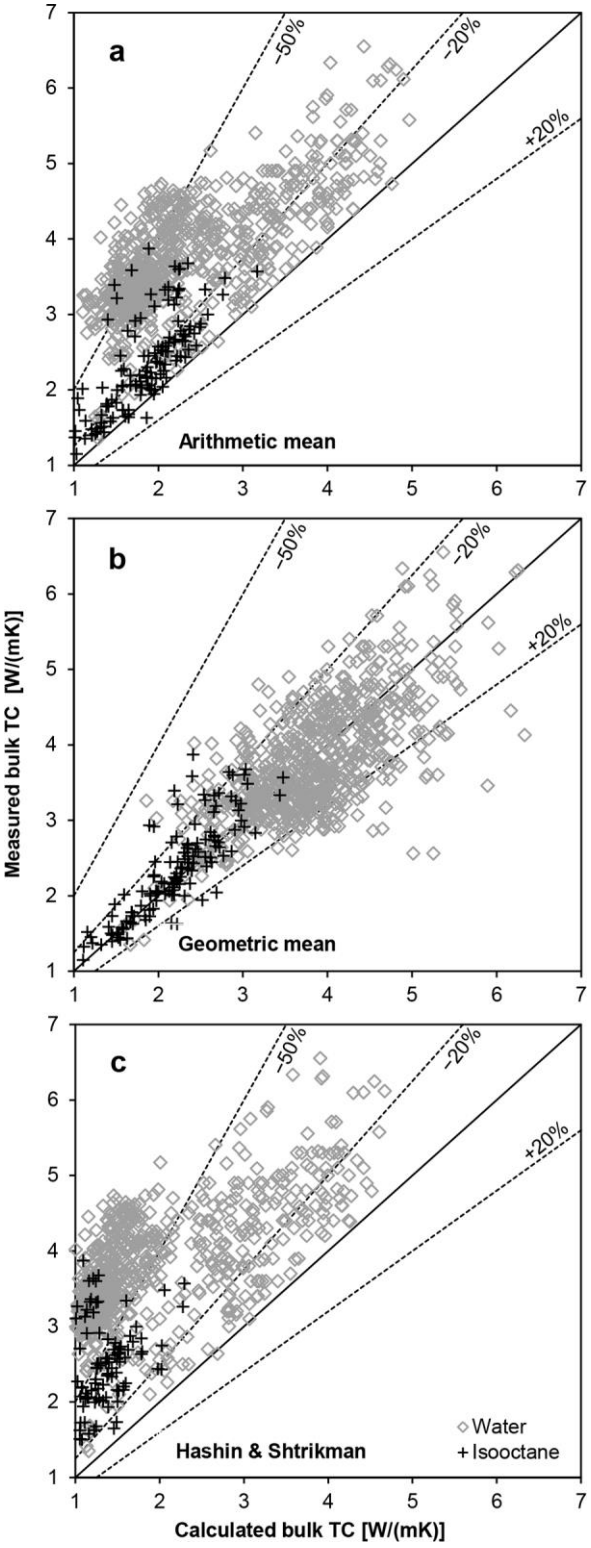

Figure 3-4 Plots of measured bulk TC versus calculated bulk TC for water-saturated (n = 757) and isooctane-saturated (n = 128).

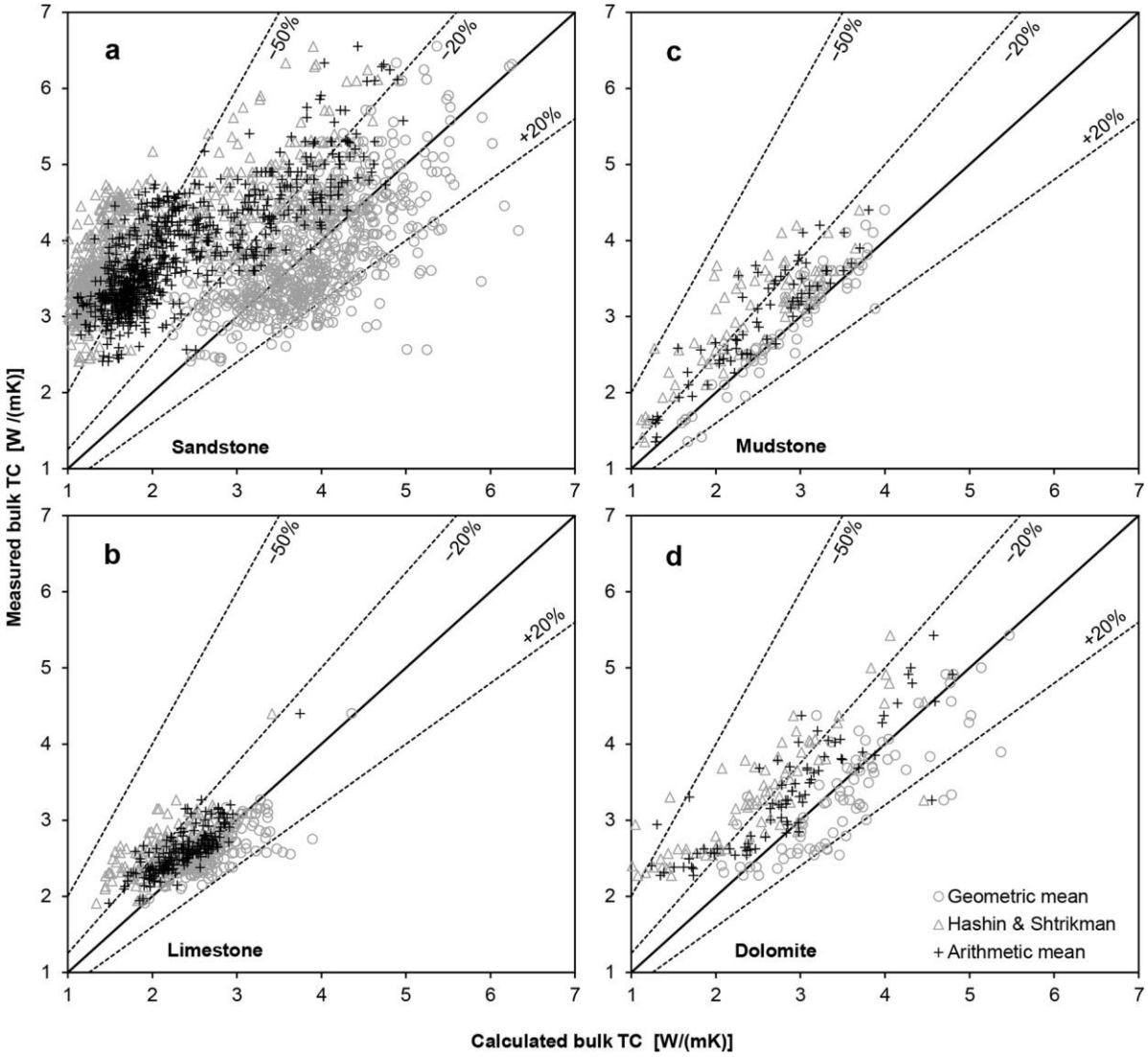

Figure 3-5 Calculated bulk TC (water-saturated) based on different mixing models compared to measured bulk TC for different lithotypes

3.6 Discussion

3.6.1 General model fit, anisotropy, and saturating fluid

The various mixing models evaluated in this study approximate measured bulk TC data in different, however mostly unsatisfying quality. Only the geometric mean consistently shows a good fit, with the bulk of calculated data deviating less than ± 20% from measured bulk TC (Fig. 3-5). Considering the entire sample suite, the deviation averages between 11% (geometric mean) to 31% (arithmetic mean) and 42% (Hashin-Shtrikman mean). Only examining the lithotype, the deviation varies between 5.7% and 13% (geometric mean), 7.6% and 40% (arithmetic mean), and 12% and 53% (Hashin-Shtrikman mean). These results are in line with observations reported by Pribnow (1994) and Buntebarth and

DOI: 10.2312/GFZ.b103-13111

Schopper (1998). The latter authors rated the geometric-mean model as best solution for situations, in which no additional criterion (*e.g.*, an empirical alpha-value describing the pore structure of the rock) is considered.

Calculation of bulk TC with the harmonic mean (Eq. 3-3) results in abnormal values (Fig. 3-2). More than 96% of the calculated bulk TC values are negative. This misfit, which was already recognized, for instance, by Beck and Beck (1965), Robertson and Peck (1974), and Pribnow (1994), can be attributed to the equation for calculating the matrix TC which allows the denominator to get zero or negative. Especially high porosities almost inevitably cause a negative denominator. Hence, this model is unfeasible and, with it, also the mean of the harmonic and arithmetic mean.

The goodness-of-fit and the effective porosity are antipathetically related also for the other models. This observation is linked with the mathematical formalisms of bulk TC calculation, causing greater uncertainties with increasing porosity.

For rocks with anisotropies > 5%, the arithmetic-mean model did not show the expected co relation with the direction of measurement (*i.e.*, the fit between measured and calculated TC should be better for data acquired parallel to bedding). The observations made in this study are just in opposition to this expectation and may question the physical concept of this model. This criticism is in line with earlier observations (*e.g.,* Zimmerman, 1989) and implies that a body (rock) consisting of alternating slabs of matrix and pore space is physically unrealistic, at least for clastic sediments. The arithmetic-mean model, however, may apply for fractured aquifers in carbonate rocks in the situation of a layered fracture pattern. Moreover, because the bulk of our samples are only weakly anisotropic, the results of this study strictly apply only to rocks with anisotropies ≤ 20%. More strongly anisotropic rocks may fit the arithmetic-mean model better.

The use of isooctane (Fig. 3 - 4) has no statistically discernible impact on the quality of fit for either model (independent *t*-test, $\alpha = 0.05$, $p > 0.1$). The lower TC of isooctane compared to water and, hence, the much smaller ratio between the TC of saturating fluid and air (factor ~ 3 for isooctane compared to factor ~ 24 for water) does not result in larger deviations between measured and predicted bulk TC, as one might expect. This observation is in contradiction to results of Buntebarth and Schopper (1998), who showed that the type of saturating fluid had a strong influence on the fitting of the geometric mean. These authors identified an acceptable fit for the geometric mean only for sandstone samples that were water-saturated (n = 11). More work is needed to explain this discrepancy.

The re-calculation of isooctane-saturated bulk TC to water-saturated bulk TC is afflicted with several uncertainties. Therefore, saturation with water should be preferred to isooctane saturation in determining bulk TC. The use of isooctane or other alkanes, such as n-heptane utilized by Woodside and Messmer (1961*b*) and Zimmerman (1989), is an expedient alternative only for determining the porosity of argillaceous rocks.

In the special situation of handling bulk TC measured with different saturation fluids (air, water, n-heptane), we recommend averaging the respective matrix values. This recommendation is rooted in the observation of a significant difference in matrix TC calculated from dry-measured bulk TC (lower by 5.2%) compared to the matrix value calculated from isooctane-saturated bulk TC (paired t-test, n = 127,

DOI: 10.2312/GFZ.b103-13111

α = 0.05, p < 0.000). A difference also is observed, but with an opposite trend, between matrix TC calculated from dry-measured bulk TC (higher by 4.9%) compared to the matrix value calculated from water-saturated bulk TC (paired *t*-test, n = 1 019, α = 0.05, p < 0.000).

3.6.2 *Correction charts*

The only mixing model that generally reproduces the measured bulk TC satisfactorily is the geometric mean, but the data scatter is still large. The other mean models examined in this paper produce TC data often significantly deviating from measured values. The question arises whether it is possible to calculate correction charts that permit reduction of the deviation and the scatter of the different mean models. In order to verify this idea, the relations between absolute deviation [in W/(m·K)] and porosity for the different lithotypes and mean models (Fig. 3-6a–d) are investigated. For this purpose, the data set is subdivided into porosity (%) classes: 0–3; 3–6; 6–10; 10–15; 15–20; 20–25; 25–30; 30–35 (Fig. 3-6e–h). The mean deviation within each porosity class is the input parameter for the regression analyses. The statistical treatment resulted in linear or logarithmic trend lines and respective equations, which in turn provided the correction values for every mean model and lithotype. For statistical reason, the initial data set was randomized into two groups. The first group (85% of data) is the regression set, from which the equations were derived; the second group (15% of data) is the testing set, from which the fitting parameters were calculated. The inversion of the curves shown in Fig. 3-6e–h gives the correction value [in W/(m·K)] for sandstone, mudstone, limestone, and dolomite, calculated by the arithmetic or geometric means.

Table 3-1 is a compilation of the computed regression parameters for the various lithotypes and mean models. The correlation coefficients for the different groups scatter between 0.76 and 0.99, indicating a remarkably good degree of tracking. The only lithotype, for which the linear regression did not result in a satisfying improvement of the fit, is dolomite, with a quiet poor correlation coefficient of 0.43 for the geometric mean. The possible reason for this unsatisfying result is the fact that in our suite of dolomite rocks, the number of samples and the TC deviations in each porosity class are highly variable and, consequently, the calculated averages of deviation display larger uncertainties.

Table 3-1 Coefficients of determination for correction charts shown in Fig. 3-6 (right panel).

	Mean Model[1]	Regression Parameter[2]					Mean Model[1]	Regression Parameter[2]			
		Type	b_0	b_1	R^2			Type	b_0	b_1	R^2
	Sandstone						*Limestone*				
A	GM	linear	0.504	-3.039	0.927	G	GM	linear	0.059	-3.833	0.967
B	AM	ln	2.091	0.340	0.887	H	AM	ln	0.820	0.178	0.986
C	H&S	ln	2.779	0.461	0.922	I	H&S	ln	1.378	0.301	0.976
	Mudstone						*Dolomite*				
D	GM	linear	0.208	-3.261	0.757	J	GM	linear	-0.104	-1.648	0.436
E	AM	ln	1.003	0.179	0.871	K	AM	ln	1.329	0.293	0.781
F	H&S	ln	1.502	0.282	0.941	L	H&S	ln	1.869	0.388	0.909

[1] GM: Geometric mean; AM: Arithmetic mean; H&S: Hashin-Shtrikman mean. [2] b_0 and b_1 are constants for regression model. Linear (linear) equation is $y = b_1x + b_0$, logarithm equation (ln) is $y = b_1 \ln(x) + b_0$, where y is the calculated correction value and x is the given porosity value. Letters A-L in the first column are equal to those from Fig. 3-6.

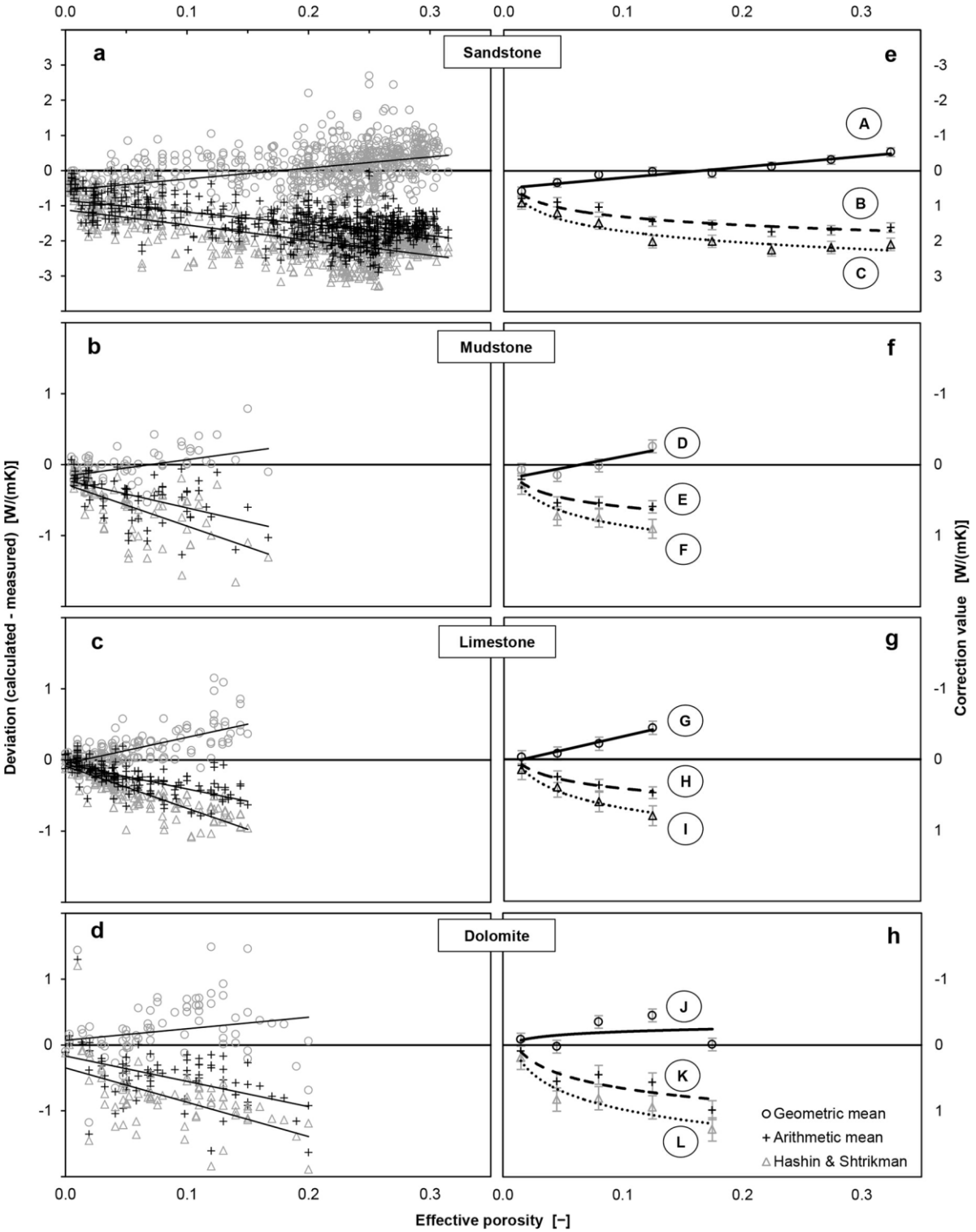

Figure 3-6 Variations between calculated and measured bulk TC values (a – d) and derived correction values (e – h) for different lithotypes and mixing models, respectively. Regression coefficients and RMS values for A–L are listed in Table 3-1.

The impact of implementing these correction coefficients in the calculation of bulk TC is shown in Fig. 3-7a and b, separately for every model and lithotype. The application of the correction results in noticeable improvements of the fits for all mean models, on average reducing the deviations for the Hashin-Shtrikman equation by 70%, for the arithmetic mean by 59%, and for the geometric mean by another 15%.

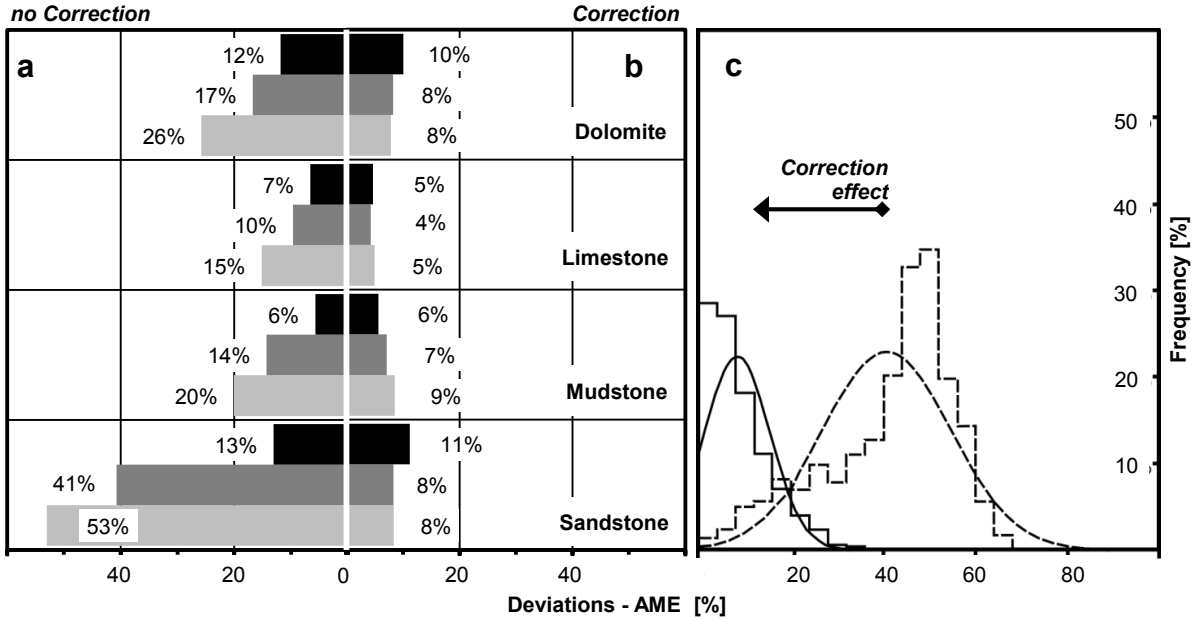

Figure 3-7 Left: Comparison of corrected (b) (Fig. 3–6 and Table 3–1) and uncorrected (a) calculations. Black bar: geometric mean; dark gray bar: arithmetic mean; light gray bar: Hashin-Shtrikman mean. Right: Distribution of percent errors (c) for corrected (solid line) and uncorrected (dashed line) values for sandstones calculated with the arithmetic mean.

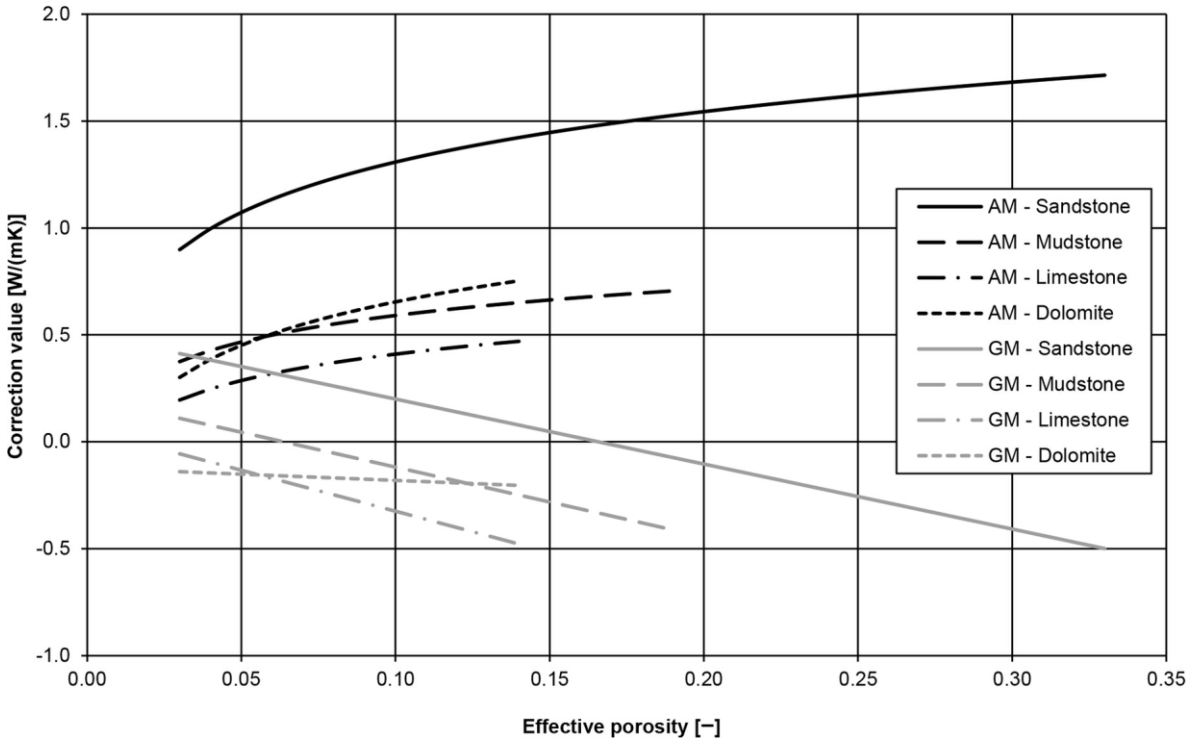

Figure 3-8 Correction values for bulk TC calculation from dry measurements for sedimentary rocks. Arithmetic mean (AM): black lines, geometric mean (GM): gray lines.

3.6.3 Conversion equations

This improvement is exemplarily shown for the arithmetic mean used for bulk TC calculation of sandstone samples (Fig. 3-7c), exposing a smaller mean deviation and variance. In order to improve the applicability of the correction chart, mean deviations were converted to user-friendly correction values (Fig. 3-8). Those porosity-dependent correction values either have to be added to or subtracted from (depending on the algebraic sign) the original mixing-model results.

The unsatisfying fitting behavior of most mean models and the necessity of applying correction charts encouraged us to examine our data set in whether is it possible to set up an equation that permits estimation of the water-saturated bulk TC directly from dry-measured bulk TC data and known porosity values.

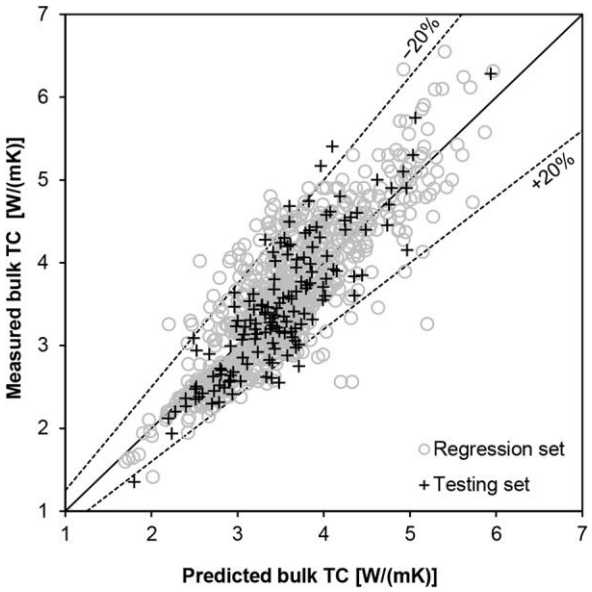

Figure 3-9 Scatter plot of predicted (conversion equation based on multiple regression analyses) vs. measured water-saturated bulk TC.

For this goal, the data set was tested using a multiple regression analysis. The fitting result of this type of analysis is shown in Fig. 3-9. For statistical reasons, the initial data set was randomized into two groups of 85% (regression set) and 15% (testing set). The plot of measured versus predicted bulk TC shows a good fit for both the regression and the testing sets, with a deviation of 10 ± 8% (AME) for the testing set.

Table 3-2 Results of multiple regression analyses of dry and saturated-measured bulk TC and effective porosity, respectively.

Samples	Regression Parameter			R^2	ANOVA			AME
	b_0	b_1	b_2		F	n	p	
All	-0.406	7.417	1.216	0.726	1348.0	740/130	< 0.001	10.2 ± 7.8%
Sandstone	1.579	2.244	0.817	0.667	581.4	494/ 87	< 0.001	8.7 ± 7.2%
Mudstone	-0.696	8.446	1.290	0.895	243.9	51/ 8	< 0.001	8.3 ± 7.7%
Limestone	0.272	3.961	0.914	0.758	243.2	134/ 23	< 0.001	4.8 ± 4.3%
Dolomite	0.631	2.527	0.890	0.779	119.6	60/ 10	< 0.001	6.5 ± 9.0%

b_0, b_1 and b_2 are constants for the multiple regression models. Equation is $y = b_1x + b_2z + b_0$, where y is the calculated bulk TC, x is the given porosity value and z is the dry bulk TC. R^2, coefficient of determination; F, F-value; n, number of samples (first value, regression set; second value, testing set); p, observed significance level; AME, arithmetic mean error ± 1 standard deviation for testing group.

The coefficients of determination resulting from the multiple regression analysis are listed in Table 3-2 for the entire sample set and, additionally, for the various lithotypes. All listed equations display an AME equal or less than 10%. If the lithotype is sufficiently well known, we recommend application of the equations elaborated for mudstone, limestone, and dolomite instead of the one based on the entire set of samples, because the specific equations exhibit significantly lower AMEs (ANOVA, Tukey's HSD, $\alpha = 0.05$).

Table 3-3 finally compares the errors after applying correction charts to the various mean models with the errors resulting from utilizing the new conversion equations. Considering all samples, the implementation of correction charts resulted in the smallest error for the arithmetic mean.

If lithotypes are concerned, the fit of all these approaches is good for every mixing model, except for the geometric mean applied to sandstone. This misfit is a consequence of the high porosity of the sandstone samples (19.8 ± 8.8%), combined with the mathematical structure of the geometric mean. For all lithotypes, both the correction equations for the mean models and the conversion equations yield to uncertainties in the bulk TC ranging between 5% and 10% (AME). These uncertainties are significantly better than those arising from application of the mean models without correction (range of AME: 11 – 42%).

Table 3-3 Bulk TC mean errors as from correction equations and direct conversion equations.

Samples	Correction Equations			Conversion Equations
	AM	GM	H&S	
All	7.4 ± 6.9%	9.5 ± 9.5%	7.6 ± 7.0%	10.2 ± 7.8%
Sandstone	8.3 ± 7.2%	11.0 ± 10.2%	8.4 ± 7.2%	8.7 ± 7.2%
Mudstone	7.1 ± 7.3%	5.7 ± 4.9%	8.5 ± 9.1%	8.3 ± 7.7%
Limestone	3.9 ± 3.7%	4.6 ± 4.5%	4.4 ± 4.0%	4.8 ± 4.3%
Dolomite	8.0 ± 7.4%	10.0 ± 9.5%	7.6 ± 7.1%	6.5 ± 9.0%

GM: Geometric mean; AM: Arithmetic mean; H&S: Hashin-Shtrikman mean.

3.7 Conclusions

In both the general geothermal characterization of sedimentary basins, including the assessment of geothermal reservoirs, as well as the modeling of other potential resources, for example oil and gas, the implementation of large numbers of bulk TC data is required. In the light of the time-extensive effort necessary to determine water-saturated TC for such large sample sets, methods are requested to reduce the work load. The mean models for bulk TC of two-phase rocks presented and evaluated in this study constitute efficient tools to transfer air-saturated bulk TC to water-saturated bulk TC, if porosity is known from independent sources (*e.g.*, derived from standard well logs). If a correction equation (see Section 3.6.2) is applied to the mean model result, the errors in water-saturated bulk TC can be reduced to 4–11%, depending on lithotype. In turn, the application of model-independent conversion

equations (reported in Section 3.6.3) allows a general reduction of the error to < 10%. This accuracy is sufficient for many industrial as well as specific scientific applications.

The more sophisticated physical rock models, that are advanced effective-medium theory models, require knowledge of additional rock parameters that are not readily available. Acquisition of such additional parameters (for instance, distribution and size of grains and pores) is labor-intensive and requires special analytical equipment's. Therefore, such models are suitable for basic research, but are unlikely to be routinely used in exploration studies.

It remains to be investigated whether the TC measuring technique, on which the data evaluated in this study are based and which do not apply pressure to the sample, eventually underestimates the measured TC, and whether these effects are statistically relevant to alter the equations and correction charts developed in this study. In addition, laboratory studies are required to eliminate the ambiguity in pressure dependency of TC in the range < 10 MPa. This would also shed light on the reasoning of the small deviation between DB and OS values recognized by Popov et al. (1999), implying a pressure dependency of TC that is much smaller than reported by other authors (*e.g.*, Buntebarth, 1991; Hurtig and Brugger, 1970; Kukkonen et al., 1999; Somerton et al., 1963; Walsh and Decker, 1966). Unless those ambiguities are overcome, we consider our results as universal for application for isotropic to weakly anisotropic sedimentary rocks.

3.8 Acknowledgments

The authors would like to thank Ilmo T. Kukkonen, an anonymous reviewer, editor-in-chief A. Ghassemi, and Daniel F. Merriam for constructive comments and suggestions which helped to improve the paper.

3.9 References

Abdulagatova, Z.Z., Abdulagatov, I.M., Emirov, S.N. (2009). Effect of temperature and pressure on the thermal conductivity of sandstone. *International Journal of Rock Mechanics and Mining Sciences* 46(6), 1055–1071.

Balling, N., Kristiansen, J., Breiner, N., Poulsen, K.D., Rasmusen, R., Saxov, S. (1981). Geothermal measurements and subsurface temperature modelling in Denmark. *Geologiske Skrifter*, vol. 16, Department of Geology Århus University, 172 pp.

Beck, A.E. (1988). Methods for determining thermal conductivity and thermal diffusivity. *In:* Haenel, R., Rybach, L., Stegena, L. (Eds.), Handbook of Terrestrial Heat-Flow Density Determination. Dordrecht, Netherlands, Kluwer Academic Publishers, pp. 87–124.

Beck, J.M., Beck, A.E. (1965). Computing thermal conductivities of rocks from chips and conventional specimens. *Journal of Geophysical Research* 70(20), 5227–5239.

Birch, F. (1950). Flow of heat in the Front Range – Colorado. *Bulletin of the Geological Society America* 61(6), 567–630.

Blackwell, D.D., Steele, J.L. (1989). Thermal conductivity of sedimentary rocks: measurement and significance. *In:* Naeser, N.D. and McCulloh, T.H. (Eds.), Thermal History of Sedimentary Basins, Methods and Case Histories, Springer, New York, pp. 13–35.

Brailsford, A.D., Major, K.G. (1964). The thermal conductivity of aggregates of several phases, including porous material. *British Journal of Applied Physics* 15, 313–319.

Brigaud, F., Chapman, D.S., Le Douran, S. (1990). Estimating thermal conductivity in sedimentary basins using lithological data and geophysical well logs. *AAPG Bulletin* 74, 1459–1477.

Bruggeman, D.A.G., 1935. Berechnung verschiedener Konstanten von heterogenen Substanzen – I. Dielektrizitätskonstanten und Leitfähigkeiten der Mischkörper aus isotropen Substanzen. *Annalen der Physik* 24, 636–679.

Budavari, S. (1989). The Merck Index - Encyclopedia of Chemicals, Drugs and Biologicals. Merck and Co., Inc., Rahway, New Jersey, 817 pp.

Buntebarth, G. (1991). Thermal properties of KTB Oberpfalz VB core samples at elevated temperature and pressure. *Scientific Drilling* 2, 73–80.

Buntebarth, G., Schopper, J.R. (1998). Experimental and theoretical investigations on the influence of fluids, solids and interactions between them on thermal properties of porous rocks. *Physics and Chemistry of the Earth* 23, 1141–1146.

Carson, J.K., Lovatt, S.J., Tanner, D.J., Cleland, A.C. (2005). Thermal conductivity bounds for isotropic, porous materials. *International Journal of Heat and Mass Transfer* 48, 2150–2158.

Clauser, C. (2006). Geothermal Energy. *In:* Heinloth, K. (Eds.), Landolt-Börnstein, Group VIII Advanced Materials and Technologies, vol. 3, Subvol. C: Renewable Energies, Springer Verlag, Heidelberg/Berlin, pp. 480-604.

Clauser, C. (2009). Heat transport processes in the earth's crust. *Surveys in Geophysics* 30, 163–191.

Clauser, C., Hartmann, A., Koch, A., Mottaghy, D., Pechnig, R., Rath V. (2007). Erstellung statistisch abgesicherter thermischer und hydraulischer Gesteinseigenschaften für den flachen und tiefen Untergrund in Deutschland, Phase 1 – Westliche Molasse und nördlich angrenzendes Süddeutsches Schichtstufenland. Final report for BMU-Project FKZ 0329985, RWTH Aachen, http://www.eonerc.rwth-achen.de/aw/cms/website/zielgruppen/gge/research_gge/geothermik/~vfa/Erstellung_statistisch_abgesicherter_thermischer/?lang=de, (last accessed: 07.03.2013).

Demongodin, L., Pinoteau, B., Vasseur, G., Gable, R. (1991). Thermal conductivity and well logs: a case study in the Paris Basin. *Geophysical Journal International* 105, 675–691.

Eucken, A. (1940). Allgemeine Gesetzmäßigkeiten für das Wärmeleitvermögen verschiedener Stoffarten und Aggregatzustände. *Forschung auf dem Gebiete des Ingenieurwesens*, Ausgabe A, 11(1), 6–20.

Fuchs, S., Förster, A. (2010). Rock thermal conductivity of Mesozoic geothermal aquifers in the Northeast German Basin. *Chemie der Erde* 70(Supplement 3), 13–22.

Goss, R.D., Combs, J. (1976). Thermal Conductivity Measurement and Prediction from Geophysical Well Log Parameters with Borehole Application. Institute for Geosciences, University of Texas at Dallas, Dallas, pp. 1019–1027.

Goutorbe, B., Lucazeau, F., Bonneville, A. (2006). Using neural networks to predict thermal conductivity from geophysical well logs. *Geophysical Journal International* 166, 115–125.

Gröber, H., Erk, S., Grigull, U. (1955). Die Grundgesetze der Wärmeübertragung. 2nd ed., Springer, Berlin, Wien, Heidelberg, 465 pp.

Hanai, T. (1968). Electrical properties of emulstons. *In:* Sherman, P. (Ed.), Emulsion Science, New York, Academic Press, pp. 354–477.

Hartmann, A., Rath, V., Clauser, C. (2005). Thermal conductivity from core and well log data. *International Journal of Rock Mechanics and Mining Sciences* 42, 1042–1055.

Hartmann, A., Pechnig, R., Clauser, C. (2008). Petrophysical analysis of regional-scale thermal properties for improved simulations of geothermal installations and basin-scale heat and fluid flow. *International Journal of Earth Sciences* 97, 421–433.

Hashin, Z., Shtrikman, S. (1962). A variational approach to the theory of the effective magnetic permeability of multiphase materials. *Journal of Applied Physics* 33, 3125–3131.

He, L., Hu, S., Huang, S, Yang, W., Wang, J., Yuan, Y., Yang, S. (2008). Heat flow study at the Chinese Continental Scientific Drilling site: borehole temperature, thermal conductivity, and radiogenic heat production, *Journal of Geophysical Research*, 113 (B02404), *http://dx.doi.org/10.1029/2007JB004958*.

Homuth, S., Sass, I., Hamm, K., Rumohr, S. (2008). In-Situ-Messungen zur Bestimmung geothermischer Untergrundkennwerte. *Grundwasser* 13(4), 241–251.

Horai, K.-I. (1991). Thermal conductivity of Hawaiian basalt: a new interpretation of Robertson and Peck's data. *Journal of Geophysical Research* 96, 4125–4132.

Hurtig, E., Brugger, H. (1970). Wärmeleitfähigkeitsmessung unter einaxialem Druck [*Heat conductivity measurements under uniaxial pressure*]. *Tectonophysics* 10, 67–77.

Hutt, J. R., Berg, J. W. (1968). Thermal and electrical conductivities of sandstone rocks and ocean sediments. *Geophysics* 33, 489–500.

Kappelmeyer, O., Haenel, R. (1974). Geothermics with Special Reference to Application. Geopublication Associates, Geoexploration Monographs, Gebrüder Borntraeger Berlin, Series 1, No. 4., 238 pp.

Kukkonen, I.T., Jokinen, J., Seipold, U. (1999). Temperature and pressure dependencies of thermal transport properties of rocks: implications for uncertainties in thermal lithosphere models and new laboratory measurements of high-grade rocks in the Central Fennoscandian Shield. *Surveys in Geophysics* 20, 33–59.

Lemmon, E.W., McLinden, M.O., Friend, D.G. (2005). Thermophysical properties of fluid systems. *In:* Linstrom, P.J., Mallard, W.G. (Eds.), NIST Chemistry WebBook, NIST Standard Reference Database, Number 69. National Institute of Standards and Technology, Gaithersburg MD, p. 20899, *http://webbook.nist.gov* (last accessed: 21.02.2013).

Lewis, T., Villinger, H., Davis, E. (1993). Thermal conductivity measurement of rock fragments using a pulsed needle probe. *Canadian Journal of Earth Sciences* 30, 480–485.

Lichtenecker, K. (1924). Der elektrische Leitungswiderstand künstlicher und natürlicher Aggregate. *Physikalische Zeitschrift* 25, pp. 169–181, 193–204, 226–233.

Liu, S., Feng, C., Wang, L, Cheng, L. (2011). Measurement and analysis of thermal conductivity of rocks in the Tarim Basin, Northwest China. *Acta Geologica Sinica - English Edition* 85, 598–609.

Majorowicz, J., Šafanda, J., Torun-1 Working Group (2008). Heat flow variation with depth in Poland: evidence from equilibrium temperature logs in 2.9-km-deep well Torun-1. *International Journal of Earth Sciences* 97, 307–315.

Maxwell, J.C. (1892). A treatise on electricity and magnetism. Clarendon Press Series, vol. 1, 3rd ed., 440, Oxford, UK, 425 pp.

Mottaghy, D., Schellschmidt, R., Popov, Y.A., Clauser, C., Kukkonen, I.T., Nover, G., Milanovsky, S., Romushkevich, R.A. (2005). New heat flow data from the immediate vicinity of the Kola super-deep borehole: Vertical variation in heat flow confirmed and attributed to advection. *Tectonophysics* 401, 119–142.

Norden, B., Förster, A. (2006). Thermal conductivity and radiogenic heat production of sedimentary and magmatic rocks in the Northeast German Basin. *AAPG Bulletin* 90, 939–962.

Orilski, J., Schellschmidt, R., Wonik, T. (2010). Temperaturverlauf und Wärmeleitfähigkeit im Untergrund der Bohrung Groß Buchholz GT1 in Hannover. Extended Abstract, Geothermiekongress 2010. Karlsruhe, Germany 17–19 November 2010, p. 10.

Popov, Y.A., Pevzner, L.A., Rumushkevich, R.A., Korostelev, V.M., Vorob'jev, M.G. (1995). Thermophysical and geothermal sections obtained from Kolvinskaya well logging data. *Physics of the Solid Earth*, English Translation 30, 778–789.

Popov, Y.A., Pribnow, D.F.C., Sass, J.H., Williams, C.F., Burkhardt, H. (1999). Characterization of rock thermal conductivity by high-resolution optical scanning. *Geothermics* 28, 253–276.

Popov, Y. A., Tertychnyi, V., Romushkevich, R., Korobkov, D., Pohl, J. (2003). Interrelations between thermal conductivity and other physical properties of rocks: Experimental data. *Pure and Applied Geophysics* 160, 1137–1161.

Popov, Y.A., Miklashevskiy, D., Romushkevich, R., Novikov, S., Safonov, S. (2010). Advanced Technique for Reservoir Thermal Properties Determination and Pore Space Characterization. *In: Proceedings of the World Geothermal Congress, Bali, Indonesia, 25-29 April 2010, p. 9.*

Popov, Y.A., Romushkevich, R., Korobkov, D., Mayr, S., Bayuk, I., Burkhardt, H., Wilhelm, H. (2011). Thermal properties of rocks of the borehole Yaxcopoil-1 (Impact Crater Chicxulub, Mexico). Geophysical Journal International 184, 729–745.

Pribnow, D.F.C. (1994). Ein Vergleich von Bestimmungsmethoden der Wärmeleitfähigkeit unter Berücksichtigung von Gesteinsgefügen und Anisotropie. *VDI Fortschrittsberichte* Reihe 19(75), VDI-Verlag, Düsseldorf, Germany, 111 pp.

Progelhof, R.C., Throne, J.L., Ruetsch, R.R. (1976). Methods for predicting the thermal conductivity of composite systems: a review. *Polymer Engineering and Science* 16, 615–625.

Reuss, A. (1929). Berechnung der Fließgrenze von Mischkristallen auf Grund von Plastizitätsbedingung für Einkristalle. *Zeitschrift für Angewandte Mathematik und Mechanik* 9, 49–58.

Revil, A. (2000). Thermal conductivity of unconsolidated sediments with geophysical applications. *Journal of Geophysical Research* 105, 16749–16768.

Robertson, E.C., Peck, D.L. (1974). Thermal conductivity of vesicular basalt from Hawaii. *Journal of Geophysical Research* 79, 4875–4888.

Schärli, U., Rybach, L. (1984). On the thermal conductivity of low-porosity crystalline rocks. *Tectonophysics* 103, 307–313.

Schön, J.-H. (1996). Physical Properties of Rocks, Fundamentals and Principles of Petrophysics. *In:* Treitel, S. and Helbig, K. (Eds.), Handbook of Geophysical Exploration: Seismic Exploration, vol. 18. Oxford, UK, Pergamon, 583 pp.

Schopper, J.R. (1991). An amendment to Gassmann's theory. *In: Proceedings of the 14th SPWLA European Formation Evaluation Symposium*, London, England, 9-11 December 1991, 19 pp.

Schütz, F., Norden, B., Förster, A., DESIRE Group (2012). Thermal properties of sediments in southern Israel: a comprehensive data set for heat flow and geothermal energy studies. *Basin Research* 24, 357–376.

Sen, P.N., Scala, C., Cohen, M.H. (1981). A self-similar model for sedimentary rocks with application to the dielectric constant of fused glass beads. *Geophysics* 46, 781–795.

Somerton, W.H. (1992). Thermal Properties and Temperature-Related Behavior of Rock/Fluid Systems. Elsevier Science Publishers B.V., Amsterdam, 257 pp.

Somerton, W.H., Ward, S.H., King, M.S. (1963). Physical properties of Mohole test site basalt. *Journal of Geophysical Research* 68; 849–856.

Sugawara, A., Yoshizawa, Y. (1961). An investigation on the thermal conductivity of porous materials and its application to porous rock. *Australian Journal of Physics* 14, 469–480.

Tinga, W.R., Voss, W.A.G., Blossey, D.F. (1973). Generalized approach to multiphase dielectric mixture theory. *Journal of Applied Physics* 44, 3897–3902.

Vasseur, G., Brigaud, F., Demongodin, L. (1995). Thermal conductivity estimation in sedimentary basins. *Tectonophysics* 244, 167–174.

Voigt, W. (1928). Lehrbuch der Kristallphysik. Teubner, Leipzig, 978 pp.

Walsh, J.B., Decker, E.R. (1966). Effect of pressure and saturating fluid on the thermal conductivity of compact rock. *Journal of Geophysical Research* 71, 3053–3061.

Watanabe, H. (2003). Thermal conductivity and thermal diffusivity of sixteen isomers of alkanes: CnH2n+2 (n = 6 to 8). *Journal of Chemical and Engineering Data* 48, 124–136.

Wiener, O.H. (1912). Die Theorie des Mischkörpers für das Feld der stationären Strömung, Erste Abhandlung: Die Mittelwertsätze für Kraft, Polarisation und Energie. *Abhandlungen der mathematisch-physischen Klasse der Königlich-Sächsischen Gesellschaft der Wissenschaften* 32, 507–604.

Woodside, W., Messmer, J. (1961a). Thermal conductivity of porous media. I. Unconsolidated Sands. *Journal of Applied Physics* 32, 1688–1699.

Woodside, W., Messmer, J. (1961b). Thermal conductivity of porous media. II. Consolidated Rocks. *Journal of Applied Physics* 32, 1699–1706.

Zimmerman, R.W. (1989). Thermal conductivity of fluid-saturated rocks. *Journal of Petroleum Science and Engineering* 3, 219–227.

4 Well-log based prediction of thermal conductivity of sedimentary successions: a case study from the North German Basin

Abstract

Data on rock thermal conductivity (TC) are important for the quantification of the subsurface temperature regime and for the determination of heat flow. If drill core is not retrieved from boreholes and thus no laboratory measurement of TC can be made, other methods are desired to determine TC. One of these methods is the prediction of TC from well logs. We have examined the relationships between TC and standard well-log data (gamma ray, density, sonic interval transit time, hydrogen index, photoelectric factor) by a theoretical analysis and by using real subsurface data from four boreholes of the North German Basin. The theoretical approach comprised the calculation of TC from well-log response values for artificial sets of mineral assemblages consisting of variable contents of 15 rock-forming minerals typical for sedimentary rocks. The analysis shows different correlation trends between TC and the theoretical well-log response in dependence on the mineral content, affecting the rock matrix TC, and on porosity. The analysis suggests the development of empirical equations for the prediction of matrix TC separately for different groups of sedimentary rocks. The most valuable input parameters are the volume fraction of shale, the matrix hydrogen index and the matrix density. The error of matrix TC prediction is on the order of 4.2 ± 3.2% (carbonates), 7.0 ± 5.6% (evaporites), and 11.4 ± 9.1% (clastic rocks). From the subsurface data, comprising measured TC values (n = 1 755) and well-log data, four prediction equations for bulk TC were developed resembling different lithological compositions. The most valuable input parameters for these predictions are the volume fraction of shale, the hydrogen index, and the sonic interval transit time. The equations predict TC with an average error between 5.5 ± 4.1% (clean sandstones of low porosity; Middle Buntsandstein), 8.9 ± 5.4% (interbedding of sandstone, silt- and claystones; Wealden), and 9.4 ± 11% (shaly sandstones; Stuttgart Fm.). An equation including all clastic rock data yields an average error of 11 ± 10%.

The subsurface data set also was used to validate the prediction equation for matrix TC established for clastic rocks. Comparison of bulk TC, computed from the matrix TC values and well-log porosity according to the geometric-mean model, to measured bulk TC results in an accuracy < 15%. A validation of the TC prediction at borehole scale by comparison of measured temperature logs and modeled temperature logs (based on the site-specific surface heat flow and the predicted TC) shows an excellent agreement in temperature. Interval temperature gradients vary on average by < 3 K/km and predicted compared to measured absolute temperature fitted with an accuracy < 5%. Compared to previously published TC-prediction approaches, the developed matrix and bulk-TC-prediction equations show significantly higher prediction accuracy. Bulk TC ranging from 1.5 to 5.5 W/(m·K) is always predicted with an average error < 10% relative to average errors between 15 and 35% resulting from the application to our data set of the most suitable methods from literature.

DOI: 10.2312/GFZ.b103-13111

Keywords

Downhole methods, Heat flow, Heat generation and transport
Sedimentary basin processes, Europe

DOI: 10.2312/GFZ.b103-13111

4.1 Introduction

Thermal conductivity (TC, λ) is an intrinsic physical property of minerals and rocks. In sedimentary basins, where the sedimentary record usually is very heterogeneous exposing various lithotypes of different mineralogy, rock TC can vary both laterally and vertically thus altering the basin's thermal structure locally and regionally. Knowledge of the TC of geological formations and its spatial variations is fundamental for quantifying the basin evolution, hydrocarbon maturation processes, but also for understanding the geothermal condition of a geological setting. Furthermore, the TC forms in conjunction with the temperature gradient (*gradT*), according to Fourier's law, the basic input parameter for the heat-flow density (q) determination of an area, which in turn is a major input parameter in temperature modeling at different scale, also including deeper crustal levels.

Subsurface rock TC usually is determined by laboratory measurements on drill cuttings or core samples recovered from boreholes. Different techniques are available for these measurements, comprising steady-state and transient techniques (*e.g.*, von Herzen and Maxwell, 1959; Beck, 1965; Sass et al., 1971; Vacquier, 1985; Popov et al., 1999).

However, as rock samples are often restricted only to some target reservoir, the TC for entire borehole profiles usually cannot be determined. Therefore, methodologies are desired to quantify the TC indirectly from a suite of other petrophysical properties measured by well logs. Such an approach would allow the determination of TC in a profile-wise fashion and, in the best situation, along an entire borehole section. Various data sets and regression parameters are known from several studies performed in different geological environments, but, up to date, no universal well-log based prediction equation for TC is developed yet. Such a universally valid prediction would need to be calculated from a global, comprehensive data set of TC measured for a full spectrum of sedimentary rocks (Williams and Anderson, 1990) and, in turn, from a well-log data set that can fully reflect and explain the TC variability within the 'global data set'.

In this paper, we address the indirect determination of TC from petrophysical well-log properties obtained in sedimentary rocks. The study specifically aims to answer the following critical questions: (A) what well-log data/parameters are most valuable in predicting TC, (B) can any universally valid statistical prediction equation be developed using conventional well logs, and if not, how can this problem circumnavigated, (C) what are major limiting factors in the well-log based approach, and (D) what method shows the best prediction quality?

4.2 Background on TC prediction from well logs

Several approaches exist to determine TC in boreholes. High-precision equilibrium temperature logs can be inverted for an indirect determination of TC by applying a value of heat-flow density to the entire log after having calculated an interval heat-flow density from TC measured on drill core and from an average temperature gradient of this particular depth interval (*e.g.*, Blackwell and Steele, 1989; Fuchs and Förster, 2010). However, the major drawback is that measurements of equilibrium

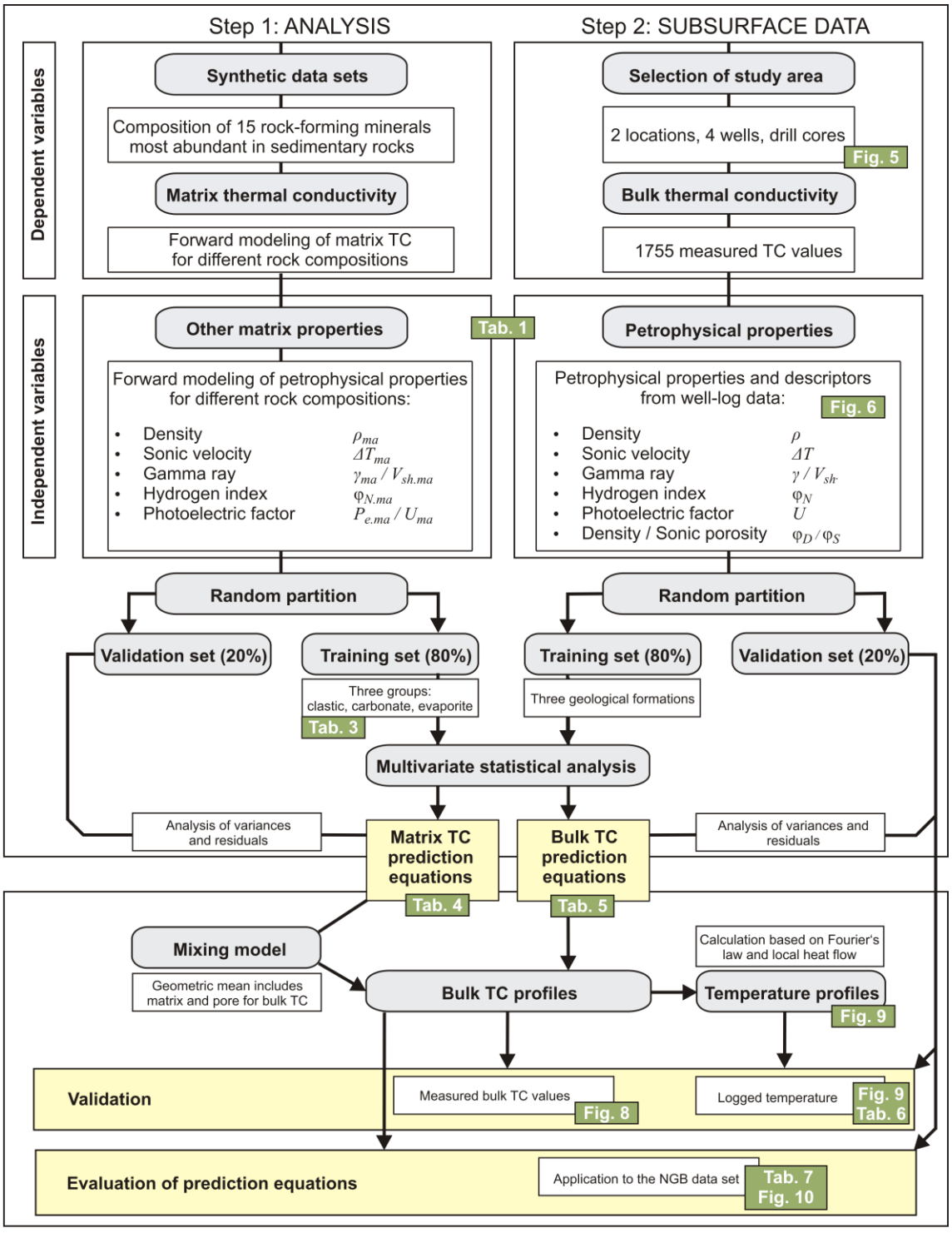

Figure 4-1 Workflow for TC prediction from petrophysical properties of sedimentary rocks.

temperature logs are rarely available. Up to now, this approach is still academic and not standard in the exploration of resources.

The utilization of petrophysical well-logs to determine TC is another basic approach. One type of methods hereby applies an appropriate mixing law to compute rock TC from the TC of mineral constituents (*e.g.*, provided by XRD analyses) and well-log-derived rock porosity (*e.g.*, Brigaud et al., 1990; Demongodin et al., 1991). Other methods derive either the lithology or the major mineralogical composition of a borehole section from well logs using an inverse solution and typical log-response values for each component (Savre, 1963; Quirein et al., 1968; Doveton and Cable, 1979), and, in turn, apply an appropriate mixing equation to calculate bulk TC for the respective lithotype using textbook TC values (*e.g.*, Merkel et al., 1976; Dove and Williams, 1989; Brigaud et al., 1990; Demongodin et al., 1991; Vasseur et al., 1995; Midttømme et al., 1997; Hartmann et al., 2005). Major uncertainties with this method are linked with the quality of the involved well logs, the local complexity of mineral composition, and the selected log-reference values. Another method applies the phonon-conduction theory to predict TC for crystalline rocks using density, sonic velocity, and temperature as predictor variables (Williams and Anderson, 1990). However, the temperature data required in this approach hinder an application in wells, in which only standard well-logs are measured.

Numerous authors have demonstrated for different rock types the direct relation of TC and single petrophysical properties (mostly density and sonic velocity) using statistical methods. (*e.g.*, Čermák 1967; Anand et al., 1973; Poulson et al., 1981; Pribnow et al., 1993; Beziat et al., 1992; Kukkonen and Peltoniemi, 1998; Sundberg, 2002; Popov et al., 2003; Hartmann et al., 2005, 2008; Goutorbe et al., 2006; Sundberg et al., 2009; Gegenhuber and Schön, 2012). However, the results gained for sedimentary as well as crystalline rocks show inconsistencies, are inhomogeneous, and the observed correlation trends differ significantly from one another. Some data show just scatter, some a positive correlation and other a negative correlation of bulk TC with different properties. Hence, no generally valid, simple linear correlation between TC and density or sonic velocity seems to exist, which is in accordance to conclusions by Kukkonen and Peltoniemi (1998). The list of empirical relationships established between well-log data and measured TC is long. Also the complexity of the proposed equations is quite different due to the developed calculation models (*e.g.*, Houbolt and Wells, 1980; Gegenhuber and Schön, 2012) or due to different regression techniques applied. Linear regression (Dachnov and Djakonov, 1952; Zierfuss and Van der Vliet, 1956; Bullard and Day, 1961; Karl, 1965; Moiseyenko et al., 1970; Molnar and Hodge, 1982; Lovell and Ogden, 1984; Lovell, 1985; Della Vedova et al., 1987; Griffith et al., 1992; Zamora et al., 1993; Sahlin and Middleton, 1997; Popov et al., 2011), multiple linear regression (*e.g.*, Thornton, 1919; Anand et al., 1973; Goss et al., 1975; Goss and Combs, 1976; Evans, 1977; Molnar and Hodge, 1982; Vacquier et al., 1988; Doveton et al., 1997; Popov et al., 2003; Hartmann et al., 2005; Goutorbe et al., 2006; Khandelwal, 2010) as well as nonlinear regression (NLR) analysis (*e.g.*, Tikhomirov, 1968; Balling et al., 1981; Özkahraman et al., 2004; Popov et al., 2011) were used. These regression-based empirical equations are typically limited to the rocks on the basis of which they were established (*e.g.*, lithotype, stratigraphy) so that they are not universally applicable (*e.g.*, Goss and Combs, 1976; Evans, 1977; Molnar and Hodge, 1982; Blackwell and Steele, 1989; Hartmann et al., 2005). Most recently, studies were published that use artificial neuronal networks (ANN) instead of linear or even NLR techniques (*e.g.*, Goutorbe et al., 2006; Singh et al., 2007; Singh et al., 2011; Khandelwal, 2010). The ANNs often show higher accuracy compared to common regression techniques. However, due the lack of

knowledge on the internal parameters deployed they do not allow a third party to use them later on for their own TC prediction.

4.3 Methods

4.3.1 Workflow

Considering the limitations that past studies have shown in the well-log based prediction of TC, we have selected a different approach whose workflow is provided in Fig. 4-1. In a first step, for large sets of mineral assemblages it is studied how the TC of the most typical rock-forming minerals of sediments is correlated with individual, conventional petrophysical well-log properties and how these correlations are influenced by an assumed porosity. Matrix-TC-prediction equations are derived, which are used to calculate bulk TC based on porosities from well logs. In a second step, prediction equations for bulk TC are developed using a set of conventional petrophysical well logs and measured TC values from the Mesozoic section of the NGB. The most accurate prediction equations in turn are used to calculate TC profiles for full borehole sections. The calculated TC profiles are validated by comparison with measured TC and by comparison of measured temperature-gradient profiles with those calculated according to Fourier's law using predicted TC values. Finally, previously published well-log based TC prediction methods are evaluated by application to our data set of measured TC values.

4.3.2 Well-log parameters and thermal conductivity

Various well-log parameters – *e.g.*, bulk density (ρ_b), natural gamma-ray (γ), sonic acoustic transit time (ΔT), hydrogen index (neutron porosity, ϕ_N), photoelectric factor (P_e) – and petrophysical descriptors – *e.g.*, volume fraction of shale (V_{sh}), density porosity (ϕ_D), matrix density (ρ_{ma}) – are important for this work. The basic well-log equations applied in this study are listed in Table 4-1.

In general, the total response of a geophysical tool (L_{total}) is determined by the volume fraction of different formation components (minerals and pore space with filling fluid, V_i) and their theoretical tool response (L_i) with the constraint that $\sum V_i = 1$ (Eq. 4-1); *e.g.*, Savre, 1963; Doveton and Cable, 1979; Serra, 1984].

$$L_{total} = \sum_1^n V_i L_i \tag{4-1}$$

Thus, the total log response of any user-defined mineral or pore-matrix composition can be calculated (*e.g.*, for ρ_b, U, ϕ_N, and in the laminated case ΔT; see Savre, 1963; Serra, 1984). Where several radioactive minerals are present, the response of the gamma-ray tool is a function (Eq. 4-2) of the

Table 4-1 Petrophysical descriptors combined with TC.

Petrophysical Descriptor	Unit	Equation
Volume fraction of shale[1]	-	$V_{sh.GR} = \frac{\gamma_{mea} - \gamma_{min}}{\gamma_{max} - \gamma_{min}}$
	-	$V_{sh.ND} = \frac{\phi_N - \phi_D}{\phi_{N.sh} - \phi_{D.sh}}$
Density porosity[2]	p.u.	$\phi_D = \frac{\rho_{ma} - \rho_b}{\rho_{ma} - \rho_{fl}}$
Sonic porosity[3]	p.u.	$\phi_S = \frac{\Delta T - \Delta T_{ma}}{\Delta T_{fl} - \Delta T_{ma}}$
Total porosity[4]	p.u.	$\phi_t = \frac{\phi_N + \phi_D}{2}$
Effective porosity[5]	p.u.	$\phi_e = \phi_t(1 - V_{sh})$
Apparent matrix hydrogen index	p.u.	$\phi_{N.ma} = \phi_N - \phi_D$
Apparent matrix density[6]	g/cm^3	$\rho_{maa} = \frac{\rho_b - (\phi_t \cdot \rho_{fl})}{1 - \phi_t}$
Apparent matrix acoustic transit time[7]	µs/m	$\Delta T_{maa} = \frac{\Delta T - (\phi_t \cdot \Delta T_{fl})}{1 - \phi_t}$
Apparent photoelectric absorption index[8]	barns/cm^3	$U_{maa} = \frac{U - (\phi_t \cdot U_{fl})}{1 - \phi_t}$

[1] Serra (1984), [2] Asquith (1982), [3] Wyllie (1958), [4] Doveton (1997) [5] Dewan (1983), [678] Western Atlas (1995).

Table 4-2 Petrophysical properties and logging-tool characteristic readings of rock-forming minerals typical in sedimentary rocks and of fluids.

Class	Name	Abbv.	TC	ρ	U	Φ_N	ΔT	γ
			W/(m·K)	g/cm^3	barns/cm^3	p.u.	µs/m	API
Carbonates	Dolomite	Dol	5.4 [b,e,f,g]	2.88 [a]	9 [a]	0.02 [a]	140 [a,d]	0 [a]
	Calcite	Cal	3.4 [b,e,f,g]	2.71 [a]	13.8 [a]	0 [a]	153 [a]	0 [a]
Clays	Kaolinite	Kln	2.7 [b,e]	2.42 [a]	6.17 [a]	0.37 [a]	211 [i]	80 [a]
	Montmorillonite	Mnt	1.85 [b,e]	2.12 [a]	4.3 [a]	0.12 [a,i]	212 [i]	150 [a]
	Illite	Ilt	1.8 [b]	2.75 [a,c]	11.1 [a]	0.2 [a]	211 [i]	250 [a]
Feldspats	Orthoclase	Or	2.25 [f,b,e]	2.57 [c]	7.5 [a]	-0.02 [a]	233 [a]	220 [a]
	Albite	Ab	2 [f]	2.62 [a]	4.35 [a]	-0.01 [a]	165 [a,d,i]	0 [a]
	Anorthite	An	1.9 [e]	2.74 [a]	8.58 [a]	-0.02 [a]	145 [f]	0 [a]
Halogenides	Sylvite	Syl	8.5 [e]	1.98 [a]	15.8 [a]	-0.02 [a]	242 [i]	747 [a]
	Halite	Hl	6.5 [f]	2.15 [a]	9.48 [a]	-0.02 [a]	229 [a]	0 [a]
Micas	Muscovite	Ms	2.33 [d,f]	2.82 [a]	7.33 [a]	0.19 [a,i]	151 [a,d,i]	270 [a]
	Biotite	Bt	2 [f]	3 [a]	19.8 [a]	0.21 [a]	195 [d]	200 [a]
Oxides	Quartz	Qz	7.7 [b]	2.65 [a]	4.79 [a]	-0.02 [a]	182 [a]	0 [a]
Sulfates	Anhydrite	Anh	4.8 [f,e,g]	2.96 [a]	14.9 [a]	-0.02 [a]	164 [a,i,e]	0 [a]
	Gypsum	Gp	1.3 [e]	2.32 [a]	9.37 [a]	0.49 [a]	174 [g]	0 [a]
Fluids	air		0.03 [j]	0.0012	-	0	3021[e]	-
	water		0.6 [h]	1.15	0.96	1.05	620[a]	-
	oil		0.14 [e]	0.88[a]	0.11[a]	-0.02	770[a]	-

[a] Serra (1984), [b] Brigaud and Vasseur (1989), [c] Fertl and Frost (1980), [d] Schön (1996), [e] Schön (1983), [f] Horai (1971), [g] Cermak and Rybach (1982), [h] Lemmon et al. (2005), [i] Crain (2013), [j] Gröber (1955). Mineral abbreviations after Whitney and Evans (2010).

concentration by the weight of *i*th mineral in the rock and the density of the rock matrix (Serra, 1984).

$$GR\rho_b = \sum_1^n \rho_i V_i A_i \tag{4-2}$$

Typical log-response values for minerals and fluids, valid for ambient conditions, are listed in Table 4-2. If volume fractions were determined from well-log data, the KIWI-tool (Doveton, 1986) was used.

Following the experience of previous authors (*e.g.*, Woodside and Messmer, 1961; Sass et al., 1971; Merkel et al., 1976; Brigaud and Vasseur, 1989) the geometric-mean model, originally introduced by Lichtenecker (1924), was used to calculate matrix TC [λ_m, Eq. (4-3)] from the mineral constituents, as well as to calculate the saturated bulk TC [λ_b, Eq. (4-4)] using the matrix TC and porosity (Φ) (*e.g.*, Fuchs et al., 2013).

$$\lambda_m = \prod_1^n \lambda_i^{V_i}, \tag{4-3}$$

with V_i volume fraction of each component.

$$\lambda_b = \lambda_m^{1-\phi} \cdot \lambda_p^{\phi}, \tag{4-4}$$

where λ_p is the TC of the pore-filling fluid.

4.3.3 *Statistics*

All data were randomly subdivided in two groups, one set of test data (80% of data) and one set of validation data (20% of total data). The test data set was used for statistical analysis, while the validation data set was used to prove the statistical quality of the deduced prediction equations (Fig. 4-1).

Simple linear (SLR), multiple linear (MLR) and nonlinear (NLR) regression analysis based on a least-squares estimation were applied to predict the values on a quantitative outcome variable (dependent variable: TC) using one or more predictor variables (independent variable: well log values). Levels of 'F to enter' and 'F to remove' were set to correspond to p-levels of 0.05 and 0.1, respectively.

The performance of the applied methods was evaluated by test (values not reported) and validation data (reported fitting data) using the arithmetic mean error (AME), the standard error of the estimate (SE), and the coefficient of determination (R^2) between predicted and measured values, respectively. SE explains the excursions of the given TC values from the computed regression line and is defined as the root mean square value (RMS):

$$RMS = \sqrt{\frac{1}{n}\sum_{i=1}^{n}\left(TC_{mea.i} - TC_{pred.i}\right)^2}, \tag{4-5}$$

where *n* is the number of samples.

R^2 describes the dependent-variable variance (TC), which is explained by the independent-variable variance (log-response values). In this study, the adjusted R^2 value is reported, which is frequently slightly smaller than R^2, but more robust by taking into consideration the number of observations and the number of predictor variables. Coefficient of variation (CV) is given as the quotient of RMS value and arithmetic mean value of the measured TC. Coefficient of variation values < 10% are assumed as an indicator for a valid prediction model. All prediction equations developed and presented hereafter show an acceptable level of multicollinearity (tolerance > 0.3), which means a low level of correlation between two predictor variables, and the standardized residuals are always (nearly) randomly distributed.

4.3.4 *Pressure and temperature correction of laboratory-measured TC*

The TC values predicted in this study from standard well-log parameters basically represent the physical properties of the rock matrix plus porosity. Pressure and temperature influences on the laboratory-measured TC are a priori not considered (see Section 4.10). For the validation of predicted bulk TC temperature-gradient plots from measured temperature logs are compared with respective plots calculated on the basis of predicted bulk TC and a site-typical value of surface heat flow (*cf.* Section 4.5.2). For this purpose, the predicted TC values are corrected to *in-situ* values by applying pressure and temperature corrections.

For the correction of the temperature effect the equation of Somerton (1992) is used. The pressure correction was made with a new equation that is based on various relations derived from laboratory experiments on sedimentary rocks (sandstone, anhydrite, greywacke, conglomerate, limestone, and dolomite) and crystalline rocks (granite, amphibolite, and gneiss) (Fig. 4-2):

$$TC_{cor} = (1.095 \cdot TC_{lab} - 0.172) \cdot p^{(0.0088 \cdot TC_{lab} - 0.0067)}, \tag{4-6}$$

where TC_{lab} is the zero-pressure TC in W/(m·K) and p is the assumed *in-situ* pressure in MPa.

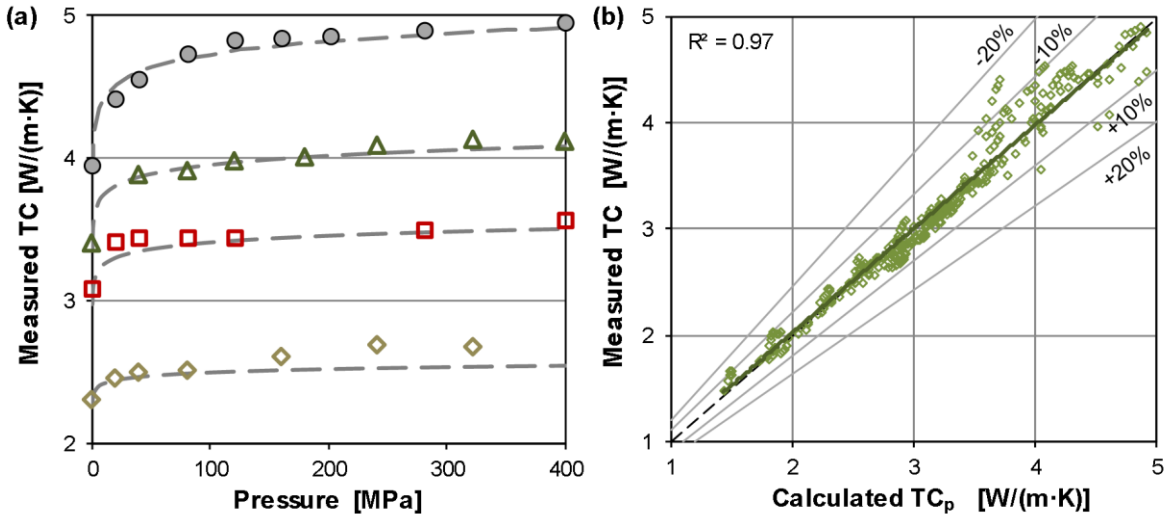

Figure 4-2 Pressure dependence of rock TC. (a) Laboratory measured TC as function of pressure for selected lithotypes (dot: anhydrite, open triangle: dolomite, open rectangle: limestone, open diamond: sandstone). Dashed lines are calculated from equation (4-6). Eq. (4-6) originated from data by Woodside and Messmer (1961), Walsh and Decker (1966), Hurtig and Brugger (1970), Balling et al. (1981), Buntebarth (1991), Seipold and Huenges (1998), Abdulagatova et al. (2009), and Abdulagatova et al. (2010). (b) Measured vs. calculated [Eq. (4-6)] TC.

The pressure build-up TC values involved in the equation were obtained under different experimental conditions (*e.g.*, uniaxial, triaxial and (quasi-)hydrostatic pressure; air, water or oil as pore-filling fluid) to maximum values of 400 MPa. With sufficient certainty, equation (4-6) can be applied to laboratory TC between 1.5 and 5.0 W/(m·K).

4.4 Analysis

4.4.1 Relations of TC and petrophysical properties of minerals

A data set was compiled, comprising TC values and logging-tool response values (ρ_b, P_e, ϕ_N, ΔT, γ) for 15 rock-forming minerals most abundant in sedimentary rocks (Table 4-2), to study the interrelations between TC and these parameters. Figure 4-3 shows that the interrelations between the different petrophysical properties and TC differ largely. The TC-density plot (Fig. 4-3a) for example is highly diffuse; no global trend is apparent. Carbonate minerals show a positive correlation with TC, which continues with increasing content of clay (*e.g.*, the carbonate-mudstone facies), except of illite. Clastic rocks, composed of quartz, mica, plagioclase, and illite are negatively correlated with TC; whereas rocks composed of quartz, orthoclase, montmorillonite, and kaolinite show a weak positive correlation, respectively. The nonexistence of a unique global TC–density correlation is in contradiction to the results of Horai and Simmons (1969), who recognized a correlation for minerals with the same mean atomic weight. Application of a regression equation formulated by Schön (1996) based on the database of Horai and Simmons did not reproduce any TC for the 15 rock-forming minerals used in this study. The difference to our results may be explained by the fact that Horai and Simmons included in their database of 119 minerals also those that are not regarded as typical rock-forming minerals of sedimentary rocks.

The interrelation between TC and sonic transit time (Fig. 4-3b) is well described by the Debye theory and the Birch relationship (Birch, 1960, 1961). Horai and Simmons (1969) determined a positively correlated trend from the data of Birch (1960, 1961) and Simmons (1964a, 1964b). However, this trend cannot be observed for all minerals included in this study. A negative correlation can be observed within halogenides, while a positive correlation can be observed in the carbonate-mudstone system. For clastic rocks, the correlation trend largely depends on the most abundant mineral after quartz.

The TC- photoelectric-factor plot (Fig. 4-3c) shows a similarly diffuse scatter as the TC versus density and sonic transit time. However, P_e, ρ_b and ΔT are suitable for the separation between evaporites, carbonates and clastic rocks.

A clear nonlinear trend is observed between TC and the hydrogen index obtained from the ϕ_N-log (Fig. 4-3d). Halogenides, feldspars, carbonate minerals, and anhydrite comprise the entire spectrum of TC values, but show only low hydrogen-index values. Only OH-bearing sheet silicates (*e.g.*, clay minerals, micas, and gypsum), exhibit a moderate or high hydrogen index (corresponding with low TC values). Thus, TC prediction from the hydrogen-index values alone is for most of the minerals impossible.

DOI: 10.2312/GFZ.b103-13111

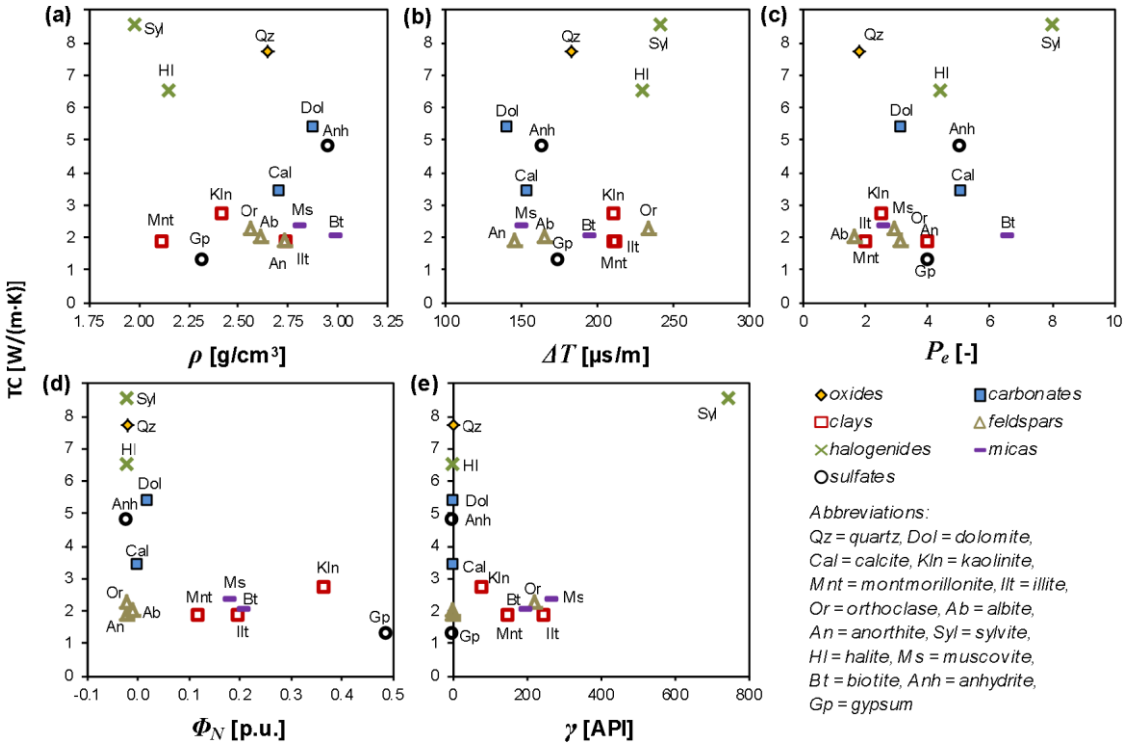

Figure 4-3 TC vs. petrophysical properties for 15 rock-forming minerals common in sedimentary rocks. Plotted mineral data are from Table 4-2.

The gamma-tool response values are completely uncorrelated (Fig. 4-3e) to TC. However, it is remarkable that the most gamma-active minerals (clay minerals, mica, alkali feldspar) show TC values in a narrow range [between 1.5 and 3.0 W/(m·K)]. Owing to this, incoherent negative correlations between TC and gamma ray can be observed in quartz-dominated sediments. However, obviously this cannot be regarded as universally valid.

The TC prediction capability of all five predictor variables is poor [best case using MLR: Adj. R^2 = 0.26, RMS = 2.02 W/(m·K)], which is no surprise. Changes of correlation trends within or between formations of different composition have a crucial impact on the prediction results, if empirically equations with fixed regression coefficients are used. Those regression coefficients are equal to the slopes for the different predictor variables, indicating the correlation trends between dependent and independent variable. The final predicted TC value is cumulative from the partial TC values coming from each (input) predictor variable. The resulting misfit coming from these trend changes results in a high inaccuracy in SLR, which can possibly, at least partly, be compensated using additional predictor variables in explanation of TC (using MLR). However, such simultaneous change of predictor variables poses an increased danger of multicollinearity for MLR techniques and, therefore, instable estimates for the coefficients. Thus, the major correlation trends are of great importance for the use of regression techniques.

Curve fitting with NLR or the application of ANN techniques (feedforward backpropagation neural networks) provides no better fit than MLR. Obviously, there is no fundamental relationship between TC and other petrophysical properties that could be obtained for the selected rock-forming minerals.

DOI: 10.2312/GFZ.b103-13111

Some pairs of petrophysical properties are clearly uncorrelated, while others show only poor correlations. Thus, it is fair to assume, that in some situations other factors must have influenced the relationships observed by various authors on rock samples. Porosity and the type of pore-filling fluid (*e.g.*, water, air, oil, gas) are obvious factors.

4.4.2 *Influence of porosity on the relations of TC and petrophysical properties of rocks*

The total log response significantly changes with different porosity because of the contrast in properties of the pore-filling fluid compared to those of the matrix mineral grains (Table 4-2). This fact is well displayed in the cross-plots for different two-component (matrix mineral and porosity) systems, exemplarily shown for ρ_b and ΔT (Fig. 4-4).

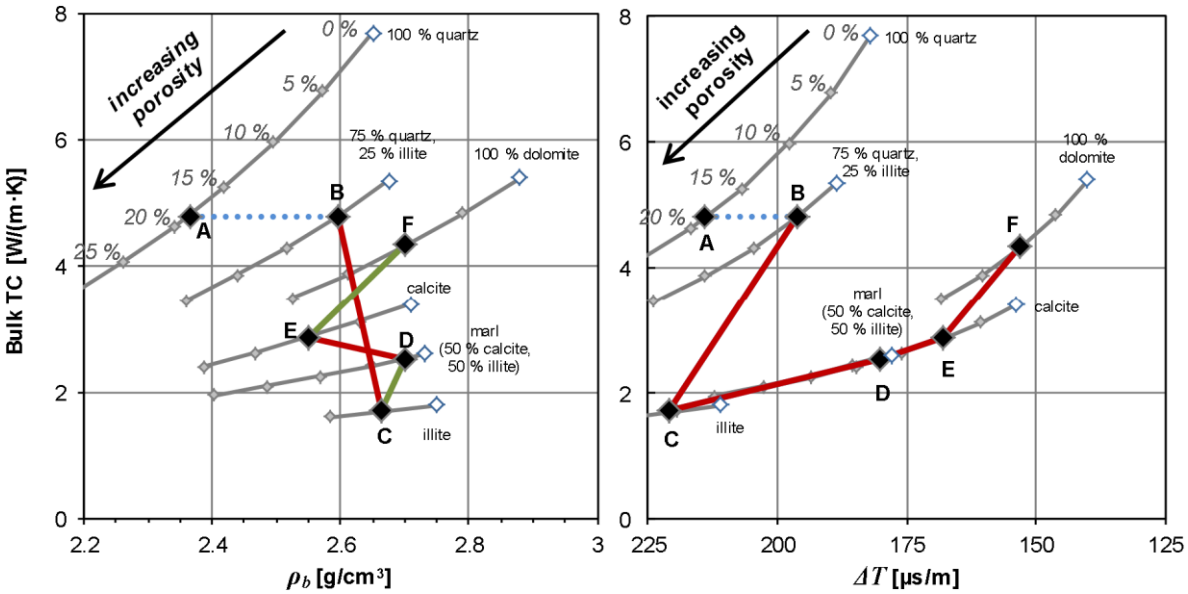

Figure 4-4 Influence of rock porosity on the correlation trends for two-component systems (matrix minerals and porosity). Black diamonds: A: sandstone (matrix: 100% quartz; 18% porosity), B: shaly sandstone (matrix: 75% quartz, 25% illite; 5% porosity), C: claystone (matrix: 100% illite; 5% porosity), D: mudstone (matrix: 50% calcite, 50% illite; 3% porosity), E: limestone (matrix: 100% calcite; 10% porosity), F: dolomite (matrix: 100% dolomite; 10% porosity). Blue dotted line: no correlation, red line: negative correlation, green line: positive correlation.

Depending on the TC value of the matrix component, different porosity values result in different slopes and slope directions (correlation coefficients). Those changes in correlation trends (positive or negative correlations) imply problems for regression techniques as previously described.

For example, the change from a clay-free 'quartz rock' (representative of clean sandstone) of high porosity to a quartz-illite mixture (argillaceous sandstone) result in positive correlations between TC and density whereas negative correlations can be expected for a low-porous 'quartz rock' (Fig. 4-4a). The same effect can be observed for numerous other lithotype combinations. In contrast, the TC-ΔT relation, exemplarily shown in Fig. 4-4b, indicates only negative correlations. In conclusion, due to the ambiguous influence of porosity on the correlation trends we proceed in the TC prediction with the focus on the mineral constituents of the rock matrix and thus the matrix TC.

DOI: 10.2312/GFZ.b103-13111

4.4.3 *Matrix-TC prediction for artificial rock compositions*

Table 4-3 Groups of sedimentary rocks with respect to their assumed rock composition, and the min-max range of the particular minerals.

Group	Mineral	Range		
		Carb.	Clast.	Evap.
		%	%	%
Oxides	Quartz	0–50	50–100	-
Feldspars	Anorthite	-	0–50	-
	Albite	-	0–50	-
	Orthoclase	-	0–50	-
Micas	Muscovite	-	0–20	-
	Biotite	-	0–20	-
Clays	Kaolinite	0–70	-	-
	Montmorillonite	0–70	0–100	-
	Illite	0–70	0–100	-
Carbonates	Calcite	0–100	0–20	0–100
	Dolomite	0–100	0–20	0–100
Sulfates	Anhydrite	-	0–20	0–100
	Gypsum	-	-	0–100
Chlorides	Halite	-	-	0–100
	Sylvite	-	-	0–100

Carb., carbonates; Clast., clastic rocks; Evap., evaporites.

For this purpose, the sedimentary rocks are classified into three major groups (I) carbonates, including mudstones, (II) clastic rocks, and (III) marine evaporites (Table 4-3). For the groups (I) and (II), multi-mineral-rock compositions are defined, based on the stepwise combination (in 10%-steps) of different rock-forming minerals common in sedimentary rocks. This procedure is performed as long as each mineral was combined with each other within the limitations defined in Table 4-3. For the group (III), the marine evaporites, an artificial data set of rock composition is generated by stepwise combination of two minerals of the calcite–dolomite–gypsum–anhydrite–halite–potassium–magnesium–salt sequence.

Petrophysical properties are calculated for each mineral combination shown in Table 4-3 using the mineral data given in Table 4-2, which in turn formed the basis for the prediction equations of matrix TC. Thus, for rocks with the same mineralogy, the matrix well-log response, computed from the bulk tools response and the porosity (applying Eqs. (4-1), (4-2) and (4-4), and typical log-response values from Table 4-1), should be equal to the petrophysical properties calculated for this mineralogy.

Prediction equations for matrix TC are calculated by using multiple regression analysis. Taking into account the balance between the use of as few as possible different well logs and the need to achieve a large explained variance (minimizing the prediction error), the 'optimal log configuration' for each rock group and the deduced empirical relationships are described in the following subsections. However, in many cases the 'optimal log configuration' for determination of matrix TC is not available, in particular in old boreholes. Then, matrix TC can be predicted by using one of the additional regression equations listed in Section 4.11 (Appendix B). The Appendix comprises regression coefficient, statistical parameters and the expected prediction errors (for artificial and subsurface data set) for each possible combination of well logs used in this study. Considering larger prediction uncertainties, this allows a TC prediction even if the required and recommended log combination is not available.

4.4.3.1 *Carbonates*

In a first attempt, all matrix well-log properties (Table 4-2) are included in the regression analysis (MLR). The result is a nearly perfect coefficient of regression ($R^2 = 0.98$). Considering that the largest impact on the explained variance is by the first three predictor variables, ρ_{ma}, V_{sh} and U_{ma} ($R^2 = 0.95$), a prediction equation with three variables [Table 4-4, Eq. (4-8)] is a proper choice if a minimal number of well logs shall be included in the TC prediction. The matrix TC is determined with an error of < 10%

DOI: 10.2312/GFZ.b103-13111

for > 96% of the predicted values. This is that 95% of the values show deviations of < 0.24 W/(m·K)]. The implementation of U_{ma} in the prediction equation results only in a slightly improved explained variance. Furthermore, ρ_{ma} and U_{ma} show signs of multicollinearity (tolerance ~ 0.3). Thus, U_{ma} could be ignored in the TC prediction if the respective log is not available. The resulting, two-predictor-equation [Table 4-4, Eq. (4-9)] shows no multicollinearity (tolerance > 0.5) and is able to predict > 60% of the values with deviations < 10%. This is that 50% of the values show deviations of < 0.25 W/(m·K). The coefficient of determination (R^2 = 0.70) is high, indicating a good degree of tracking. The prediction errors (AME, RMS) are in the order of 9.2% and 0.39 W/(m·K).

Table 4-4 Matrix-TC equations derived from regression analysis for major sedimentary rock types.

Rock group	Matrix-TC-prediction equations	R^2	n	RMS	AME	SD	CV	T	F	B_{s1}	B_{s2}	B_{s3}	eq.
				W/(m·K)	%	%	%						
Evaporites	$\lambda_m = 14.06 - 10.35\,\phi_{N.ma} - 3.37\rho_{ma}$	0.92	51	0.45	7.0	5.6	8.8	0.99	237	-0.81	-0.50	-	(4-7)
Carbonates	$\lambda_m = -0.55 + 3.093\,\rho_{ma} - 2.727\,V_{sh} - 0.332\,U_{ma}$	0.95	2252	0.17	4.2	3.2	5.1	0.38	14891	0.46	-0.79	-0.67	(4-8)
Carbonates	$\lambda_m = 5.058 \pm 0.1\,\rho_{ma} - 2.915\,V_{sh}$	0.7	2252	0.39	9.2	6.8	10.6	0.58	2653	-0.15	-0.85	-	(4-9)
Clastics	$\lambda_m = 5.281 - 2.961\,\phi_{N.ma} - 2.797\,V_{sh}$	0.43	3484	0.48	11.4	9.1	14.7	0.55	1336	-0.58	-0.11	-	(4-10)

All predictor variables are highly significant (p < 0.001). For statistics see Section 4.3.3, for abbreviations see Appendix A (Section 4.10).

4.4.3.2 *Clastic rocks*

The high variability of ρ_{ma} and ΔT_{ma} of major clay minerals (illite, montmorillonite and kaolinite) are the main challenging factors for a valid prediction equation for matrix TC using MLR. For these properties, changes in the correlation trend from one clay mineral to another as well as from one rock composition to another (see also Fig. 4-3) do not allow a development of a valid empirical prediction equation for matrix TC. Even for the simplest rock matrix model, consisting of quartz and different clay minerals, the prediction failed by using the full suite of available well-log parameters. Only for rocks composed of quartz, feldspar, and mica and one clay mineral only a nearly perfect coefficient of variation is achieved. That is why ρ_{ma} and ΔT_{ma} were not taken into further consideration, and the prediction model is reduced to the use of V_{sh} and ϕ_{Nma}. The resulting two-predictor-equation [Table 4-4, Eq. (4-10)] shows no multicollinearity (tolerance > 0.55) and is able to predict > 67% of values with deviations of < 10% or 92% with deviations < 20%, respectively.

4.4.3.3 *Evaporites*

A stepwise MLR was performed using ϕ_{Nma}, U_{ma}, ΔT_{ma} and ρ_{ma} as predictor variables. Regarding that none of the considered minerals (Table 4-3) show an intrinsic natural gamma response, the gamma-ray log, and thus the calculated V_{sh} are no useful TC predictors for the evaporate sequence. However, they are certainly useful for a lithological identification. The ϕ_{Nma} log response delivers the largest part of the shared explained variance for the predicted TC. Step 1 results in R^2 = 0.67. In step 2, ρ_{ma} was added as further predictor variable, which improved the result significantly to R^2 = 0.92 [Table 4-4, Eq. (4-7)].

ΔT_{ma} and U_{ma} provided no further explained variance and thus were not implemented in the prediction equation. Using this equation, > 80% of the predicted values show deviations < 10%. This is that 60% of values show deviations < 0.25 W/(m·K). The AME value is in the order of 7.0%.

4.4.4 Bulk-TC prediction from laboratory measured TC and well-log data of the NGB

For the TC prediction, well-log data were used from two sites (Fig. 4-5). At site A, the Ketzin site, data were available from three wells (the Ktzi 200, Ktzi 201, Ktzi 202 boreholes) drilled to a total depth of approximately 800 m as part of the CO_2SINK project (Norden et al., 2010). The wells bottom in the Upper Triassic (Stuttgart Formation, Middle Keuper). At site B, the Hannover site, well-log data from the Groß-Buchholz well (GT 1) are used (Schäfer et al., 2012; Hübner et al., 2012). The well, drilled in the framework of the GeneSys project, has a total depth of approximately 3,900 m and bottoms in the Lower Triassic (Middle Buntsandstein). Thus, the four boreholes represent a combined subsurface section of the whole Mesozoic in the NGB.

A total of 1 755 TC values was measured under ambient laboratory conditions on drill cores retrieved from these boreholes and used in this study to develop prediction equations for bulk TC from well logs. 733 TC values (B. Norden, personal communication, 2013) are from the Stuttgart Formation (~80 m

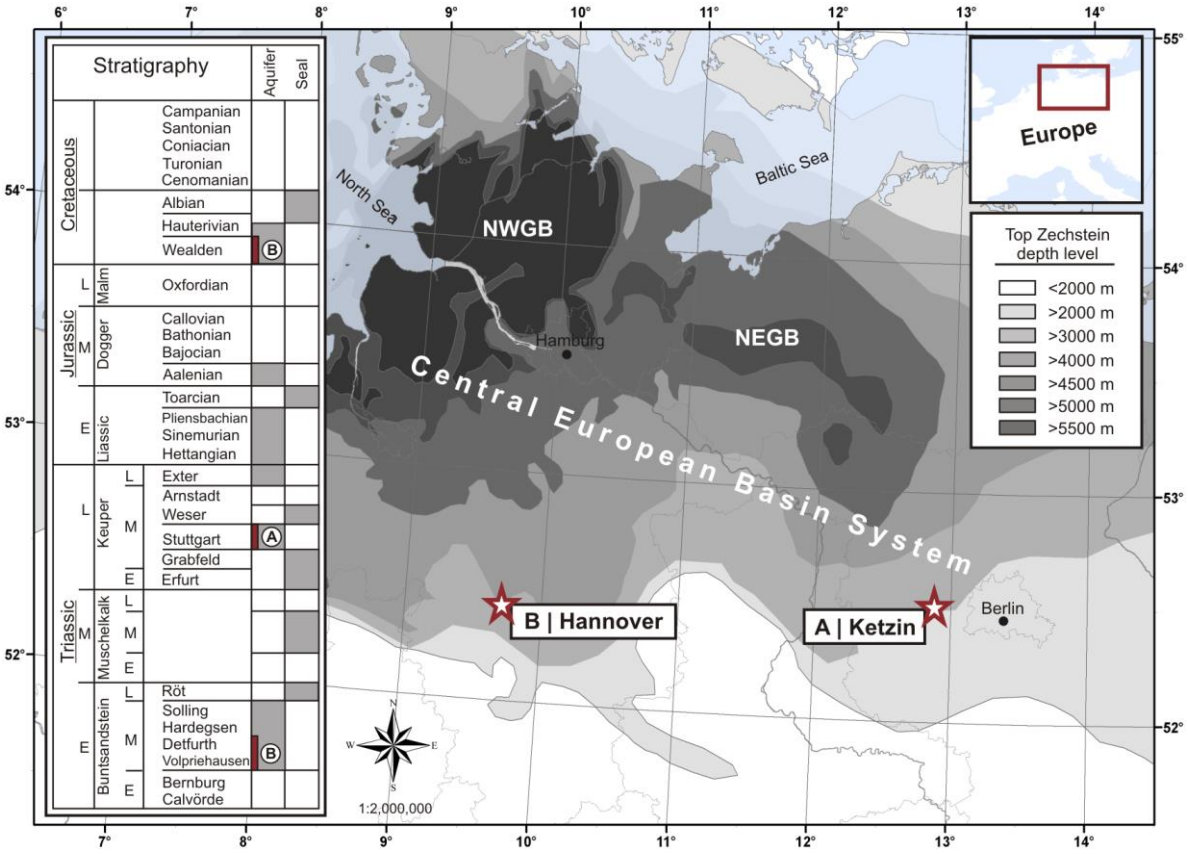

Figure 4-5 Studied borehole sites in the North German Basin. A. the Ketzin site; B, the Hannover site. NEGB, Northeast German Basin, NWGB, Northwest German Basin. Generalized stratigraphic column of the Mesozoic with major geothermal sandstone aquifers and major aquitards (modified after Feldrappe et al., 2008). Red bar indicates the section studied in this paper.

DOI: 10.2312/GFZ.b103-13111

thick) at the Ketzin site. The Stuttgart Formation is lithologically heterogeneous and made up of fluvial sandstones (feldspathic litharenites and lithic arkoses) and siltstones interbedded with mudstones showing remarkable differences in porosity caused by high contents of anhydritic cementation in some extent (Förster et al., 2006, 2010; Norden et al., 2010). 1 022 values are from the Wealden Formation (190 m thick, cored between 1,208 and 1,223 m) and the Middle Buntsandstein (250 m thick) at the Hannover site (Orilski et al., 2010). The Wealden Formation is dominated by sandy siltstones and silty claystones, which are interbedded by thin well-sorted sandstones (subarkoses and sublitharenites). Medium porosity values (10–15%), low densities, and clay-mineral, carbonate, and silicaceous cementation were commonly observed (Hesshaus et al., 2010, Hübner et al., 2012). Middle Buntsandstein samples from this site are dominated by carbonate and anhydrite cemented, fine- to medium grained, well-sorted sandstones of low porosity (< 3%; Röhling & Heinig, 2012), siltstones, and claystones (Hesshaus et al., 2010), respectively. On both locations, the neutron porosity was logged as limestone porosity.

For the Ketzin site, measurements of water-saturated bulk TC (n = 733) on drill-core samples were performed by B. Norden (personal communication, 2013). For the Hannover location, bulk TC was measured (n = 1 022) on dry drill-core samples by J. Orilski (Orilski et al., 2010).

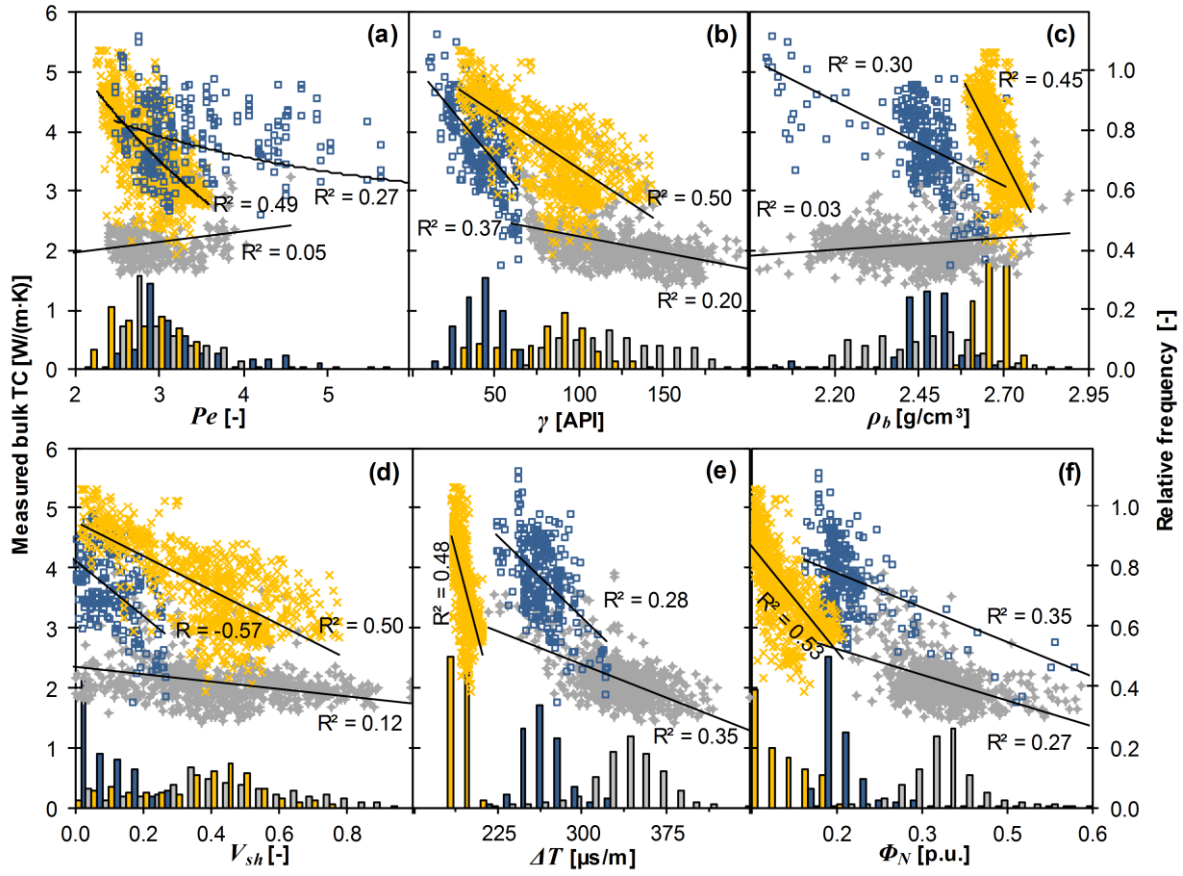

Figure 4-6 Cross-plots of well-log data and measured bulk TC (y-axis on the left) for the NGB data set. Colored bars (histogram) represent the relative frequency (y-axis on the right) of the petrophysical property values. R, Pearson's correlation coefficient. Yellow cross, Middle Buntsandstein; blue rectangle, Wealden Fm.; grey diamond, Stuttgart Fm.

Both sets of TC data were obtained under ambient conditions (T ~ 293 K; atmospheric pressure) using the high-resolution optical scanning method developed by Popov et al. (1999). The dry measured TC data from the Hannover location were converted to water-saturated bulk TC using well-log derived porosity and the corrected geometric-mean model (Fuchs et al., 2013). The data set was analyzed for the relations of measured bulk TC and single petrophysical well-log parameters (Fig. 4-6). Density and photoelectric factor show different correlation coefficients for the three geological formations analyzed. TC is negatively correlated with ρ_b and P_e for the Middle Buntsandstein (R = -0.67 and R = -0.7) and weakly positive correlated for the Stuttgart Fm. (R = 0.17 and R = 0.23), respectively. For gamma ray (and thus V_{sh}), ΔT, and ϕ_N only positive correlations are observed, whereby Stuttgart Fm. samples show always significantly lower correlation coefficients than the other two formations.

The data set of measured bulk TC formed the basis for development of a prediction equation of bulk TC using the petrophysical well-log properties shown in Fig. 4-6. This analysis was performed for the full data set on the one hand and individually for the three geological formations on the other hand.

4.4.4.1 Analysis of the full data set

A first MLR with all five predictor variables resulted in a moderate coefficient of determination of approximately 0.79. However, caused by the large number of input variables, a high level of multicollinearity was present (tolerance < 0.4), so that the model was rejected. The largest impact on the explained variance was by ϕ_N and V_{sh}. MLR including only these two variables [Table 4-5, Eq. (4-11)] shows a somewhat lower coefficient of determination (R^2 = 0.75) and a very low level of multicollinearity (tolerance = 0.96) compared to the five-variable model. Both the AME value [0.33 ± 0.26 W/(m·K)] and the CV value (12.8%) are acceptable. More than 70% of samples show deviations < 20%.

4.4.4.2 Analysis of Wealden Formation

A first stepwise regression analysis showed that ϕ_N, ρ_b, V_{sh} and U were useful predictor variables. However, V_{sh} and U provided only a low additional explained variance (ΔR^2: 0.041). Thus, a reduction of the regression model to ϕ_N and ρ_b [Table 4-5, Eq. (4-12); Fig. 4-7a] results in a somewhat larger error [ΔRMS: 0.017 W/(m·K)], which, however, is insignificant for applications. More than 76% of samples show deviations < 10% and nearly all samples (98%) show deviations < 20%.

4.4.4.3 Analysis of Stuttgart Formation

The most accurate bulk-TC prediction using MLR was obtained by using V_{sh}, ϕ_N and ΔT as predictor variables. The coefficient of determination (R^2 = 0.53) indicated a good degree of tracking [Table 4-5, Eq. (4-13); Fig. 4-7b]. The additional use of ρ_b and U as predictor variables would result in a statistically significant improvement of the prediction quality, which, however, is insignificant for applications. The average error [AME: 0.16 ± 0.15 W/(m·K)] is low, more than 73% of samples show deviations < 10% and nearly all samples (96%) show deviations < 20%.

DOI: 10.2312/GFZ.b103-13111

4.4.4.4 *Analysis of Middle Buntsandstein*

Bulk density and the V_{sh} are the most important predictor variables for these samples [Table 4-5, Eq. (4-14)]. The coefficient of determination (R^2 = 0.83) is high, indicating a fair degree of tracking for the full formation (Detfurth and Volpriehausen samples). The error distribution is small [AME: 0.2 ± 0.14 W/(m·K)], resulting in CV of approximately 7%. The qualitative agreement between measured and predicted values (Fig. 4-7c) is obvious with most of the predicted conductivities within ± 10%. More than 88% of samples show deviations < 10% and nearly all samples (99%) show deviations < 20%. In summary, four equations for bulk-TC prediction are developed. They display different errors of determination. The application of an overall prediction equation for clastic rocks results in errors (AME) on the order of 11.2 ± 9.9%. Significantly smaller errors can be achieved by the application of individual prediction equations for the specific geological formations (AME values between 5.5 ± 4.1% and 9.4 ± 10.6%).

Table 4-5 Bulk-TC equations derived from regression analysis for subsurface data.

Data set	Bulk-TC-prediction equation	R^2	n	RMS	AME	SD	CV	T	F	B_{s1}	B_{s2}	B_{s3}	Eq.
				W/(m·K)	%	%	%						
Full data set	$\lambda_b = 4.75 - 4.19\,\phi_N - 1.81\,V_{sh}$	0.75	1755	0.43	11	9.9	13	0.9	2024	-0.64	-0.40	-	(4-11)
Wealden Fm.	$\lambda_b = 4.97 - 2.24\,V_{sh} - 1.87\,\phi_N$	0.65	288	0.33	6.8	5.3	8.7	0.7	260	-0.55	-0.35	-	(4-12)
Stuttgart Fm.	$\lambda_b = 4.05 - 0.48\,V_{sh} - 2.06\,\phi_{N.ma} - 0.003\,\Delta T$	0.53	325	0.28	9.4	11	9.8	0.3	123	-0.34	-0.29	-0.26	(4-13)
M. Buntsdst.	$\lambda_b = 11.95 - 1.81\,V_{sh} - 0.038\,\Delta T$	0.84	734	0.25	5.5	4.1	6.7	0.6	1843	-0.58	-0.43	-	(4-14)

All predictor variables are highly significant (p < 0.001). For statistics see Section 4.3.3, for abbreviations see Section 4.10 (Appendix A).

4.4.5 *Discussion*

The weak positive correlation of TC and density obtained for the Stuttgart Fm. (Fig. 4-6c) is in line with previous results for shaly sediments (*e.g.*, Beziat et al., 1992, clay-sand mixtures; Hartmann et al., 2005, shaly sands and carbonates). In contrast, the strong negative correlation of TC and density observed for the clean sandstones of the Middle Buntsandstein and the interbedded sandstones of the Wealden was not previously known, but was reported for crystalline rocks (*e.g.*, Pribnow et al., 1993; Kukkonen and Peltoniemi, 1998; Sundberg, 2002). The negative correlation trends are consistent with the theoretical models including the rock-forming minerals (Fig. 4-3a). Thus, given the ambiguity in the observed trends for different rock types, the density does not seem to be a useful discriminator for clastic rocks to overcome the known limitations of previously published equations.

The weak to strong negative correlations of TC with sonic sonic interval transit time (Fig. 4-6e) and, vice versa the positive correlation with sonic velocity, observed for shaly sediments and low-porosity sandstones support previous observations (*e.g.*, Sahlin and Middleton, 1997; Hartmann et al., 2005; Goutorbe et al., 2006; Gegenhuber and Schön, 2012). They also correlate with the theoretical observations presented in this study (Fig. 4-4b). However, the wide range of negative correlations caused by porosity hinders the use of this well-log parameter as a predictor variable for clastic rocks. Therefore, it is expected that most of the approaches published in literature using ΔT as a predictor variable (see

Table 4-7) will not work for our data set, especially if the standardized beta-coefficient for ΔT from MLR analysis is large.

The weak to strong negative correlations of TC with V_{sh} observed on the full data set (Fig. 4-6d) are generally comparable to the results of Brigaud and Vasseur (1989), who obtained similar results for sandstones of variable clay content. Also the TC-V_{sh} data scatter of the Ketzin samples and of the shaly rocks of Sahlin and Middleton (1997) are similar. Sahlin and Middleton (1997) found no obvious prediction trend for bulk TC for shales and claystones, which they explained by the large range of TC of clay minerals. On the contrary, V_{sh} is important for each of the deduced bulk-TC equations in this study [Eqs. (4-11), (4-12), (4-13), and (4-14)] and for matrix TC calculated for clastic and carbonate rocks [Eqs. (4-8), (4-9), and (4-10)], respectively.

The negative correlation between TC and ϕ_N (Fig. 4-6f) has not yet been widely discussed in the literature. As the analysis of the (matrix) TC-ϕ_N interrelation indicates a nonlinear behavior for the group of major minerals itself, quartz-dominated rock compositions consistently generate this range of negative correlations.

The photoelectric factor was suggested by many authors (*e.g.*, Sahlin and Middleton, 1997; Doveton et al., 1997; Goutorbe et al., 2006) to be a valuable predictor variable. Our observation however delineate both positive and negative correlations with TC (Fig. 4-6a) making it questionable to include this variable into prediction equations for clastic rocks. In addition, following Fig. 4-3c, the correlation between TC and P_e in carbonate-mudstone systems strongly depends on the major carbonate and clay minerals, respectively. All in all, P_e may be more useful for the discrimination between the major depositional groups than as predictor variable in MLR analysis.

In general, different types of electrical resistivity logs are commonly available in deep wells. Thus, the implementation of this petrophysical property would be an attractive option to enlarge the application range of the proposed method. However, the method presented herein based on reliable and largely invariant log-response values of the selected minerals. Following the data of Serra (1984), that cannot be assumed for the most important minerals selected in this work (*cf.* the large resistivity range of quartz, calcite, and halite, respectively). Depending on the chosen reference value the correlation of matrix resistivity with matrix TC might be positive, negative or neutral for the same composition. Thus, the resistivity log was not considered in this study.

4.5 *Validation*

4.5.1 Comparison of calculated and measured TC data

The validation of the prediction equations for TC of clastic rocks by comparison of calculated and measured TC values is made on the validation data set (Fig. 4-1). Matrix TC values are calculated from equations (4-9) and (4-10) (Table 4-4) for carbonates and clastic rocks and transposed to water-saturated bulk TC using the geometric-mean model (Eq. 4-4) and log values of effective porosity. In addition, bulk TC values are calculated using equation (4-11) (developed for clastic rocks independent

of rock type) and using equations (4-12) – (4-14) (developed for single rock types/geological formations).

In general, the calculated TC values mimic very well the trends of TC changes along geological sections (Fig. 4-7). Bulk TC calculated from equation (4-10) for the Stuttgart Fm. match well measured bulk TC, but slightly overestimate those layers exhibiting a low hydrogen index. The quantification of error (Fig. 4-8) shows that the misfit due the hydrogen index (deviations of > 50%) pertains only to < 8% of the data. Bulk TC values calculated from equation (4-11) slightly underestimate measured TC in the Wealden Fm. especially in the layers with high hydrogen index values. The RMS value of the bulk TC values predicted by equations (4-10) – (4-14) for sections shown in Fig. 4-7 (full data set) is between 0.24 and 0.41 W/(m·K). This error is comparable to the values noted by Hartmann et al. (2005). The lowest RMS value was achieved for the Middle Buntsandstein [Eq. 4-14: 9.8%; Eq. 4-10: 7.8%] of homogeneous composition and the highest for the heterogeneous Stuttgart Fm. [Eq. 4-13: 12.5%; Eq. 4-10: 28%], respectively.

Although it was originally assumed that empirical equations for the calculation of TC are valid only for the geological formations for which they were determined (*e.g.*, Goss and Combs, 1975; Evans, 1977; Molnar and Hodge, 1982; Blackwell, 1989; Hartmann et al., 2005), the results from using equation (4-10) (Fig. 4-7) seem to be valid for all formations analyzed in this study. This can be explained by the use of an artificial data set for model development. Thus it is likely to assume that equation (4-10) also can be successfully applied for any clastic rock. The use of such an artificial data set in combination with MLR is different to other approaches (*e.g.*, Goutorbe et al., 2006), which favor nonlinear techniques such as neural networks as ultimate technique for 'universal' TC estimations.

DOI: 10.2312/GFZ.b103-13111

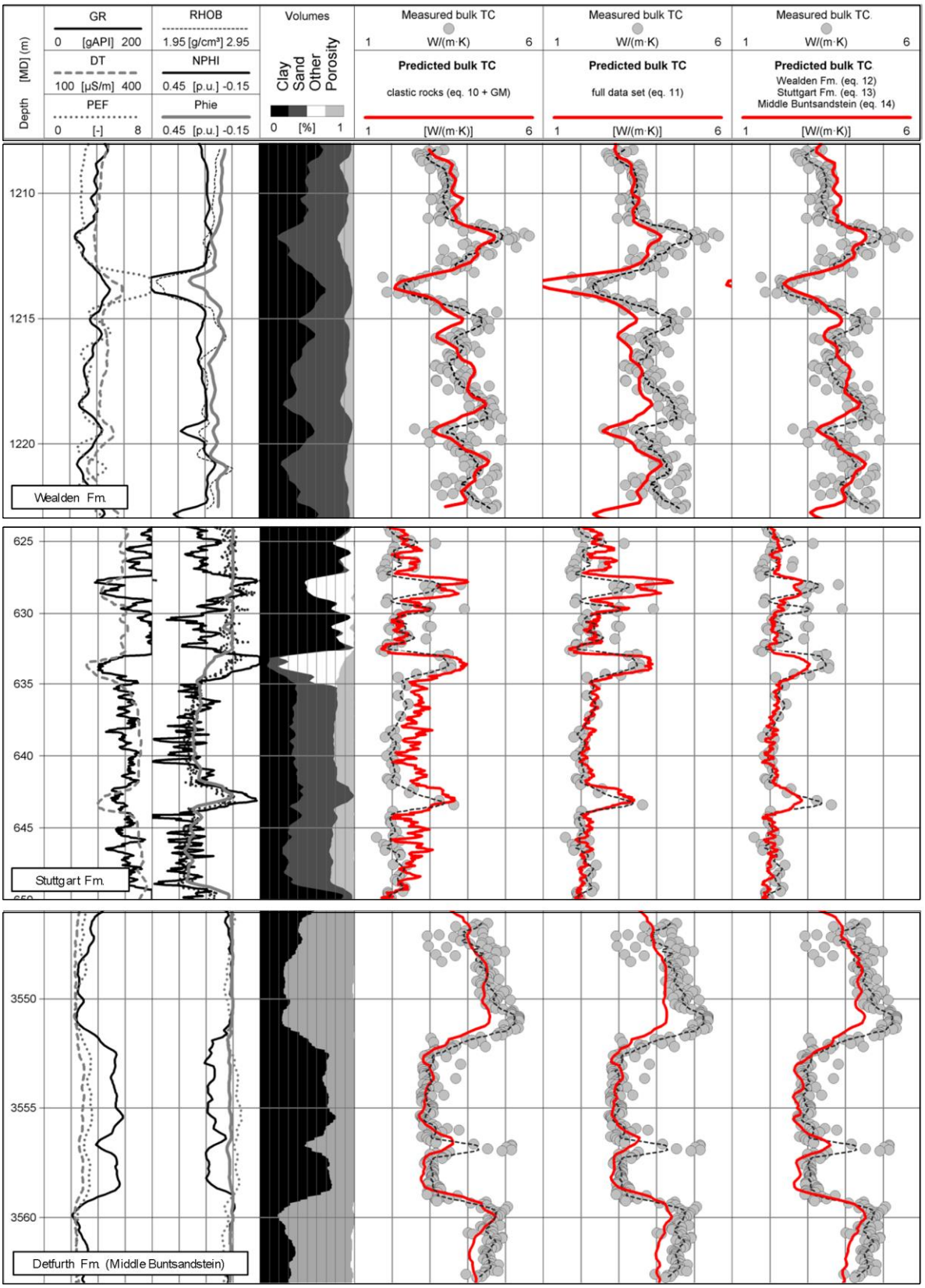

Figure 4-7 Comparison of well-log based TC (three right tracks). Predicted bulk TC (red line) vs. laboratory-measured bulk TC (measured values: grey dots, moving average (1m): dashed line) for three selected well sections. For abbreviations see the Appendix (Section 4.10).

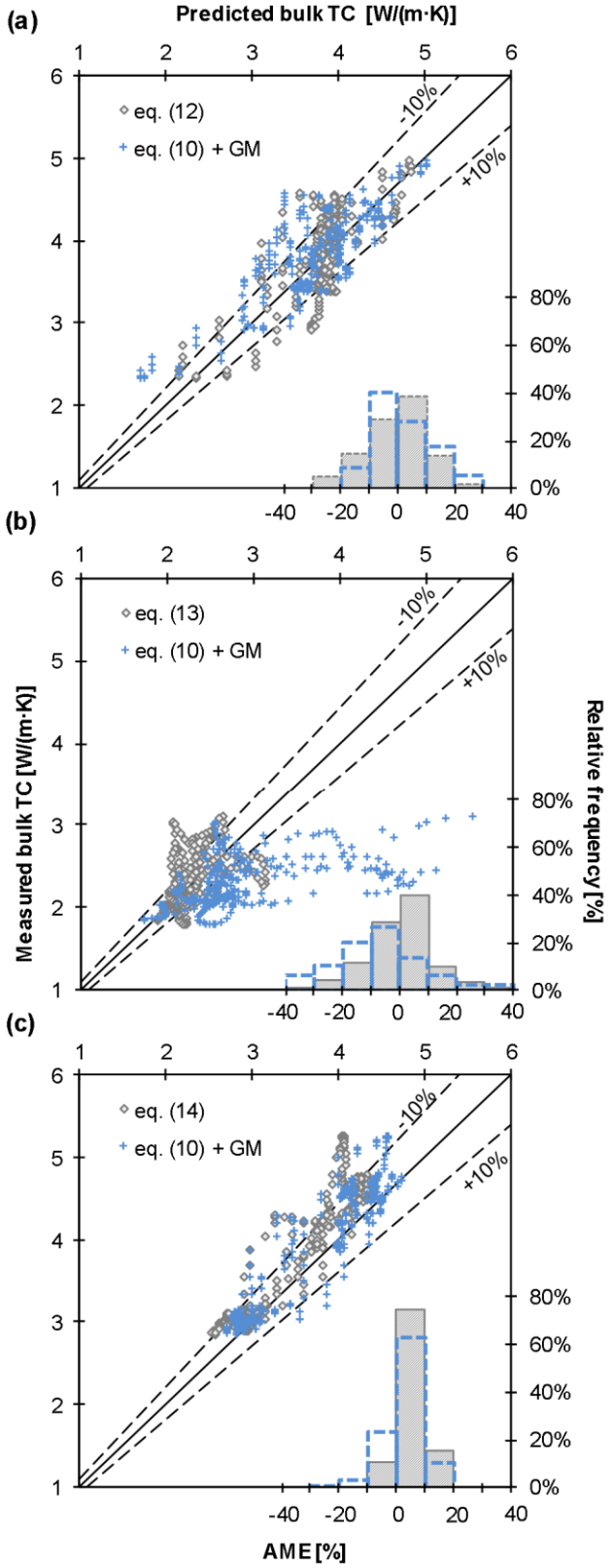

The validation of the matrix TC equation for carbonates was made against the Doveton et al. (1997) data. The data set consists of matrix values for density and sonic transit time, gamma ray and calculated total porosity as well as bulk TC (originally published by Blackwell and Steele, 1989). The AME value between measured and predicted bulk TC is 22 ± 13% [Eq. (4-9)], which is comparable to the error (AME: 19 ± 16%) that would stem from the application of the Doveton et al. (1997) TC-prediction equation.

Both error estimates are acceptable, given the uncertainties linked with the original data (TC measurements on cuttings using the chip technique described by Sass et al., 1971, sampling in 10-ft intervals, log-depth matching, up-scaling, etc.) Indeed, significantly smaller prediction errors could be achieved if equation (4-9) would be applied to a data set of higher quality.

For both equations, ρ_{ma} and V_{sh} have the largest impact on TC prediction in carbonate-shale systems. All in all, more data would be useful to further verify prediction equations developed in this paper for both carbonate and evaporite rocks.

4.5.2 Comparison of calculated and measured temperature profiles

The value of any predictive TC equation must be based on its ability to reproduce the thermal characteristics of a section logged by a high-resolution temperature device to within an acceptable error tolerance (Doveton et al., 1997). We assume that an

Figure 4-8 Scatter plots of predicted vs. measured bulk TC. (a) Wealden Fm., (b) Stuttgart Fm., and (c) Middle Buntsandstein. The histogram shows the distribution (right y-axis) of percent errors (lower x-axis) between measured and predicted bulk TC [crosshatched bars; Eqs. (4-12) – (4-14), see Table 4-5] and for combination of theoretically derived matrix TC equations and geometric mean [dashed-bordered, unfilled bars; Eq. (4-10), see Table 4-4].

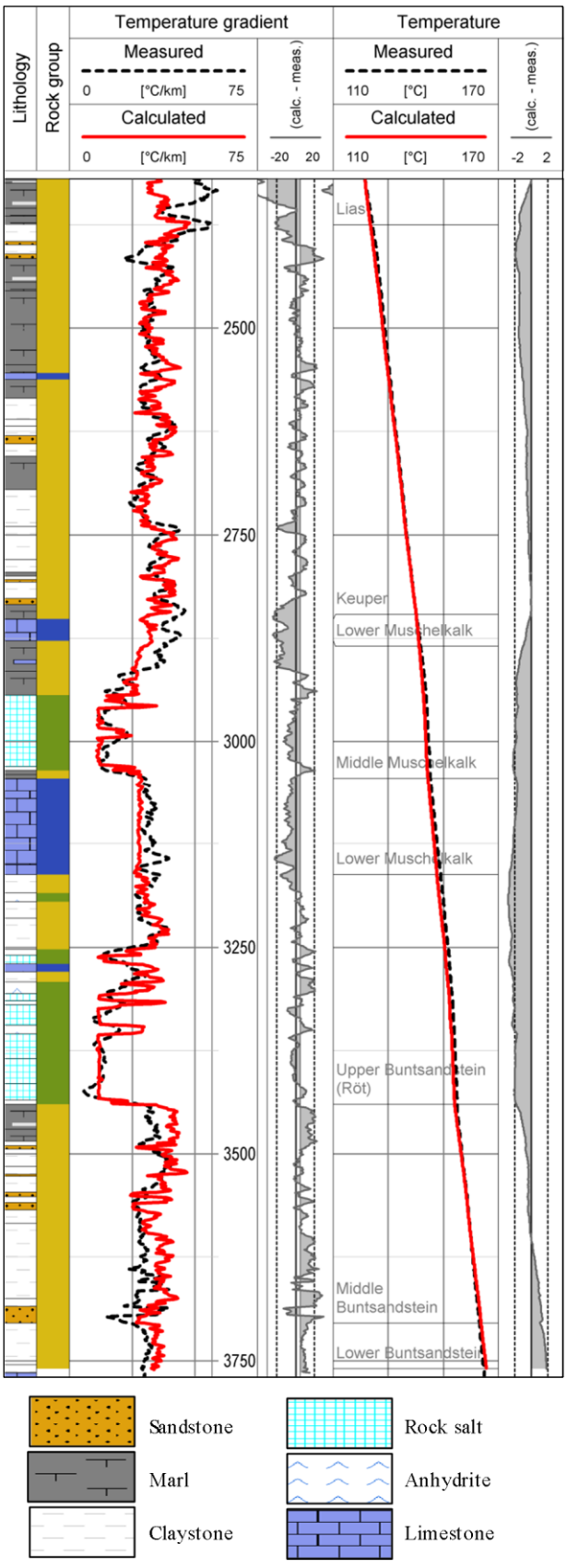

acceptable error would be on the order of < 5%, which is < 1.5 K/km for an average temperature gradient of 30 K/km and < 2 K/km for a gradient of 40 K/km, respectively.

For both borehole locations in the NGB (Fig. 4-5), high-precision temperature logs are available (Hannover location: Orilski et al., 2010) that are processed as temperature-gradient plots and compared with temperature gradients calculated from predicted TC.

The temperature logs were measured at 0.01 m recording intervals; the logging systems had a precision of 0.001 K. The logs were obtained at least one year after borehole completion, and thus are regarded as to reproduce thermal borehole equilibrium.

For the calculation of full borehole TC profiles a differentiation between various types of sedimentary rock into evaporite, carbonate, and clastic rock is made using standard lithology mapping techniques (*e.g.*, Asquith and Gibson, 1982; Serra, 1984). *In-situ* bulk TC then is calculated according to equations (4-7), (4-8), and (4-10). In addition, the universal equation [Eq. (4-11)] is applied to intervals of clastic rock. The computation was performed for borehole sections of approx. 630 m length at the Ketzin location and of approximately 1.7 km length at the Hannover site. The predicted TC values are corrected for *in-situ* temperature and pressure.

The predicted TC profiles are used together with a site-specific value of surface heat flow to calculate temperature-gradient profiles according to Fourier's law of heat conduction [Eq. (4-25)]:

$$gradT = \frac{q}{TC}, \qquad (25)$$

Figure 4-9 Comparison of measured and calculated temperature and temperature gradients. Depth in meters. Lithology is from drill core and cutting analysis as well as from well-log interpretation. Rock-group classification is a simplification of lithology consisting of clastic (yellow), carbonate (blue) and evaporites (green).

where *gradT* is the temperature gradient, *q* is heat flow and *TC* is thermal conductivity.

For the Ketzin site a heat-flow value of 70 mW/m² was determined using measured laboratory values of TC that were pressure and temperature corrected. For the Hannover site, a value of 82 mW/m² was used (Orilski et al., 2010).

The theoretical temperature-gradient plots for the two sites fully reflect the lithological pattern changes of the sedimentary succession. There is also a good agreement in absolute values between measured and calculated temperature-gradient plots. At the Hannover site, differences in the temperature gradients obtained for the four intervals (Middle Keuper: 2 460–2 540 m, Middle Muschelkalk: 2 960–3 040 m, Upper Buntsandstein: 3 165–3 250 m, Middle Buntsandstein: 3,440–3,590 m) are on the order of < 2 K/km (Fig. 4-9). For the Ketzin site, similar results are observed (Table 4-6). The maximum difference in absolute temperature (measured vs. calculated, Fig. 4-9) on both sites is < 0.8 K and < 1.3 K. This yields an average error in absolute temperature of 2.4% (Hannover location) and 5.8% (Ketzin location). The error is within the threshold of accepted prediction accuracy.

Table 4-6 Comparison of logged and computed temperature inverted from bulk TC profiles.

Well	#	Depth interval			Logged T			Predicted T		Error	
		top	bottom	length	top	bottom	Δ	bottom	Δ	Interval	Total
		m	m	m	°C	°C	°C	°C	°C	%	°C/km
Ketzin 200/07	1	168.0	775.0	607.0	17.12	39.68	22.56	40.99	+ 1.31	5.8	2.2
Hannover	1	1172.0	1363.0	191.0	69.24	76.02	6.78	75.57	- 0.45	6.6	2.4
	2	1642.0	1743.5	101.5	87.05	91.07	4.02	90.27	- 0.8	19.9	7.9
	3	2321.5	3748.0	1426.5	121.55	164.38	42.83	164.61	+ 0.23	0.5	0.2
			total length:	1719.0 m					**mean:**	**4.4%**	**1.6 °C/km**

Temperature was predicted starting in each interval from top downwards. $\Delta_{predicted\ T}$ is the difference between the bottom-logged and bottom-predicted temperature value. The interval error was calculated as quotient of $\Delta_{predicted\ T}$ and $\Delta_{logged\ T}$. The total error was calculated as quotient of $\Delta_{predicted\ T}$ and the length of the depth interval.

4.6 *Evaluation of previous approaches*

None of the previously published prediction equations seems to be valid universally for all types of sedimentary rocks. As the last comprehensive comparison work in this field dates back to Goss and Combs (1975) and the current state of knowledge on the applicability and prediction quality of other data sets is poor, it is timely to evaluate in this work the validity of the available prediction equations on a defined data set comprising clastic rock of the NGB.

Owing to the results of theoretical analysis performed in this paper, simple linear regression equations considering just one predictor variable were excluded from the evaluation. Also excluded are those equations that have not fully disclosed the regression coefficients (*e.g.*, Sahlin and Middleton, 1997; Goutorbe et al., 2006), equations in which matrix TC values were assumed (*e.g.*, Griffiths et al., 1992), and approaches, which included well-logs not considered in this study (*e.g.*, Khandelwal, 2010). Thus the comparison of TC prediction includes equations from Tikhomirov (1968), Goss et al. (1975), Goss and Combs (1976), Evans (1977), Vacquier et al. (1988), and Hartmann et al. (2005).

Table 4-7 Selected previously published TC prediction equations.

Author	TC Prediction Equation[2]	Lithotpye[3]	R^2	n	RMS W/(m·K)	AME %	SD W/(m·K)	comment	eq.
Tikhomirov (1968)[1]	$\lambda_b = (1.3\exp(0.58\,\rho_b + 0.4\,WAT)) / 2.388$	*SS, CS, LS*	0.6	139	*n.a.*	*n.a.*	*n.a.*	- dry/partially saturated rocks from different authors	(4-15)
Goss et al. (1975)[1]	$\lambda_b = 1.34 - 2.55\,\phi_N + 0.38\,V_P$	*SiS, GW, SS (cemented)*	0.9	39	*n.a.*	10	0.29	- TC range: 1.46–3.35, 24°C, 20 MPa uniax., data from Imperial Valley of Southern California	(4-16)
Goss and Combs (1976)[1]	$\lambda_b = 0.842 - 3.978\,\phi_N + 0.695\,V_p$	*SiS, GW, SS (cemented)*	0.9	25/14	*n.a.*	10	0.29	- TC range: 1.2–4.2, 29°C, 7 MPa uniax., cutting samples, Mesozoic sediments, North Sea Basin	(4-17)
Evans (1977)	$\lambda_b = -4.9\,\phi_N - 0.160\,V_p + 3.6\,\rho_b - 5.5$	*SS,SiS, SH, LI, MA, DO, AN*	0.8	39(191)	*n.a.*	5-10	*n.a.*		(4-18)
Vacquier et al. (1988)[1]	$\lambda_b = -0.845 - 2.91\,(1/V_p) + 1.8\,\rho_b + 1.714\,(1/\phi_N)^2 - 3.23\,V_{sh}$	*SS*	0.30	25	*n.a.*	14.7	0.38		(4-19)
	$\lambda_b = 1.955 - 0.3\,(1/V_p) - 0.37\,\rho_b + 3.139\,(1/\phi_N)^2 - 1.369\,V_{sh}$	*SH, M*	0.30	6	*n.a.*	12.1	0.27	- TC range: 1–3, core samples, Eocene and Cretaceous (Parisian Basin), Triassic and Jurassic (Aquitaine Basin)	(4-20)
	$\lambda_b = -3.43 + 3.67\,(1/V_p) + 0.72\,\rho_b + 7.04\,(1/\phi_N)^2 - 1.218\,V_{sh}$	*SS,SSH*	0.50	42	*n.a.*	9.7	0.31		(4-21)
	$\lambda_b = 9.15 - 5.116\,(1/V_p) - 2.663\,\rho_b + 1.915\,(1/\phi_N)^2 - 0.5\,V_{sh}$	*mixtures*	0.66	20	*n.a.*	16.2	0.77		(4-22)
Hartmann et al. (2005)	$\lambda_b = 1.07 + 0.239\,V_p + 0.504\,\rho_b + 0.042\,\phi_N$	*SSS*	*n.a.*	>100	0.12	*n.a.*	*n.a.*	- TC range: 2.5–3.7, cutting samples (Molasse Basin)	(4-23)
	$\lambda_b = -0.22 + 0.243\,V_p + 0.913\,\rho_b + 1.11\,\phi_N$	*SS,DO, LI*	*n.a.*	>100	0.17	*n.a.*	*n.a.*		(4-24)

[1] Equations were reformulated to standard units (conversion see Appendix A; Section 4.10). [2] TC was measured under laboratory conditions (20°C, 0.1 MPa), otherwise, it is noted above. [3] Lithological abbreviations (e.g. SS, CS, LS) are described in Appendix A (Section 4.10). Statistical paprameters are taken from the original literature.

Equations were reformulated to SI-units if necessary and listed in Table 4-7. In addition, the inverse method was applied, which derives the lithology or major mineralogy of rocks from well logs (Savre, 1963; Quirein et al., 1968; Doveton and Cable, 1979), and, in turn, applies an appropriate mixing equation to calculate bulk TC for the respective lithotype using textbook TC values (*e.g.*, Merkel et al., 1976; Dove and Williams, 1989; Brigaud et al., 1990; Demongodin, et al., 1991; Vasseur et al., 1995; Midttømme et al., 1997; Hartmann et al., 2005).

Bulk TC, calculated by implementing the well-log parameters of the NGB into these approaches is compared to measured TC, and the deviations are quantified as a prediction error (Fig. 4-10). The smallest prediction error is achieved by using equation (4-11) (this study) (AME: 11 ± 10%) and by applying the matrix-TC equation [Eq. (4-13), AME: 16 ± 15%] and the geometric-mean model. Both equations show a similar structure by using ϕ_N and V_{sh} as predictor variables and by avoiding the problematic ρ_b and ΔT.

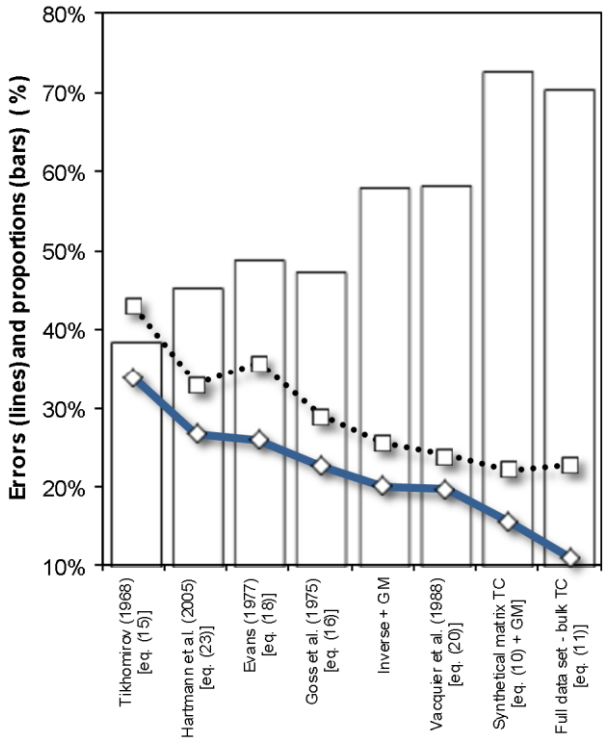

Figure 4-10 Comparison of results from different prediction methods. Relative AME (blue solid line), relative RMS (black dotted line), bars represent proportion of deviations less than 20%.

Agreements of less quality are achieved for the full data of clastic rock by application of the Vacquier et al. (1988) equation [Eq. (4-20); AME: 20 ± 13%] developed for argillaceous rocks. Equations (4-19), (4-21), and (4-22) (also from Vacquier et al., 1988) show better agreements for selected lithotypes only. For example, equation (4-19) shows valid results only for sandstone of the Middle Buntsandstein (AME: 8 ± 6%), and equation (4-21) for interbedded sandstone and argillaceous rock of the Wealden Fm. (AME: 15 ± 24%). The observed AME values fit into the range originally provided by these authors. Surprisingly, the equation proposed to be valid for mixtures of clastic and carbonate rocks (Eq. 4-22) completely fails on our data set.

Application of a simple inverse model, consisting of four components (clay, sand, carbonate, and porosity), on the full data set results in an AME of 20 ± 16% (Fig. 4-10). Application of an advanced inverse model to the Stuttgart Fm., consisting of nine components derived from elemental log analysis and detailed core analysis (Norden et al., 2010), results in a much lower AME value of 9 ± 12%. However, it is expected, that in situations of less data on the formation mineralogy and petrography, the use of such a multi-component advanced model may cause larger errors. Indeed, the quality of the predicted TC is directly related to the prediction quality of the component volume fractions (Hartmann et al., 2005).

DOI: 10.2312/GFZ.b103-13111

The application of the approaches of Tikhomirov (1969, Eq. 4-15), Goss et al. (1975, Eq. 4-16), Goss and Combs (1976, Eq. 4-17), Evans (1977, Eq. 4-18), and Hartmann et al. (2005, Eqs. 4-23 and 4-24) show reasonable agreements (AME: < 15%, RMS: < 20%) only for the low-porosity sandstone samples of the Middle Buntsandstein, but failed completely for all other litho-stratigraphical units (AME: > 23%, RMS > 30%). None of these presented equations shows an acceptable match for the full data set of clastic rocks. This could result from the implementation of sonic velocity and/or bulk density into the equations as predictor variables, for which strongly varying correlations were observed for the NGB data set (Fig. 4-6).

4.7 *Conclusion*

(1) Standard well-log data (bulk density, natural gamma-ray, sonic interval transit time, hydrogen index, and photoelectric factor) and petrophysical descriptors derived from these are obviously not able to sufficiently reflect and explain the TC variability of an artificial 'global data set' of sedimentary rocks. Thus we conclude that no universally valid TC-prediction equation can be developed with standard well-log data and regression techniques.

(2) However, a subdivision into clastic, carbonate and evaporite rocks resulted in individual equations that predict matrix TC with a high accuracy (AME: between 4 and 11%). Volume fraction of shale (carbonate and clastic rocks), matrix hydrogen index (evaporite and clastic rocks) and matrix density (carbonate and evaporite) predominantly show the largest potential as predictor variable, while sonic and photoelectric factor log often provide no additional explained variance. By combining the results of these equations [Eqs. (4-7), (4-8), (4-9), and (4-10)], entire borehole profiles can be calculated for sedimentary successions with an error on average < 9.2%. In this approach, knowledge of single lithotypes or mineral composition is dispensable. We recommend to use the equations (Table 4-4) that are fully based on matrix log-response values for predicting matrix TC of borehole profiles.

(3) The approach of using subsurface data (well logs and measured TC) restricted to clastic rocks results in a suggestion to delineate bulk-TC-prediction equations for different geological formations representing a typical composition of different lithotypes. Formation-specific equations show slightly smaller prediction uncertainties (AME: between 5 and 9%), than the equation developed for the available, full subsurface data set of clastic rocks (AME: 11%). For bulk TC prediction of clastic rocks, hydrogen index and volume fraction of shale show the largest potential as predictor variable. Bulk density and sonic-log data are questionable input parameters and even the implementation of the photoelectric factor log provides no advantage for reducing the errors. We recommend the use of formation-specific bulk TC equations as developed in this paper for TC prediction in formations that are similar to those described in this study. Although afflicted with some error, equation (4-11) seems to be a good approximator for clastic rocks in general.

(4) All presented prediction equations show better prediction capabilities than any other previously published approach.

(5) Computed borehole TC profiles may be used as prerequisites for the calculation of temperature profiles with high accuracy (< 5% error). This opens up new opportunities, *e.g.*, (i) to quantify the

paleoclimatic effect on a local scale; to estimate the heat-flow density (ii) in the absence of detailed temperature logs; and (iii) by using bottom-hole temperature (BHT) measurements; and (iv) to validate temperature maps provided by web-based geothermal information systems.

(6) More work is needed to extend the multi-mineral rock composition approach to crystalline rocks.

4.8 Acknowledgments

This work was performed in the framework of the German GeoEn (Verbundvorhaben GeoEnergie-Forschung) project (www.geoen.de). The GeoEn project was funded by the Federal Ministry of Education and Research (BMBF) in the program 'Spitzenforschung und Innovation in den Neuen Ländern'. We are grateful to Ben Norden (GFZ Potsdam, Potsdam) and the Leibniz Institute for Applied Geophysics (LIAG) in Hannover for providing background data from boreholes, logging data, and core material.

4.9 References

Abdulagatova, Z.Z., Abdulagatov, I.M. and Emirov, S.N. (2009). Effect of temperature and pressure on the thermal conductivity of sandstone. *International Journal of Rock Mechanics and Mining Sciences* 46, 1055–1071.

Abdulagatova, Z.Z., Abdulagatov, I.M. and Emirov, S.N. (2010). Effect of pressure, temperature, and oil-saturation on the thermal conductivity of sandstone up to 250 MPa and 520 K. *Journal of Petroleum Science and Engineering* 73(1–2), 141–155.

Anand, J., Somerton, W.H. and Gomaa, E. (1973). Predicting thermal conductivities of formations from other known properties *Society of Petroleum Engineers Journal* 13(5), 267–272.

Asquith, G.B. and Gibson, C.R. (1982). Basic Well Log Analysis for Geologists. American Association of Petroleum Geologists, Tulsa, Oklahoma, 216 pp.

Balling, N., Kristiansen, J., Breiner, N., Poulsen, K.D., Rasmusen, R. and Saxov, S. (1981). Geothermal measurements and subsurface temperature modelling in Denmark. *Geologiske Skrifter* 16(1), 172.

Beck, A.E. (1965). Techniques of Measuring Heat Flow on Land. *In:* W. H. K. Lee (Ed.): Terrestrial Heat Flow, 24–57, Am. Geophys. Union, Washington D.C.

Beziat, A., Dardaine, M. and Mouche, E. (1992). Measurements of the thermal conductivity of clay-sand and clay-graphite mixtures used as engineered barriers for high-level radioactive waste disposal. *Applied Clay Science* 6(4), 245–263.

Birch, F. (1960). The velocity of compressional waves in rocks to 10 kilobars, part 1. *Journal of Geophysical Research* 65(4), 1083–1102.

Birch, F. (1961). The velocity of compressional waves in rocks to 10 kilobars, part 2. *Journal of Geophysical Research* 66(7), 2199–2224.

Blackwell, D.D. and Steele, J.L. (1989). Thermal Conductivity of Sedimentary Rocks; Measurement and Significance. *In:* Naeser, N.D. and McCulloh, T.H. (Eds.), Thermal History of Sedimentary Basins, Methods and Case Histories, Springer, New York, pp. 13–35.

Brigaud, F., Chapman, D.S. and Le Douaran, S. (1990). Estimating thermal conductivity in sedimentary basins using lithologic data and geophysical well logs. *AAPG Bulletin* 74(9), 1459–1477.

Brigaud, F. and Vasseur, G. (1989). Mineralogy, porosity and fluid control on thermal conductivity of sedimentary rocks. *Geophysical Journal International* 98(3), 525–542.

Bullard, E.C. and Day, A. (1961). The fow of heat through the floor of the Atlantic Ocean. *Geophysical Journal of the Royal Astronomical Society* 4(S 1), 282–292.

Buntebarth, G. (1991). Thermal properties of KTB Oberpfalz VB core samples at elevated temperature and pressure. *Scientific Drilling* 2(2–3), 73–80.

Čermák, V. (1967). Coefficient of thermal conductivity of some sediments and its dependence on density and water content of rocks. *Chemie Der Erde-Geochemistry* 26(–), 271–278.

Čermák, V. and Rybach, L. (1982). Thermal Conductivity and Specific Heat of Minerals and Rocks. *In:* M. Beblo, A. Berktold, U. Bleil, H. Gebrande, B. Grauert, U. Haack, V. Haak, H. Kern, H. Miller, N. Petersen, J. Pohl, F. Rummel and J. R. Schopper (Eds.): Landolt-Bornstein Numerical Data and Functional Relationships in Science and Technology, New Series, Group V, Geophysics and Space Research. Geophysics - Physical Properties of Rocks, 305–343, Springer, Berlin.

Crain, E.R. (2013). Crains petrophysical handbook. url: http://www.spec2000.net, last accessed: 12.04.2013

Dachnov, V.N. and Djakonov, D.J. (1952). Thermal Investigation of Fissures (in Russian, Термические исследования скважин). Gostoptehizdat (Гостоптехиздат), Leningrad (Ленинград), 214 pp.

Della Vedova, B. and Von Herzen, R.F. (1987). Geothermal Heat Flux at the COST B-2 and B-3 Wells, U. S. Atlantic Continental Margin. Woods Hole Oceanographic Institution, Woods Hole, Massachusetts, 79 pp.

Demongodin, L., Pinoteau, B., Vasseur, G. and Gable, R. (1991). Thermal conductivity and well logs: a case study in the Paris Basin. *Geophysical Journal International* 105(3), 675–691.

Dewan, J.T. (1983). Essentials of Modern Open-Hole Log Interpretation. PennWell Books, Tulsa, Oklahoma, 361 pp.

Dove, R.E. and Williams, C.F. (1989). Thermal conductivity estimated from elemental concentration logs. *Nuclear Geophysics* 3(2), 107–112.

Doveton, J.H. (1986). Log Analysis of Subsurface Geology: Concepts and Computer Methods. Wiley-Interscience, New York, 273 pp.

Doveton, J.H., Förster, A. and Merriam, D.F. (1997). Predicting thermal conductivity from petrophysical logs: a Midcontinent Paleozoic case study. *Proceedings of the International Association for Mathematical Geology, Annual Meeting 1997*, Barcelona, 212–217 pp.

Doveton, J.H. and Cable, H.W. (1979). Fast matrix methods for the lithological interpretation of geophysical logs. *Computers &. Geology* 3(–), 101–116.

Evans, T.R. (1977). Thermal properties of North Sea rocks. *Log Analyst* 18(2), 3–12.

Feldrappe, H., Obst, K. and Wolfgramm, M. (2008). Die mesozoischen Sandsteinaquifere des Norddeutschen Beckens und ihr Potential für die geothermische Nutzung. *Zeitschrift für geologisch Wissenschaften* 36(4–5), 199–222.

Fertl, W.H. and Frost Jr., E. (1980). Evaluation of shaly clastic reservoir rocks. *Journal of Petroleum Technology* 32(9), 1641–1646.

Förster, A., Norden, B., Zinck-Jørgensen, K., Frykman, P., Kulenkampff, J., Spangenberg, E., Erzinger, J., Zimmer, M., Kopp, J., Borm, G., Juhlin, C., Cosma, C.-G. and Hurter, S. (2006). Baseline characterization of the CO2SINK geological storage site at Ketzin, Germany. *Environmental Geosciences* 13(3), 145–161.

Förster, A., Schöner, R., Förster, H.J., Norden, B., Blaschke, A.W., Luckert, J., Beutler, G., Gaupp, R. and Rhede, D. (2010). Reservoir characterization of a CO_2 storage aquifer: The Upper Triassic Stuttgart Formation in the Northeast German Basin. *Marine and Petroleum Geology* 27(10), 2156–2172.

Fuchs, S. and Förster, A. (2010). Rock thermal conductivity of mesozoic geothermal aquifers in the Northeast German Basin. *Chemie Der Erde-Geochemistry* 70(S 3), 13–22.

Fuchs, S., Schütz, F., Förster, H.-J. and Förster, A. (2013). Evaluation of common mixing models for calculating bulk thermal conductivity of sedimentary rocks: correction charts and new conversion equations. *Geothermics* 47, 40–52.

Gegenhuber, N. and Schön, J. (2012). New approaches for the relationship between compressional wave velocity and thermal conductivity. *Journal of Applied Geophysics* 76, 50–55.

Goss, R.D. and Combs, J. (1976). Thermal Conductivity Measurement and Prediction from Geophysical Well Log Parameters with Borehole Application, Final Report, Institute for Geosciences, University of Texas at Dallas, NSF/RA–760364, 31 pp.

Goss, R.D., Combs, J. and Timur, A. (1975). Prediction of thermal conductivity in rocks from other physical parameters and from standard geophysical well logs. *Proceedings of the SPWLA 16th Annual Logging Symposium*, 1975, 21 pp.

Goutorbe, B., Lucazeau, F. and Bonneville, A. (2006). Using neural networks to predict thermal conductivity from geophysical well logs. *Geophysical Journal International* 166(1), 115–125.

Griffiths, C.M., Brereton, N.R., Beausillon, R. and Castillo, D. (1992). Thermal conductivity prediction from petrophysical data: a casestudy. *Geological Society, London, Special Publications* 65(1), 299–315.

Gröber, H., Erk, S. and Grigull, U. (1955). Die Grundgesetze der Wärmeübertragung. Springer, Berlin, 465 pp.

Hartmann, A., Pechnig, R. and Clauser, C. (2008). Petrophysical analysis of regional-scale thermal properties for improved simulations of geothermal installations and basin-scale heat and fluid flow. *International Journal of Earth Sciences* 97(2), 421–433.

Hartmann, A., Rath, V. and Clauser, C. (2005). Thermal conductivity from core and well log data. *International Journal of Rock Mechanics and Mining Sciences* 42(7–8), 1042–1055.

Hesshaus, A., Heinig, S., Kringel, R. and Röhling, H.-G. (2010). GeneSys Hannover - Hydrochemische und petrographische Untersuchungen an der Geothermiebohrung Groß Buchholz GT1. *Proceedings of the Geothermiekongress 2010*, Karlsruhe, 17.-19. November 2010, 10 pp.

Horai, K.-I. (1971). Thermal conductivity of rock-forming minerals. *Geophysical Research Letters* 76(5), 1278–1308.

Horai, K.-I. and Simmons, G. (1969). Thermal conductivity of rock-forming minerals. *Earth and Planetary Science Letters* 6(5), 359–368.

Houbolt, J.J.H.C. and Wells, P.R.A. (1980). Estimation of heat flow in oil wells based on a relation between heat conductivity and sound velocity. *Geologie en Mijnbouw / Netherlands Journal of Geosciences* 59(3), 215–224.

Hübner, W., Hunze, S., Baumgarten, H., Orilski, J. and Wonik, T. (2012). Petrophysical and sedimentary petrographic characterisation of the Bückeburg Formation (German Wealden) in the geothermal well Groß Buchholz Gt-1 (Hanover, Germany). *Zeitschrift der Deutschen Gesellschaft für Geowissenschaften* 163(4), 483–492.

Hurtig, E. and Brugger, H. (1970). Wärmeleitfähigkeitsmessung unter einaxialem Druck. *Tectonophysics* 10(1–3), 67–77.

Karl, R. (1965). Gesteinsphysikalische Parameter (Schallgeschwindigkeit und Wärmeleitfähigkeit). *Freiberger Forschungshefte* C197, 7–76.

Khandelwal, M. (2010). Prediction of thermal conductivity of rocks by soft computing. *International Journal of Earth Sciences* 100(6), 1383–1389.

Kukkonen, I.T. and Peltoniemi, S. (1998). Relationships between thermal and other petrophysical properties of rocks in Finland. *Physics and Chemistry of the Earth* 23(3), 341–349.

Lemmon, E.W., McLinden, M.O. and Friend, D.G. (2005). Thermophysical properties of fluid systems. NIST Chemistry WebBook, NIST Standard Reference Database 69, 20899 pp.

Lichtenecker, K. (1924). Der elektrische Leitungswiderstand künstlicher und natürlicher Aggregate. *Physikalische Zeitschrift* 25(8), 169–181, 193–204, 226–233.

Lovell, M.A. (1985). Thermal conductivity and permeability assessment by electrical resistivity measurements in marine sediments. *Marine Geotechnology* 6(2), 205–240.

Lovell, M.A. and Ogden, P. (1984) Remote Assessment of Permeability/thermal Diffusivity of Consolidated Clay Sediments: Final Report. Commission of the European Communities, Directorate-General Science, Research and Development, Luxembourg, 168 pp.

Merkel, R.H., Maccary, L.M. and Chico, R.S. (1976). Computer techniques applied to formation evaluation. *Log Analyst* 17(3), 3–10.

Midttømme, K., Roaldset, E. and Aagaard, P. (1997). Thermal Conductivity of Argillaceous Sediments. *In:* D. M. McCann, M. Eddleston, P. J. Fenning and G. M. Reeves (Eds.): Modern Geophysics in Engineering Geology, 355-363, Geological Society Engineering Geology,

Moiseyenko, U.I., Sokolova, L.S. and Istomin, V.E. (1970). Electrical and Thermal Properties of Rocks (in Russian: Elektricheskiye i teplovyye svoystva gornykh porod v usloviyakh normalnykh i vysokikh temperatur i davleniy). Epaminond Ėpaminondovič Fotiadi, Novosibirsk, Russia, 59 pp.

Molnar, P.S. and Hodge, D. (1982). Correlation of thermal conductivity with physical properties obtained from geophysical well logs. *Proceedings of the AAPG Annual Convention with Divisions SEPM/EMD/DPA*, Calgary, AB, Canada, June 27–30, 1982, 608–609 pp.

Norden, B. and Förster, A. (2006). Thermal conductivity and radiogenic heat production of sedimentary and magmatic rocks in the Northeast German Basin. *AAPG Bulletin* 90(6), 939–962.

Norden, B., Förster, A., Vu-Hoang, D., Marcelis, F., Springer, N. and Le Nir, I. (2010). Lithological and Petrophysical Core-Log Interpretation in CO2SINK, the European CO2 Onshore Research Storage and Verification Project. *SPE Reservoir Evaluation & Engineering* 13(2), 179-192.

Orilski, J., Schellschmidt, R. and Wonik, T. (2010). Temperaturverlauf und Wärmeleitfähigkeit im Untergrund der Bohrung Groß Buchholz GT1 in Hannover. *Proceedings of the Geothermiekongress 2010*, Karlsruhe, 17.-19. November 2010, 10 pp.

Özkahraman, H.T., Selver, R. and Işık, E.C. (2004). Determination of the thermal conductivity of rock from P-wave velocity. *International Journal of Rock Mechanics and Mining Sciences* 41(4), 703–708.

Popov, Y., Romushkevich, R., Korobkov, D., Mayr, S., Bayuk, I., Burkhardt, H. and Wilhelm, H. (2011). Thermal properties of rocks of the borehole Yaxcopoil-1 (Impact Crater Chicxulub, Mexico). *Geophysical Journal International* 184(2), 729–745.

Popov, Y., Tertychnyi, V., Romushkevich, R., Korobkov, D. and Pohl, J. (2003). Interrelations between thermal conductivity and other physical properties of rocks: Experimental data. *Pure and Applied Geophysics* 160(5–6), 1137–1161.

Popov, Y.A., Pribnow, D.F.C., Sass, J.H., Williams, C.F. and Burkhardt, H. (1999). Characterization of rock thermal conductivity by high-resolution optical scanning. *Geothermics* 28(2), 253–276.

Poulsen, K.D., Saxov, S., Balling, N. and Kristiansen, J.I. (1981). Thermal conductivity measurements on Silurian limestones from the Island of Gotland, Sweden. *Geologiska Foreningen i Stockholm Forhandlingar* 103(3), 349–356.

Pribnow, D., Williams, C.F. and Burkhardt, H. (1993). Well log-derived estimates of thermal conductivity in crystalline rocks penetrated by the 4-KM deep KTB Vorbohrung. *Geophysical Research Letters* 20(12), 1155–1158.

Quirein, J., Kimminau, S., La Vigne, J., Singer, J. and Wendel, F. (1986). A coherent framework for developing and applying multiple formation evaluation models. *Proceedings of the SPWLA 27th Annual Logging Symposium*, 09–13 June 1986, 17 pp.

Röhling, H.-G. and Heinig, S., 2012. Lithostratigraphie und Petrographie des Mittleren Buntsandsteins in der Geothermiebohrung Groß Buchholz Gt1 und der Bohrung Hämelerwald Z1. *Erdöl Erdgas Kohle*, 128(4), 144–153.

Sahlin, T. and Middleton, M.F. (1997). Correlation of thermal conductivity with well log derived petrophysical parameters. Proceedings of the Second Nordic Symposium on Petrophysics, Reykjavík, Orkustofnun, 263–281 pp.

Sass, J.H., Lachenbruch, A.H. and Munroe, R.J. (1971). Thermal conductivity of rocks from measurements on fragments and its application to heat-flow determinations. *Journal of Geophysical Research* 76(14), 3391–3401.

Savre, W.C. (1963). Determination of a more accurate porosity and mineral composition in complex lithologies with the use of the sonic, neutron and density Surveys. *Journal of Petroleum Technology* 15(9), 945–959.

Schäfer, F., Hesshaus, A., Hunze, S., Jatho, R., Luppold, F.-W., Orilski, J., Pletsch, T., Röhling, H.G., Tischner, T. and Wonik, T. (2012). Kurzprofil der Geothermiebohrung Groß Buchholz Gt 1. *Erdöl Erdgas Kohle* 128(1), 20–26.

Schön, J. (1983). Petrophysik. Physikalische Eigenschaften von Gesteinen und Mineralien. Enke Ferdinand, Stuttgart, 405 pp.

Schön, J.-H. (1996). Physical Properties of Rocks, Fundamentals and Principles of Petrophysics. *In:* K. Helbig and S. Treitel (Eds.): Handbook of Geophysical Exploration: Seismic Exploration, vol. 18, Pergamon, Oxford, UK, 583 pp.

Seipold, U. and Huenges, E. (1998). Thermal properties of gneisses and amphibolites - high pressure and high temperature investigations of KTB-rock samples. *Tectonophysics* 291(1–4), 173–178.

Serra, O. (1984). Fundamentals of Well-Log Interpretation - The Acquisition of Logging Data. Elsevier, Amsterdam - Oxford - New York - Tokyo, 423 pp.

Simmons, G. (1964a). Velocity of compressional waves in various minerals at pressures to 10 kilobars. *Journal of Geophysical Research* 69(6), 1117–1121.

Simmons, G. (1964b). Velocity of shear waves in rocks to 10 kilobars, 1. *Journal of Geophysical Research* 69(6), 1123–1130.

Singh, R., Bhoopal, R.S. and Kumar, S. (2011). Prediction of effective thermal conductivity of moist porous materials using artificial neural network approach. *Building and Environment* 46(12), 2603–2608.

Singh, T.N., Sinha, S. and Singh, V.K. (2007). Prediction of thermal conductivity of rock through physico-mechanical properties. *Building and Environment* 42(1), 146–155.

Somerton, W.H. (1992). Thermal Properties and Temperature-Related Behavior of Rock/Fluid Systems. Elsevier Science Publishers B.V., Amsterdam, 257 pp.

Sundberg, A. (2002). Determination of Thermal Properties at Äspö HRL. Comparison and Evaluation of Methods and Methodologies for Borehole KA 2599 G01. SKB Rapport Report: SKB R-02-27, Stockholm, 73 pp.

Sundberg, J., Back, P.-E., Ericsson, L.O. and Wrafter, J. (2009). Estimation of thermal conductivity and its spatial variability in igneous rocks from in situ density logging. *International Journal of Rock Mechanics and Mining Sciences* 46(6), 1023–1028.

Thornton, W.M. (1924). CI. The thermal conductivity of solid electric insulators.—II. *Philosophical Magazine Series 6* 48(288), 1054–1056.

Tikhomirov, V.M. (1968). The thermal conductivity of rocks and its relationship to density, moisture content, and temperature (in Russian: Теплопроводность горных пород и ее связь с плотностью, влажностью и температурой). *Neftânoe Hozâjstvo (Нефтяное хозяйство)* 46(4), 36–40.

Vacquier, V. (1985). The measurement of thermal conductivity of solids with a transient linear heat source on the plane surface of a poorly conducting body. *Earth and Planetary Science Letters* 74(2–3), 275–279.

Vacquier, V., Mathieu, Y., Legendre, E. and Blondin, E. (1988). Experiment on estimating thermal conductivity of sedimentary rocks from oil well logging. *AAPG Bulletin* 72(6), 758–764.

Vasseur, G., Brigaud, F. and Demongodin, L. (1995). Thermal conductivity estimation in sedimentary basins. *Tectonophysics* 244(1–3), 167–174.

Von Herzen, R. and Maxwell, A.E. (1959). The measurement of thermal conductivity of deep-sea sediments by a needle-probe method. *Journal of Geophysical Research* 64(10), 1557–1563.

Walsh, J.B. and Decker, E.R. (1966). Effect of pressure and saturating fluid on the thermal conductivity of compact rock. *Journal of Geophysical Research* 71(12), 3053–3061.

Western Atlas International (1992). Log Interpretation Charts, Houston.

Western Atlas International (1995). Introduction to Wireline Log Analysis, Houston, 312 pp.

Whitney, D.L. and Evans, B.W. (2010). Abbreviations for names of rock-forming minerals. *American Mineralogist* 95(1), 185–187.

Williams, C.F. and Anderson, R.N. (1990). Thermophysical properties of the Earth's crust: In situ measurements from continental and ocean drilling. *Journal of Geophysical Research* 95(6), 9209–9236.

Woodside, W. and Messmer, J.H. (1961). Thermal conductivity of porous media. II. Consolidated rocks. *Journal of Applied Geophysics* 32(9), 1699–1706.

Wyllie, M.R.J., Gregory, A.R. and Gardner, G.H.F. (1958). An experimental investigation of factors affecting elastic wave velocities in porous media. *Geophysics* 23(3), 459–493.

Zamora, M., Dung, V.T., Bienfait, G. and Poirier, J.P. (1993). An empirical relationship between thermal conductivity and elastic wave velocities in sandstone. *Geophysical Research Letters* 20(16), 1679–1682.

Zierfuss, H. and van der Vliet, G. (1956). Laboratory measurements of heat conductivity of sedimentary rocks. *AAPG Bulletin* 40(10), 2475–2488.

4.10 Appendix A: Nomenclature

Subscripts:

b	bulk
fl	fluid
i	index of point
ma	matrix
maa	apparent matrix
max	maximum
mea	measured
min	minimum
ND	neutron–density
p	pore
sh	shale
z	depth level

Litho:

AS	anhydrite
CS	claystone
DO	dolomite
GW	greywacke
LI	limestone
M	mudstone
MA	marlstone
SH	shale
SiS	siltstone
SS	sandstone
SSH	sandy shale
SSS	shaly sandstone

Statistics:

AM	arithmetic mean
AME	arithmetic mean error
B_{si}	standardized beta coefficients for input variable i
CV	coefficient of variation
d_f	degree of freedom
F	F-value
n	number of samples
p	significance level
RMS	root mean square error
R^2	coefficient of determination
SD	standard deviation
T	tolerance

Well logging:

ANN	artificial neural networks
ΔT	sonic interval transit time (DT), [µs/m]
γ	(natural) gamma ray (GR), [API]
gradT	temperature gradient, [K/km]
MLR	multiple linear regression
NLR	nonlinear regression

DOI: 10.2312/GFZ.b103-13111

ϕ_D	density porosity, [p.u.]
ϕ_e	effective porosity (Phie), [p.u.]
ϕ_N	neutron porosity (hydrogen index, NPHI), [p.u.]
ϕ_S	sonic porosity, [p.u.]
ϕ_t	total porosity, [p.u.]
p	pressure, [MPa]
P_e	photoelectric factor log, [pe]
ρ_b	bulk density (RHOB), [g/cm³]
ρ_m	matrix density (RHOM), [g/cm³]
SLR	simple linear regression
T	temperature, [°C; K]
U	photoelectric absorption index, [barns/cm³]
VP	sonic velocity, [km/s]
V_{sh}	volume fraction of shale, [-]
WAT	water content, [-]

Conversion:

Thermal conductivity	1 W/(m·K)	=	2.388 mcal/(cm·s·K)
		=	0.578 Btu/(hr·ft·F)
Sonic interval transit time	1 µs/ft	=	304.799 km/s

DOI: 10.2312/GFZ.b103-13111

4.11 Appendix B: Matrix-TC equations for variable well-log combinations

Matrix-thermal-conductivity-prediction equations													Validation					
		Regression coefficients						Artificial data set								Subsurface data set		
Eq.	No. of logs	const.	Predictor variables / Log combinations					Regression set				Testing set			All samples			
		b_0	RHO.ma	PHIN.ma	U.ma	DT.ma	V_{SH}	R^2	F	p	T^1	AME	SD	RMS	AME	SD	RMS
		[-]	[g/cm³]	[-]	[barns/cm³]	[µs/m]	[-]	[-]				[%]	[%]	[%]	[%]	[%]	[%]
Evaporites								*n = 41*				*n = 10*					
-		-	VSH is not correlated to the set of evaporite rocks														
A1	1	5.527		-10.48				0.665	80.47	<0.001	1.00	19.2%	12.7%	22.7%			
A2	1	-0.213			0.41			0.145	7.785	0.01	1.00	45.4%	44.6%	62.0%			
A3	1	-3.200				0.043		0.533	46.73	<0.001	1.00	37.7%	55.1%	64.5%			
4-7	2	14.060	-3.38	-10.35				0.922	237.4	<0.001	1.00	7.0%	5.6%	8.8%			
A4	2	8.584	-3.35		0.39			0.383	13.41	<0.001	1.00	40.4%	58.5%	68.7%			
A5	2	-24.667	5.43			0.086		0.647	37.70	<0.001	0.18	30.5%	32.3%	43.2%			
A6	2	5.477		-10.46	0.00			0.656	39.21	<0.001	0.76	19.2%	12.8%	22.7%	no data available		
A7	2	-0.193		-8.26		0.031		0.913	210.7	<0.001	0.89	10.0%	7.4%	12.2%			
A8	2	-4.849			0.20	0.040		0.557	26.18	<0.001	0.90	34.2%	51.5%	59.6%			
A9	3	14.403	-3.38	-10.52	-0.03			0.920	155.3	<0.001	0.41	7.0%	5.4%	8.6%			
A10	3	9.438	-2.31	-9.64		0.010		0.923	160.3	<0.001	0.09	7.6%	6.0%	9.5%			
A11	3	-25.030	5.56		-0.02	0.087		0.638	24.48	<0.001	0.11	30.1%	31.2%	42.3%			
A12	3	0.893		-8.84	-0.11	0.032		0.919	152.4	<0.001	0.73	8.4%	6.5%	10.4%			
A13	4	8.108	-1.83	-9.71	-0.07	0.015		0.923	121.5	<0.001	0.08	7.3%	5.5%	9.0%			
Carbonates								*n = 2,252*				*n = 562*					
A14	1	-5.983	3.60					0.285	897.2	<0.001	1.00	15.3%	13.7%	20.5%			
A15	1	4.195		-7.44				0.349	1208	<0.001	1.00	15.1%	11.4%	18.9%			
A16	1	3.599			-0.03			0.004	9.265	0	1.00	19.0%	15.4%	24.4%			
A17	1	10.537				-0.039		0.480	2076	<0.001	1.00	12.4%	8.5%	15.0%			
A18	1	4.785					-2.88	0.702	5306	<0.001	1.00	9.2%	6.8%	11.5%			
A19	2	-2.139	2.37	-5.63				0.451	927.3	<0.001	0.83	13.8%	10.3%	17.2%			
A20	2	-11.369	6.85		-0.37			0.589	1614	<0.001	0.57	12.8%	10.9%	16.8%			
A21	2	7.968	0.70			-0.035		0.485	1061	<0.001	0.52	12.3%	8.5%	15.0%			
4-9	2	5.058	-0.10				-2.92	0.702	2654	<0.001	0.58	9.2%	6.8%	11.5%			
A22	2	5.324		-8.31	-0.12			0.406	769.7	<0.001	0.92	14.5%	12.4%	19.1%			
A23	2	9.472		-2.14		-0.032		0.492	1092	<0.001	0.45	12.3%	8.5%	14.9%			
A24	2	4.782		4.55			-3.92	0.741	3229	<0.001	0.30	8.3%	6.7%	10.6%			
A25	2	15.673			-0.27	-0.055		0.706	2701	<0.001	0.75	9.9%	7.6%	12.5%			
A26	2	6.913			-0.22		-3.46	0.872	7639	<0.001	0.86	6.9%	5.6%	8.9%			
A27	2	-0.683				0.035	-4.87	0.755	3474	<0.001	0.14	8.7%	6.4%	10.8%			
A28	3	-7.507	5.63	-5.75	-0.37			0.763	2417	<0.001	0.51	10.1%	7.3%	12.4%	no data available		
A29	3	5.656	0.98	-2.57		-0.025		0.503	759	<0.001	0.27	12.2%	8.4%	14.8%			
A30	3	6.780	-0.73	5.14			-4.30	0.747	2221	<0.001	0.19	8.0%	6.7%	10.4%			
A31	3	3.733	3.88		-0.39	-0.039		0.835	3804	<0.001	0.39	7.4%	5.4%	9.2%			
4-8	3	-0.550	3.09		-0.33		-2.73	0.952	14892	<0.001	0.38	4.2%	3.2%	5.3%			
A32	3	-2.947	0.63			0.039	-4.86	0.760	2372	<0.001	0.12	9.2%	6.9%	11.5%			
A33	3	15.255		-0.71	-0.27	-0.052		0.707	1812	<0.001	0.35	9.9%	8.2%	12.9%			
A34	3	6.995		5.25	-0.23		-4.68	0.924	9110	<0.001	0.28	5.3%	4.6%	7.0%			
A35	3	-1.591		5.52		0.041	-6.46	0.812	3239	<0.001	0.09	7.5%	6.1%	9.7%			
A36	3	5.288			-0.21	0.010	-3.96	0.875	5238	<0.001	0.11	7.2%	5.9%	9.2%			
A37	4	2.084	4.05	-1.88	-0.39	-0.031		0.845	3060	<0.001	0.26	7.9%	5.9%	9.9%			
A38	4	0.838	2.54	3.44	-0.32		-3.66	0.972	19500	<0.001	0.18	3.1%	2.9%	4.2%			
A39	4	-1.573	-0.01	5.53		0.041	-6.46	0.812	2428	<0.001	0.09	7.5%	6.1%	9.7%			
A40	4	-3.145	3.18		-0.31	0.014	-3.45	0.959	13111	<0.001	0.11	4.0%	3.0%	5.0%			
A41	4	4.389		5.55	-0.21	0.015	-5.56	0.932	7700	<0.001	0.09	4.9%	4.7%	6.8%			
A42	5	-2.206	2.59	3.73	-0.29	0.017	-4.61	0.982	24473	<0.001	0.08	2.4%	2.8%	3.7%			
Clastics								*n = 21,617*				*n = 5404*					
A43	1	-3.684	2.53					0.110	2676	<0.001	1.00	20.8%	15.3%	25.8%	19.5%	13.6%	29.9%
A44	1	4.171		-16.47				0.585	30498	<0.001	1.00	14.1%	11.0%	17.9%	25.2%	65.9%	79.6%
A45	1	4.126			-0.14			0.072	1667	<0.001	1.00	21.4%	15.3%	26.3%	21.1%	12.9%	40.2%
A46	1	12.532				-0.051		0.312	9819	<0.001	1.00	17.9%	13.1%	22.2%	45.0%	77.3%	88.7%
A47	1	4.783					-3.38	0.688	47759	<0.001	1.00	11.8%	9.3%	15.0%	15.4%	11.1%	35.0%
A48	2	-2.889	2.70	-16.69				0.711	26531	<0.001	1.00	11.5%	8.8%	14.5%	26.5%	85.3%	97.4%
A49	2	-10.721	6.61		-0.44			0.509	11199	<0.001	0.58	15.4%	12.3%	19.7%	26.8%	38.3%	108.5%
A50	2	8.691	1.12			-0.046		0.331	5343	<0.001	0.87	17.8%	13.2%	22.2%	41.7%	75.0%	84.9%
A51	2	3.385	0.52				-3.29	0.692	24337	<0.001	0.89	11.7%	9.2%	14.9%	15.4%	12.0%	36.2%
A52	2	3.371		-19.20	0.12			0.621	17715	<0.001	0.69	13.2%	10.0%	16.5%	27.4%	81.0%	88.6%
A53	2	8.031		-13.94		-0.022		0.627	18174	<0.001	0.75	13.0%	10.0%	16.4%	33.0%	97.1%	97.6%
4-10	2	5.281		-2.96			-2.80	0.430	1336	<0.001	0.55	11.4%	9.1%	14.7%	15.7%	15.8%	22.3%
A54	2	12.995			-0.11	-0.049		0.352	5884	<0.001	0.99	17.1%	12.9%	21.4%	44.5%	72.9%	83.9%
A55	2	4.901			-0.02		-3.35	0.689	23980	<0.001	0.92	11.8%	9.3%	15.0%	15.5%	11.1%	36.9%
A56	2	0.308				0.027	-4.33	0.719	27641	<0.001	0.36	11.5%	9.5%	14.9%	17.9%	19.5%	89.8%
A57	3	-4.913	3.78	-14.11	-0.12			0.725	19016	<0.001	0.29	11.2%	8.8%	14.3%	24.9%	78.7%	100.4%
A58	3	-1.224	2.50	-15.93		-0.006		0.713	17940	<0.001	0.61	11.7%	9.2%	14.9%	28.4%	92.4%	98.0%
A59	3	-0.092	1.75	-10.10			-1.45	0.730	19441	<0.001	0.15	10.8%	8.6%	13.8%	19.0%	50.2%	65.9%
A60	3	6.770		-16.54	0.10	-0.018		0.649	13340	<0.001	0.50	12.5%	9.9%	15.9%	31.5%	105.3%	105.4%
A61	3	4.454		-6.18	0.04		-2.46	0.703	17076	<0.001	0.17	11.3%	9.0%	14.4%	17.2%	26.9%	43.3%

Matrix-TC-prediction equations												Validation					
		Regression coefficients						Artificial data set							Subsurface data set		
Eq.	No. of logs	const.	Predictor variables / Log combinations					Regression set				Testing set			All samples		
		b_0	RHO.ma	PHIN.ma	U.ma	DT.ma	V_{SH}	R^2	F	p	T^1	AME	SD	RMS	AME	SD	RMS
		[-]	[g/cm³]	[-]	[barns/cm³]	[µs/m]	[-]	[-]				[%]	[%]	[%]	[%]	[%]	[%]
A62	3	0.528		-0.63		0.025	-4.18	0.719	18441	<0.001	0.09	11.0%	8.6%	13.9%	16.8%	18.2%	83.7%
A63	3	0.287			0.00	0.027	-4.34	0.719	18427	<0.001	0.32	11.4%	9.3%	14.7%	17.9%	19.4%	89.4%
A64	3	-2.358	0.81			0.029	-4.29	0.729	19335	<0.001	0.35	10.9%	8.4%	13.7%	18.5%	20.3%	93.4%
A65	3	-4.294	5.35		-0.37	-0.020		0.539	8418	<0.001	0.38	14.6%	11.3%	18.5%	32.2%	55.0%	75.3%
A66	3	-0.096	2.16		-0.14		-2.70	0.713	17897	<0.001	0.30	11.3%	9.1%	14.6%	16.9%	17.9%	58.3%
A67	4	-3.872	3.61	-13.81	-0.11	-0.004		0.726	14325	<0.001	0.28	11.2%	8.5%	14.0%	26.1%	83.0%	97.2%
A68	4	-2.119	2.76	-8.78	-0.10		-1.27	0.739	15328	<0.001	0.15	10.6%	8.6%	13.7%	18.8%	49.8%	74.7%
A69	4	-2.336	1.48	-6.44		0.018	-2.73	0.738	15232	<0.001	0.06	10.7%	8.5%	13.6%	14.3%	17.5%	77.9%
A70	4	-5.336	2.31		-0.13	0.028	-3.70	0.746	15867	<0.001	0.25	10.5%	8.4%	13.4%	20.4%	23.7%	112.9%
A71	4	0.569		-1.19	0.01	0.024	-4.09	0.719	13842	<0.001	0.07	11.1%	8.5%	14.0%	16.6%	18.0%	79.7%
A72	5	-4.917	2.58	-4.47	-0.11	0.020	-2.70	0.750	12986	<0.001	0.06	10.4%	8.2%	13.3%	15.4%	18.3%	96.3%

[1] For equations with more than 3 predictor variables, the lowest tolerance value is noted. For statistics see Section 4.3.3, for abbreviations see Section 4.10.

DOI: 10.2312/GFZ.b103-13111

5 Synthesis

5.1 *Main Results and Discussion*

Each of the first-author manuscripts that are part of this thesis concentrates either on a specific issue, such as the determination of rock TC of Mesozoic sediments in the Northeast German Basin (Manuscript 1), the evaluation of the prediction quality of two-component mixing models (Manuscript 2), or the development of new well-log based TC-prediction equations (Manuscript 3). Here, in a chronological order a synthesis of the most important results is presented.

The analysis of thermal and petrophysical rock properties was successfully applied on sedimentary drill cores obtained from eight deep boreholes from the major Mesozoic aquifers in the NEGB. Those aquifers (especially the Aalenian, the Rhaethian-Liassic Complex, the Stuttgart Fm. and the Middle Buntsandstein) are of paramount interest as hydro-geothermal exploration target in the NGB. This study presents for the first time a well-documented set of TC measurements on drill-core samples (mostly on sandstone samples) obtained from these target horizons. Average bulk TC of sandstones corrected for *in-situ* thermal conditions varies between 2.1 ± 0.11 (Stuttgart Formation) and 3.9 ± 0.27 W/(m·K) (Rhaethian). Excluding the influence of the porosity (range: 16% - 30%), the TC of the rock matrix ranges widely between 3.4 (Stuttgart Fm.) and 7.4 W/(m·K) (Postera Fm.). This range reflects the mineralogical diversity within sandstone samples of different formations. The reported TC data expands on earlier work on Permian and Permo-Carboniferous samples from Lotz (2004) and Norden et al. (2006), respectively. Our studies displaced the results of earlier thermal investigations by Hurtig and Schlosser (1975, 1976), *in toto*. These previously studies were heretofore used for the parameterization of thermal models in the NGB (*e.g.*, Bayer et al., 1997; Clauser et al., 2003; Noack et al., 2010; Kaiser et al., 2011; Noack et al., 2012), but show large uncertainties. These uncertainties are caused by incomplete methodologies in the TC determination (*e.g.*, ignoring the pore-filling fluid, temperature and pressure dependence; sample depth and borehole locations are not reported; published TC values are often lithotype mean values ordered by their stratigraphic system). Thus, TC data for Mesozoic rocks presented for the first time in this work (the full data set is documented in the appendix), together with data from Norden et al. (2006), form a robust new database for thermal modeling in the NEGB.

Moreover, significant changes in the bulk and matrix TC are detected in relation to the drilling location within the basin. While changes in matrix TC reflects changes in the lithological and/or mineralogical composition, changes in bulk TC may be caused by changes in porosity. For example, the average TC values for sandstone samples of Postera and Contorta are higher in the Schwerin boreholes [3.9 ± 0.08 W/(m·K) and 3.8 ± 0.18 W/(m·K)] than in the Neubrandenburg boreholes [3.3 ± 0.27 W/(m·K) (kCs) and 3.4 ± 0.39 W/(m·K)]. The differences in TC could reflect regionally different facies and mineralogy in the formations (*e.g.*, Norden et al., 2006; Norden et al., 2012; Schütz et al., 2013).

The average interval heat flow are 74 ± 5 mW/m² and 78 ± 5 mW/m² for the Gt Ss 1/85 borehole and Gt Ss 2/85 borehole, respectively. All calculated interval heat-flow values are within 8% and 4% of the

mean value, respectively. By regarding the radiogenic heat production in the overburden, the resulting average surface heat-flow density is in the order of 78 mW/m², which is in good agreement with previously reported mean values for the NEGB of approx. 77 mW/m² (Norden et al., 2008).

In turn, based on the calculated surface heat-flow density and temperature log information, *in-situ* bulk TC was indirectly calculated for the entire borehole profiles at the Stralsund location. Formation *in-situ* bulk TC values, calculated as the average value from the TC log for different Cenozoic and Mesozoic stratigraphical intervals, ranges from 1.5 ± 0.3 (Toarcian, mostly claystones) to 3.1 ± 0.4 W/(m·K) (Hardegsen, mostly sandstones). The calculated formation values presented herein offer an excellent foundation for the detailed parameterization of small-scale (local) thermal models, for which facies-induced changes are mostly of negligible importance. However, applying these locally derived data to other parts of the NGB is questionable, considering a detailed analysis of the spatial TC variation within the NGB by Schütz et al. (2013). These authors demonstrated that the use of average formation TCs in large-scale thermal models may cause errors in the depth prediction of approx. 500 m for the 70 °C isotherm and of approx. 1,000 m for the 120 °C isotherm. Beyond the limited availability of drill-core and temperature measurements, this further requires a much more detailed vertical and lateral resolution of thermal rock properties across the sedimentary succession of the NGB.

Such an increased TC data resolution was achieved through the application of continuous standard petrophysical well-logs. New well-log based TC-prediction equations were developed following two different approaches. The first approach is based on the comprehensive statistical analysis of the interrelations of TC and other petrophysical properties of 15 rock-forming minerals that are most abundant in sedimentary rocks. These analyses reveal the large inhomogeneity of the interrelations between different petrophysical properties and TC and underline the importance of constant (unchanging) correlation trends for the deduction of suitable prediction equations. Matrix-TC-prediction equations were calculated separately for the three major sedimentary rock types, *i.e.* clastic, carbonate, and evaporite rocks, applying multivariate regression analysis on large artificial data sets of rock compositions. The most valuable input parameters are the volume fraction of shale, the matrix hydrogen index and the matrix density. The error of matrix TC prediction is on the order of 4.5 ± 3.7% (carbonates), 8.2 ± 7.1% (clastic rocks), 8.4 ± 8.9% (evaporites). These equations are not affected by restrictions, commonly associated with empirical prediction equations published earlier (*e.g.*, regional or lithotype-specific limitations).

The second approach includes the development of classical empirical prediction equations for bulk TC using conventional petrophysical well logs (*e.g.*, volume fraction of shale, hydrogen index, sonic interval transit time) and TC values measured on drill cores sampled from four deep wells in the NGB. The most valuable input parameters for bulk TC prediction are the volume fraction of shale and the hydrogen index. Although, density and sonic velocity are often used as predictor variables (*e.g.*, Vacquier, 1988; Doveton et al., 1997; Hartmann et al., 2005), they were neglected in this study due to the puzzling effect of porosity changes on their correlation to TC. The equations predict bulk TC with an average error between 5.5 ± 4.1% (clean sandstones of low porosity; Middle Buntsandstein), 8.9 ± 5.4% (interbedding of sandstone, silt- and claystones; Wealden) and 9.4 ± 11% (shaly sandstones; Stuttgart Fm.). An equation including all clastic rock data yields an average error of 11 ± 10%.

DOI: 10.2312/GFZ.b103-13111

The subsurface data set was used to validate the prediction equation for matrix TC established for clastic rocks. Comparing of bulk TC computed from the matrix TC values and well-log porosities, to measured bulk TC results in < 15% error. A validation of the TC prediction at borehole scale by comparing measured temperature logs and modeled temperature logs (based on the site-specific surface heat flow and the predicted TC) shows an excellent agreement in temperature. Interval temperature gradients vary on average by < 3 K/km and predicted compared to measured absolute temperature fitted with an error < 5%. Compared to previously published TC-prediction approaches, the developed matrix and bulk-TC-prediction equations show significantly higher prediction accuracy. Bulk TC ranging from 1.5 to 5.5 W/(m·K) is always predicted with an average error < 10% relative to average errors between 15 and 35% resulting from the application to our data set of the most suitable methods from literature.

In dependence on porosity and pore-filling fluid, calculation from rock bulk TC to matrix TC and vice versa needs the application of a suitable mixing model. Several models widely used in geothermal exploration (arithmetic mean, geometric mean, harmonic mean, Hashin-Shtrikman mean, and effective-medium theory mean) are evaluated statistically to examine their quality of fit on a large data set of sedimentary rocks (sandstone, mudstone, dolomite, and limestone). The analyses show that most of the evaluated mixing models predict the measured bulk TC unsatisfactorily. The geometric mean (Fig. 3-2d) show the lowest average error for both carbonate (AME: 6 ± 10%) and clastic (AME: 5 ± 17%) rocks. However, the large standard deviation indicates a high variability in prediction quality. Correction charts are calculated using multiple regression analyses that permit reduction of the deviation and scatter of the different mean models. The application of these corrections results in noticeable improvements of the fits for all mean models, on average reducing the deviations for the Hashin-Shtrikman equation by 70%, for the arithmetic mean by 59%, and for the geometric mean by another 15%. The unsatisfying fitting behavior of most mean models and the necessity of applying correction equations to achieve a mean-model result with sufficient error diffusion encouraged us to develop conversion equations that permit the estimation of the water-saturated bulk TC directly from dry-measured bulk TC data and known porosity values. For all lithotypes, both the conversion equations and the correction equations for the mean models yield uncertainties in the bulk TC ranging from 5% to 10% (AME). These uncertainties are significantly lower than those arising from applying of the mean models without correction (range of AME: 11 – 42%).

5.2 Conclusion and Recommendations

The results of this thesis highlight the importance of suitable TC data.

- Together with Permo-Carboniferous data from Norden and Förster (2006), thermal-conductivity data of Mesozoic sediments measured and obtained in this study builds-up a nearly complete data set available for the parameterization of thermal models. Although a growing base of rock thermal conductivity studies is available for the NEGB, measured borehole sections are often limited to the potential targets of geothermal exploration. More data are needed for the nontargeted borehole sections, particularly to improve the vertical solution of thermal models.

DOI: 10.2312/GFZ.b103-13111

- Different approaches to calculate bulk TC from matrix TC and vice versa lead to significantly different results. However, the corrected mean models for bulk TC determination of two-phase rocks constitute efficient tools to transfer air-saturated bulk TC to water-saturated bulk TC, if porosity is known from independent sources (*e.g.*, derived from standard well logs). The application of model-independent conversion equations allows a calculation with an error < 10%, which is sufficient for many industrial as well as specific scientific applications.
- Standard well-log data (bulk density, natural gamma-ray, sonic interval transit time, hydrogen index, and photoelectric factor) and petrophysical descriptors derived therefrom are not able to sufficiently reflect and explain the TC variability of an artificial 'global data set' of sedimentary rocks. Based on these data, the sufficient prediction of rock TC will always fail for the global group of sedimentary rocks.
- A subdivision of the 'global data set' into clastic, carbonate and evaporite rock data allows the prediction of matrix TC with a high accuracy (error between 5 and 8%). In contrast to many other studies, the application of the matrix TC equations is not restricted to the particular local conditions in a specific basin (*e.g.*, lithotypes, type of diagenesis) and can be considered as universally applicable within these groups.
- By combining the predictions of these equations, entire borehole profiles can be calculated for sedimentary successions with an average error of < 8.5%. In this approach, knowledge of single lithotypes or mineral composition is not necessary. Computed borehole TC profiles may be used as prerequisites for the calculation of temperature profiles with high accuracy (< 5% error).
- All new developed prediction equations applied on the North-German-Basin data set show better prediction capabilities than any other previously published approach.

The approaches used and developed in this study open up a broad range of application opportunities.

- In combination with lithofacial analysis, the calculation of borehole TC profiles at different locations in a sedimentary basin allows an advanced thermal parameterization of thermal models.
- The paleoclimatic effect on the temperature and heat flow of the subsurface has been an issue of debate for years. If available under conductive conditions, the comparison between measured and calculated temperature profiles (using the presented approach) may provide a method that helps to quantify the depth-dependent paleoclimatic effect on the lateral heat-flow-density distribution in boreholes.
- The measurement of bottom-hole temperatures (BHT) is a widespread standard method for decades, especially in the oil and gas business. However, estimating temperature-gradient logs and reliable heat-flow densities are hardly possible. In boreholes with both a set of standard well-logs and corrected BHT measurements only the latter one can be used, in combination with the surface temperature as end-member temperature anchor point, for the calculation of artificial temperature profiles and reliable heat-flow values.
- Great efforts were made in the past to establish web-based temperature map services on a regional (*e.g.*, temperature maps of state geological surveys) or national scale (*e.g.*, German GeotIS: Schulz et al., 2007; Agemar et al., 2012). However, the proposed method can be used to val-

DOI: 10.2312/GFZ.b103-13111

idate the interpolated spatial temperature-depth distribution in areas with poor temperature database (*i.e.* where no unperturbed temperature logs or reservoir temperatures are available).

Resulting from the presented study, future aspects of research regarding thermal rock properties should involve the following paragraphs:

- Over the past 10 years, the fast-working, optical scanning technology has become established in laboratory investigations of both TC and thermal diffusivity, respectively. This technique works under ambient pressure and temperature conditions, which made it necessary to empirically correct the laboratory values to *in-situ* conditions. The development of quick working measurement devices regarding the *in-situ* conditions (formation and fluid pressure, temperature, saturation fluid) is necessary for a more precise and detailed parameterization of large-scaled thermal models.
- TC data presented in this study are mainly obtained on Mesozoic sandstones. More work is needed to enlarge the database for other lithotypes, in particular to explain facies-dependent changes in formation TC across the North German Basin.
- The presented approach for developing matrix-TC-prediction equations can be extended to crystalline rocks.

DOI: 10.2312/GFZ.b103-13111

References

Abdulagatova, Z.Z., Abdulagatov, I.M., Emirov, S.N. (2009). Effect of temperature and pressure on the thermal conductivity of sandstone. *International Journal of Rock Mechanics and Mining Sciences* 46(6), 1055–1071.

Agemar, T., Schellschmidt, R., Schulz, R. (2012). Subsurface temperature distribution in Germany. *Geothermics* 44(0), 65–77.

Anand, J., Somerton, W.H., Gomaa, E. (1973). Predicting thermal conductivities of formations from other known properties. *Society of Petroleum Engineers Journal* 13(5), 267–272.

Balling, N., Kristiansen, J., Breiner, N., Poulsen, K.D., Rasmusen, R., Saxov, S. (1981). Geothermal measurements and subsurface temperature modelling in Denmark. *Geologiske Skrifter* 16(1), 172.

Barth, G., Franz, M., Luppold, F.W., Wolfgramm, M. (2012). The Rhaetian fluvial-dominated deltaic system in the North German Basin: facies, controls and geothermal reservoir characteristics. *Proceedings of the GV+Sediment 2012,* Hamburg, 23.-28. September 2012, pp 1.

Bayer, U., Scheck, M., Koehler, M. (1997). Modeling of the 3D thermal field in the northeast German basin. *International Journal of Earth Sciences(Geologische Rundschau)* 86(2), 241–251.

Beck, A.E. (1965). Techniques of Measuring Heat Flow on Land. *In:* W. H. K. Lee (Ed.): Terrestrial Heat Flow, 24–57, Am. Geophys. Union, Washington D.C.

Beck, A.E., Anglin, F.M., Sass, J.H. (1971). Analysis of heat flow data — in situ thermal conductivity measurements. *Canadian Journal of Earth Sciences* 8(1), 1–19.

Beutler, G., Röhling, H.-G., Schulz, R., Werner, K.-H., Rockel, W., Becker, U., Kabus, F., Kellner, T., Lenz, G., Schneider, H. (1994). Regionale Untersuchung von geothermischen Reserven und Ressourcen in Nordwestdeutschland. Final report, Hannover, report number: 111 758, 161 pp.

Blackwell, D.D., Steele, J.L. (1989). Thermal Conductivity of Sedimentary Rocks; Measurement and Significance. *In:* N. D. Naeser and T. H. McCulloh (Eds.): Thermal History of Sedimentary Basins; Methods and Case Histories, 13–36, Springer, Berlin.

Brandt, W., Rockel, E., Lenz, G., Kellner, T. (1995). Geologischer Bericht zur Thermalwasserbohrung Gt Rheinsberg 1 (Gt RhM 1/95). Geothermie Neubrandenburg, 82 pp.

Bruggeman, D.A.G. (1935). Berechnung verschiedener physikalischer Konstanten von heterogenen Substanzen. I. Dielektrizitätskonstanten und Leitfähigkeiten der Mischkörper aus isotropen Substanzen. *Annalen der Physik* 24(5), 636–664.

Bullard, E.C., Day, A. (1961). The fow of heat through the floor of the Atlantic Ocean. *Geophysical Journal of the Royal Astronomical Society* 4(S 1), 282–292.

Buntebarth, G., Schopper, J.R. (1998). Experimental and theoretical investigations on the influence of fluids, solids and interactions between them on thermal properties of porous rocks. *Physics and Chemistry of the Earth* 23(9-10), 1141–1146.

Burkhardt, H., Honarmand, H., Pribnow, D. (1995). Test measurements with a new thermal conductivity borehole tool. *Tectonophysics* 244(1–3), 161–165.

Burkhardt, H., Troschke, B. (1998). Bestimmung von in situ Wärmeleitfähigkeiten - Abschlußbericht. 66 pp.

Clauser, C. (2006). Geothermal Energy. *In:* K. Heinloth (Ed.): Renewable Energy, 480–604, Springer, Heidelberg-Berlin.

Clauser, C., Koch, A., Hartmann, R.J., Rath, V., Wolf, A., Mottaghy, D., Pechnig, R. (2007). Erstellung statistisch abgesicherter thermischer und hydraulischer Gesteinseigenschaften füur den flachen und tiefen Untergrund in Deutschland - Phase 1 – Westliche Molasse und nördlich angrenzendes Süddeutsches Schichtstufenland. Final report, 228 pp.

Clauser, C., Vosteen, H.D., Lehmann, H., Schmidt-Mumm, A. (2003). 3-D Inversion von Temperatur und Wärmeleitfähigkeit im nordostdeutschen Sedimentbecken mit Hilfe Bayesscher inverser Parameterschätzung. Final report, 37 pp.

Dachnov, V.N., Djakonov, D.J. (1952). Thermal Investigation of Fissures (in Russian, Термические исследования скважин). Gostoptehizdat (Гостоптехиздат), Leningrad (Ленинград), 214 pp.

Della Vedova, B., Von Herzen, R.F. (1987). Geothermal Heat Flux at the COST B-2 and B-3 Wells, U. S. Atlantic Continental Margin. Woods Hole Oceanographic Institution, Woods Hole, Massachusetts, 79 pp.

Deming, D., Nunn, J.A., Jones, S., Chapman, D.S. (1990). Some problems in thermal history studies. *In:* V. F. Nuccio and C. E. Barker (Eds.): Applications of Thermal Maturity Studies to Energy Exploration, 61–80, MS-SEPM.

Doveton, J.H., Förster, A., Merriam, D.F. (1997). Predicting thermal conductivity from petrophysical logs: a Midcontinent Paleozoic case study. *Proceedings of the International Association for Mathematical Geology Annual Meeting,* Barcelona, 212–217.

Erbaş, K. (1988). Entwicklung einer Bohrlochsonde zur Bestimmung der in situ Wärmeleitfähigkeit für größere Tiefen. Final report, Deutsche Forschungsgemeinschaft, Be 331/19-1, 22 pp.

Evans, T.R. (1977). Thermal properties of North Sea rocks. *Log Analyst* 18(2), 3–12.

Feldrappe, H., Obst, K., Wolfgramm, M. (2007). Evaluation of sandstone aquifers of the North German Basin: a contribution to the „Geothermal Information System of Germany". *Proceedings of the Proceedings European Geothermal Congress 2007,* Unterhaching, Germany, 30.05 - 01.06.2007, 8 pp.

Feldrappe, H., Obst, K., Wolfgramm, M. (2008). Die mesozoischen Sandsteinaquifere des Norddeutschen Beckens und ihr Potential für die geothermische Nutzung. *Zeitschrift für geologisch Wissenschaften* 36(4–5), 199–222.

Förster, A., Schöner, R., Förster, H.J., Norden, B., Blaschke, A.W., Luckert, J., Beutler, G., Gaupp, R., Rhede, D. (2010). Reservoir characterization of a CO2 storage aquifer: The Upper Triassic Stuttgart Formation in the Northeast German Basin. *Marine and Petroleum Geology* 27(10), 2156–2172.

Franz, M. (2008). Litho- und Leitflächenstratigraphie, Chronostratigraphie, Zyklo- und Sequenzstratigraphie des Keupers im östlichen zentraleuropäischen Becken (Deutschland, Polen) und Dänischem Becken (Dänemark, Schweden). Thesis, Martin-Luther-University Halle-Wittenberg, 266 pp.

Franz, M., Wolfgramm, M. (2008). Sedimentologie, Petrologie und Fazies geothermischer Reservoire des Norddeutschen Beckens am Beispiel der Exter-Formation (Oberer Keuper, Rhaetium) NE-Deutschlands. *Zeitschrift für geologisch Wissenschaften* 36(4-5), 223–248.

Franz, M., Wolfgramm, M., Barth, G., Rauppach, K., Zimmermann, J. (2012). Triassic Geothermal Reservoirs of the North German Basin. *Proceedings of the GeoHannover 2012,* Hannover, 1 pp.

Fromme, K., Michalzik, D., Wirth, W. (2010). The geothermal potential of salt structures in Northern Germany. *Zeitschrift der Deutschen Gesellschaft für Geowissenschaften* 161(3), 323–333.

Gegenhuber, N., Schön, J. (2012). New approaches for the relationship between compressional wave velocity and thermal conductivity. *Journal of Applied Geophysics* 76(-), 50–55.

Goss, R.D., Combs, J. (1976). Thermal Conductivity Measurement and Prediction from Geophysical Well Log Parameters with Borehole Application. Final Report, Institute for Geosciences, University of Texas at Dallas, NSF/RA–760364, 31 pp.

Goss, R.D., Combs, J., Timur, A. (1975). Prediction of thermal conductivity in rocks from other physical parameters and from standard geophysical well logs. *Proceedings of the SPWLA 16th Annual Logging Symposium, 1975,* 21 pp.

Goutorbe, B., Lucazeau, F., Bonneville, A. (2006). Using neural networks to predict thermal conductivity from geophysical well logs. *Geophysical Journal International* 166(1), 115–125.

Griffiths, C.M., Brereton, N.R., Beausillon, R., Castillo, D. (1992). Thermal conductivity prediction from petrophysical data: a casestudy. *Geological Society, London, Special Publications* 65(1), 299–315.

Hanai, T. (1968). Electrical properties of emulstons. *In:* P. Sherman (Ed.): Emulsion science, Academic Press, New York.

Hartmann, A., Rath, V., Clauser, C. (2005). Thermal conductivity from core and well log data. *International Journal of Rock Mechanics and Mining Sciences* 42(7–8), 1042–1055.

Hashin, Z., Shtrikman, S. (1962). A variational approach to the theory of the elastic behaviour of multiphase materials. *Journal of Applied Physics* 33, 3125–3131.

Horai, K.-i. (1991). Thermal conductivity of Hawaiian Basalt: a new interpretation of Robertson and Peck's data. *Journal of Geophysical Research* 96, 4125–4132.

Hornamand, H. (1993). Bohrlochsonden zur Bestimmung der Wärmeleitfähigkeit in größeren Tiefen. *Akademische Abhandlungen zu den Geowissenschaften*, Thesis, Technical University of Berlin, 190 pp.

Houbolt, J.J.H.C., Wells, P.R.A. (1980). Estimation of heat flow in oil wells based on a relation between heat conductivity and sound velocity. *Geologie en Mijnbouw / Netherlands Journal of Geosciences* 59(3), 215–224.

Hurtig, E. (1968). Zum Problem der Anisotropie petrophysikalischer Parameter in geologischen Körpern. *Geophysik und Geologie* 12(3–36.

Hurtig, E., Schlosser, P. (1975). Untersuchung des terrestrischen Wärmeflusses in der DDR. *Gerlands Beitrage zur Geophysik* 84(2/3), 235–246.

Hurtig, E., Schlosser, P. (1976). Geothermal studies in the GDR and relations to the geological structure. *In:* A. Adam (Ed.): Geoelectric and geothermal studies (East-Central Europe, Soviet Asia), KAPG Geophysical Monograph, 384–394, Akademiai Kiado, Budapest, Budapest (Hungary).

Hutt, J.R., Berg, J.W. (1968). Thermal and electrical conductivities of sandstone rocks and ocean sediments. *Geophysics* 33(3), 489–500.

Hyndman, R.D., Davis, E.E., Wright, J.A. (1979). The measurement of marine geothermal heat flow by a multipenetration probe with digital acoustic telemetry and insitu thermal conductivity. *Marine Geophysical Research* 4(2), 181–205.

Kaiser, B.O., Cacace, M., Scheck-Wenderoth, M., Lewerenz, B. (2011). Characterization of main heat transport processes in the Northeast German Basin: Constraints from 3-D numerical models. *Geochemistry Geophysics Geosystems* 12(7), Q07011, doi:10.1029/2011GC003535.

Karl, R. (1965). Gesteinsphysikalische Parameter (Schallgeschwindigkeit und Wärmeleitfähigkeit). *Freiberger Forschungshefte* C197(-), 7–76.

Khandelwal, M. (2010). Prediction of thermal conductivity of rocks by soft computing. *International Journal of Earth Sciences* 100(6), 1383–-1389.

Kuriyagawa, M., Matsunaga, I., Yamaguchi, T. (1983). An in situ determination of the thermal conductivity of granitic rock. *5th ISRM Congress*, 147–150.

Lichtenecker, K. (1924). Der elektrische Leitungswiderstand künstlicher und natürlicher Aggregate. *Physikalische Zeitschrift* 25(8), 169–181, 193–204, 226–233.

Lotz, B. (2004). Neubewertung des rezenten Wärmestroms im Nordostdeutschen Becken. *Scientific Technical Report STR 04/04*, 226 pp.

Lovell, M.A. (1985). Thermal conductivity and permeability assessment by electrical resistivity measurements in marine sediments. *Marine Geotechnology* 6(2), 205–240.

Lovell, M.A. and Ogden, P. (1984) Remote Assessment of Permeability/thermal Diffusivity of Consolidated Clay Sediments: Final Report. Commission of the European Communities, Directorate-General Science, Research and Development, Luxembourg, 168 pp.

Moiseyenko, U.I., Sokolova, L.S., Istomin, V.E. (1970). Electrical and Thermal Properties of Rocks (in Russian: Elektricheskiye i teplovyye svoystva gornykh porod v usloviyakh normalnykh i vysokikh temperatur i davleniy). Epaminond Ėpaminondovič Fotiadi, Novosibirsk, Russia, 59 pp.

Molnar, P.S. and Hodge, D. (1982). Correlation of thermal conductivity with physical properties obtained from geophysical well logs. *Proceedings of the AAPG Annual Convention with Divisions SEPM/EMD/DPA*, Calgary, AB, Canada, June 27–30, 1982, 608–609 pp.

Noack, V., Cherubini, Y., Scheck-Wenderoth, M., Lewerenz, B., Höding, T., Simon, A., Moeck, I. (2010). Assessment of the present-day thermal field (NE German Basin) – Inferences from 3D modelling. *Chemie Der Erde-Geochemistry* 70(S 3), 47–62.

Noack, V., Scheck-Wenderoth, M., Cacace, M. (2012). Sensitivity of 3D thermal models to the choice of boundary conditions and thermal properties: a case study for the area of Brandenburg (NE German Basin). *Research Journal of Environmental and Earth Sciences* 67(6), 1695–1711.

Norden, B., Förster, A. (2006). Thermal conductivity and radiogenic heat production of sedimentary and magmatic rocks in the Northeast German Basin. *AAPG Bulletin* 90(6), 939–962.

Norden, B., Förster, A., Balling, N. (2008). Heat flow and lithospheric thermal regime in the Northeast German Basin. *Tectonophysics* 460(1–4), 215–229.

Norden, B., Förster, A., Behrends, K., Krause, K., Stecken, L., Meyer, R. (2012). Geological 3-D model of the larger Altensalzwedel area, Germany, for temperature prognosis and reservoir simulation. *Environmental Earth Sciences* 67(2), 551–526.

Oelsner, C., Hurtig, E. (1979). Zur geothermischen Situation im Erzgebirge. *Freiberger Forschungshefte* C350, 7–17.

Ondrak, R., Wenderoth, F., Scheck, M., Bayer, U. (1998). Integrated geothermal modeling on different scales in the Northeast German Basin. *Geologische Rundschau* 87(1), 32–42.

Özkahraman, H.T., Selver, R., Işık, E.C. (2004). Determination of the thermal conductivity of rock from P-wave velocity. *International Journal of Rock Mechanics and Mining Sciences* 41(4), 703–708.

Popov, Y., Romushkevich, R., Korobkov, D., Mayr, S., Bayuk, I., Burkhardt, H., Wilhelm, H. (2011). Thermal properties of rocks of the borehole Yaxcopoil-1 (Impact Crater Chicxulub, Mexico). *Geophysical Journal International* 184(2), 729–745.

Popov, Y., Tertychnyi, V., Romushkevich, R., Korobkov, D., Pohl, J. (2003). Interrelations between thermal conductivity and other physical properties of rocks: Experimental data. *Pure and Applied Geophysics* 160(5–6), 1137–1161.

Popov, Y.A., Pribnow, D.F.C., Sass, J.H., Williams, C.F., Burkhardt, H. (1999). Characterization of rock thermal conductivity by high-resolution optical scanning. *Geothermics* 28(2), 253–276.

Pribnow, D. (1994). Ein Vergleich von Bestimmungsmethoden der Wärmeleitfähigkeit unter Berücksichtigung von Gesteinsgefügen und Anisotropie. *Fortschritt-Berichte VDI Reihe 19,* 75, 118 pp.

Progelhof, R.C., Throne, J.L., Ruetsch, R.R. (1976). Methods for predicting the thermal conductivity of composite systems: a review. *Polymer Engineering & Science* 16(9), 615–625.

Rauppach, K., Wolfgramm, M., Thorwart, K., Seibt, P. (2008). Hydraulic Features of Geothermal Aquifers in the North German Basin. *Zeitschrift für geologisch Wissenschaften* 36(4-5), 268–279.

Reuss, A. (1929). Berechnung der Fließgrenze von Mischkristallen auf Grund der Plastizitätsbedingung für Einkristalle. *Zeitschrift für Angewandte Mathematik und Mechanik* 9(1), 49–58.

Robertson, E.C., Peck, D.L. (1974). Thermal conductivity of vesicular basalt from hawaii. Journal of Geophysical Research 79(32), 4875–4888.

Rybach, L. (1986). Amount and significance of radioactive heat sources in sediments. *Proceedings of the Thermal Modelling in Sedimentary Basins: 1st IFP Exploration Research Conference Carcans,* Carcans, June 3-7, 1985, 311–322 pp.

Sahlin, T., Middleton, M.F. (1997). Correlation of thermal conductivity with well log derived petrophysical parameters. *Proceedings of the Second Nordic Symposium on Petrophysics,* Reykjavík, Orkustofnun, 263–281 pp.

Sass, J.H., Lachenbruch, A.H., Munroe, R.J. (1971). Thermal conductivity of rocks from measurements on fragments and its application to heat-flow determinations. *Journal of Geophysical Research* 76(14), 3391–3401.

Schopper, J.R. (1991). An amendment to Gassmann's theory. *14th SPWLA European Formation Evaluation Symposium*, London, England, December 9-11, 19 pp.

Schulz, R., Agemar, T., Alten, A.-J., Kühne, K., Maul, A.-A., Pester, S., Wirth, W. (2007). Aufbau eines geothermischen Informationssystems für Deutschland. *Erdöl Erdgas Kohle* 123(2), 76–81.

Schulz, R., Röhling, H.G. (2000). Geothermische Ressourcen in Nordwestdeutschland. *Zeitschrift für Angewandte Geologie* 46(3), 122–129.

Schütz, F., Fuchs, S., Förster, A., Förster, H.-J. (2013). Facies-related trends of rock thermal conductivity and the impact on temperature prognosis for geothermal target reservoirs. *General Assembly European Geosciences Union* 15(EGU2013-3187), 1 pp.

Sen, P.N., Scala, C., Cohen, M.H. (1981). A self-similar model for sedimentary rocks with application to the dielectric constant of fused glass beads. *Geophysics* 46(5), 781–795.

Singh, R., Bhoopal, R.S., Kumar, S. (2011). Prediction of effective thermal conductivity of moist porous materials using artificial neural network approach. *Building and Environment* 42(1), 146–155.

Singh, T.N., Sinha, S., Singh, V.K. (2007). Prediction of thermal conductivity of rock through physico-mechanical properties. *Building and Environment* 42(1), 146–155.

Sugawara, A., Yoshizawa, Y. (1961). An investigation on the thermal conductivity of porous materials and its application to porous rook. *Australian Journal of Physics* 14(4), 469–480.

Thornton, W.M. (1924). CI. The thermal conductivity of solid electric insulators.—II. *Philosophical Magazine Series 6* 48(288), 1054–1056.

Tikhomirov, V.M. (1968). The thermal conductivity of rocks and its relationship to density, moisture content, and temperature (in Russian: Теплопроводность горных пород и ее связь с плотностью, влажностью и температурой). *Neftânoe Hozâjstvo (Нефтяное хозяйство)* 46(4), 36–40.

Tinga, W.R., Voss, W.A.G., Blossey, D.F. (1973). Generalized approach to multiphase dielectric mixture theory. *Journal of Applied Physics* 44(9), 3897–3902.

Vacquier, V. (1985). The measurement of thermal conductivity of solids with a transient linear heat source on the plane surface of a poorly conducting body. *Earth and Planetary Science Letters* 74(2–3), 275–279.

Vacquier, V., Mathieu, Y., Legendre, E., Blondin, E. (1988). Experiment on estimating thermal conductivity of sedimentary rocks from oil well logging. *AAPG Bulletin* 72(6), 758–764.

Villinger, H. (1983). In-situ-Bestimmung der Wärmeleitfähigkeit in Bohrungen. *Thesis*, Technical University of Berlin, 152 pp.

Voigt, W. (1928). Lehrbuch der Kristallphysik. Teubner, Leipzig, 978 pp.

Von Herzen, R., Maxwell, A.E. (1959). The measurement of thermal conductivity of deep-sea sediments by a needle-probe method. *Journal of Geophysical Research* 64(10), 1557–1563.

Vosteen, H.D., Rath, V., Schmidt-Mumm, A., Clauser, C. (2004). The thermal regime of the Northeastern-German Basin from 2-D inversion. *Tectonophysics* 386(1–2), 81–95.

Wiener, O.H. (1912). Die Theorie des Mischkörpers für das Feld der stationären Strömung. *Abhandlungen der Mathematisch-physischen Klasse der Königlich-sächsischen Gesellschaft der Wissenschaften* 32(6), 604.

Wolfgramm, M., Franz, M., Barth, G., Rauppach, K., Thorwart, K., Zimmermann, J. (2011). Relevanz der Sandsteinfazies im Norddeutschen Becken für die Produktivität von Geothermiebohrungen. *Proceedings of the Geothermiekongress 2011*, Bochum, Germany, November 15–17, 12 pp.

Wolfgramm, M., Rauppach, K., Seibt, P. (2008). Reservoir-geological characterization of Mesozoic sandstones in the North German Basin by petrophysical and petrographical data. *Zeitschrift für geologisch Wissenschaften* 36(4–5), 249–265.

Woodside, W., Messmer, J.H. (1961). Thermal conductivity of porous media. II. Consolidated rocks. *Journal of Applied Physics* 32, 1699–1706.

Zamora, M., Dung, V.T., Bienfait, G., Poirier, J.P. (1993). An empirical relationship between thermal conductivity and elastic wave velocities in sandstone. *Geophysical Research Letters* 20(16), 1679–1682.

Zierfuss, H., van der Vliet, G. (1956). Laboratory measurements of heat conductivity of sedimentary rocks. *AAPG Bulletin* 40(10), 2475–2488.

Zimmerman, R.W. (1989). Thermal conductivity of fluid-saturated rocks. *Journal of Petroleum Science and Engineering* 3(3), 219–227.

DOI: 10.2312/GFZ.b103-13111

Appendix: Petrophysical measurements

	Sample	Depth	Stratigraphy	Petrography	Table 2-1	Lime content	Measured bulk TC		Calculated bulk TC[1]		Aniso-tropy	Effective porosity	Matrix density
							TC⊥	TC ||	TC⊥	TC ||			
		m					W/(m·K)	W/(m·K)	W/(m·K)	W/(m·K)	-	%	g/cm³
1	Gt Ss 1/85 002	1404.59	(smS)	sandstone	+	+	2.56	2.88			1.13	19.0	1.99
2	Gt Ss 1/85 003	1406.55	(smS)	sandstone	+	+	3.22	3.14			0.98	18.8	2.62
3	Gt Ss 1/85 004a	1408.15	(smS)	sandstone	+	++	3.23	2.61			0.81	23.2	2.64
4	Gt Ss 1/85 006	1412.33	(smS)	sandstone	+	+	4.17	3.60			0.86	18.5	2.82
5	Gt Ss 1/85 007a	1414.70	(smS)	limestone		++	3.49	3.26			0.93	0.0	2.62
6	Gt Ss 1/85 009a	1423.97	(smH)	sandstone	+	+	2.81	2.71			0.96	24.0	2.03
7	Gt Ss 1/85 011	1430.35	(smH)	sandstone	+	0	2.75	3.04			1.10	24.0	2.88
8	Gt Ss 1/85 012	1434.75	(smH)	sandstone	+	+	2.75	3.22			1.17	24.0	2.69
9	Gt Ss 1/85 013a	1435.61	(smH)	sandstone	+	+	2.90					24.0	2.61
10	Gt Ss 1/85 014	1462.88	(smH)	sandstone		0	3.27	3.35			1.02	24.1	2.62
11	Gt Ss 1/85 015	1467.37	(smD)	sandstone	+	0	3.82	3.60			0.94	19.1	2.48
12	Gt Ss 1/85 016	1475.21	(smD)	sandstone		0	3.67	3.45			0.94	22.9	2.65
13	Gt Ss 1/85 017a	1480.27	(smD)	sandstone		0	3.21	3.47			1.08	24.3	2.61
14	Gt Ss 1/85 019	1491.20	(smD)	sandstone	+	0	3.47	3.21			0.92	22.5	2.56
15	Gt Ss 1/85 021	1530.34	(smD)	sandstone	+	0	2.98	2.98			1.00	19.1	2.55
16	Gt Ss 1/85 022	1540.91	(smD)	sandstone	+	0	3.26	3.09			0.95	18.0	2.51
17	Gt Ss 2/85 001a	1448.06	(smS)	sandstone	+	++	3.42	3.07			0.90	19.8	2.64
18	Gt Ss 2/85 002	1452.30	(smS)	sandstone	+	+	3.91	3.73			0.95	21.5	2.65
19	Gt Ss 2/85 003	1454.29	(smS)	sandstone	+	++	3.18	3.13			0.99	16.9	2.64
20	Gt Ss 2/85 005	1459.30	(smS)	limestone		++	2.83	2.54			0.90	2.5	2.66
21	Gt Ss 2/85 006	1463.02	(smS)	sandstone	+	+	4.29	4.05			0.94	6.0	2.66
22	Gt Ss 2/85 008	1485.52	(smH)	sandstone	+	+	3.26	3.14			0.96	23.5	2.59
23	Gt Ss 2/85 009a	1489.45	(smH)	sandstone	+	+	3.63	3.36			0.93	24.1	2.62
24	Gt Ss 2/85 010a	1496.17	(smH)	sandstone	+	+	3.43	3.56			1.04	21.0	2.59
25	Gt Ss 2/85 012	1504.93	(smH)	sandstone	+	+	3.06	3.32			1.08	23.5	2.58
26	Gt Ss 2/85 013	1514.05	(smH)	sandstone	+	+	3.56	3.35			0.94	21.7	2.63
27	Gt Ss 2/85 014	1518.65	(smH)	sandstone	+	++	3.34	3.33			1.00	26.4	2.64
28	Gt Ss 2/85 015	1519.30	(smH)	sandstone	+	+	3.50	3.28			0.94	21.4	2.59
29	Gt Ss 2/85 016a	1533.90	(smD)	sandstone	+		3.65	3.58			0.98	17.1	2.62
30	Gt Ss 2/85 018a	1540.55	(smD)	sandstone	+	0	3.26	3.13			0.96	21.7	2.61
31	Gt Ss 2/85 019	1545.18	(smD)	sandstone	+	+	2.99	3.14			1.05	21.0	2.64
32	Gt Ss 2/85 020a	1547.55	(smD)	sandstone	+		3.18	3.15			0.99	23.0	2.62
33	Gt Ss 2/85 022	1560.10	(smD)	sandstone	+		3.48	3.27			0.94	21.6	2.63
34	Gt Ss 2/85 023	1562.15	(smD)	sandstone	+	0	3.30	3.40			1.03	20.4	2.62
35	Gt Ss 2/85 026	1568.88	(smD)	sandstone	+	+	3.76	3.59			0.96	23.7	2.61
36	Gt Ss 2/85 027	1577.60	(smD)	sandstone	+	+	3.59	3.68			1.02	25.7	2.62
37	Gt Ss 2/85 028	1581.75	(smD)	sandstone		+		3.41				23.9	2.60
38	Gt Ss 2/85 030	1602.06	(smD)	siltstone	+	+	3.54	2.70			0.76	9.6	2.62
39	Gt Ss 2/85 031a	1603.59	(smV)	siltstone		0	2.93	2.52			0.86	7.3	2.56
40	Gt Ss 2/85 032	1607.73	(smV)	siltstone		0	2.27					11.6	2.62
41	Gt Ss 2/85 033	1613.12	(smV)	sand-siltstone		+	2.58					16.7	2.65
42	Gt N 2/85 001	1222.10	(kCs)	sandstone	+	+	3.38	4.08			1.21	20.0	2.58
43	Gt N 2/85 003	1225.32	(kCs)	sandstone	+	0	3.22	2.99			0.93	25.3	2.58
44	Gt N 2/85 004	1229.40	(kCs)	sandstone	+	0	3.80	3.57			0.94	18.7	2.49
45	Gt N 2/85 006	1255.50	(kOPS)	sandstone	+	++	3.63					30.5	2.60
46	Gt N 2/85 007	1261.00	(kOPS)	sandstone	+	++	3.08					30.0	
47	Gt N 2/85 012	1517.50	(kmS)	siltstone	+	0	1.94	1.95			1.01	11.0	2.14
48	Gt N 2/85 013	1525.40	(kmS)	sandstone	+	0	2.09					13.7	2.58
49	Gt N 2/85 015	1528.03	(kmS)	sandstone	+	0	1.96	2.13			1.09	17.0	
50	Gt N 2/85 017	1537.65	(kmS)	sandstone	+	0	2.11	2.01			0.95	26.3	2.61
51	Gt N 2/85 018	1541.70	(kmS)	sandstone	+	0	2.24	2.36			1.05	25.8	2.62
52	Dp N 1/82 001	841.08	(jmal)	sandstone					2.52	3.30	1.31	26.5	1.99
53	Dp N 1/82 003	849.33	(jmal)	siltstone					1.65			18.2	2.57
54	Dp N 1/82 008	867.37	(jmal)	sandstone			3.25	3.11			0.96	17.5	2.40
55	Dp N 1/82 009	868.56	(jmal)	sandstone			3.25	3.11			0.96	26.8	2.74
56	Dp N 1/82 014	889.43	(jutc)	siltstone					1.56			19.4	2.61
57	Dp N 1/82 015	991.20	(jupl)	sandstone	+		3.64					21.4	2.59
58	Dp N 1/82 022	1007.83	(jupl)	sandstone			3.03					22.0	
59	Dp N 1/82 023	1009.40	(jupl)	sandstone					1.66	2.36	1.43	18.0	2.61
60	Dp N 1/82 025	1013.78	(jupl)	sandstone					2.41	3.01	1.25	25.0	2.89
61	Dp N 1/82 027	1017.02	(jupl)	sandstone	+		3.07					26.1	2.44
62	Dp N 1/82 028	1020.80	(jupl)	sandstone					2.91	2.64	0.91	17.3	2.66

DOI: 10.2312/GFZ.b103-13111

	Sample	Depth	Stratigraphy	Petrography	Table 2-1	Lime content	Measured bulk TC		Calculated bulk TC[1]		Aniso-tropy	Effective porosity	Matrix density
							TC⊥	TC ||	TC⊥	TC ||			
		m					W/(m·K)	W/(m·K)	W/(m·K)	W/(m·K)	-	%	g/cm³
63	Dp N 1/82 030	1024.97	(jupl)	siltstone					2.22	2.82	1.27	15.7	2.63
64	Dp N 1/82 031	1028.11	(jupl)	sandstone			3.35	3.01			0.90	19.5	2.32
65	Dp N 1/82 032	1029.95	(jupl)	siltstone					1.87	2.60	1.39	14.3	2.62
66	Dp N 1/82 033	1038.95	(jupl)	sandstone			3.29	3.30			1.00	25.6	2.67
67	Dp N 1/82 034	1042.29	(jupl)	sandstone					2.74	3.00	1.10	21.2	2.75
68	Dp N 1/82 036	1251.00	(kCs)	siltstone					2.46	2.86	1.16	10.9	2.61
69	Dp N 1/82 037	1252.00	(kCs)	sandstone	+		3.46	3.50			1.01	21.9	2.53
70	Dp N 1/82 041	1261.15	(kOPS)	siltstone					3.23	3.38	1.05	12.0	2.65
71	Dp N 1/82 044	1274.55	(kOPS)	sandstone	+		3.75					22.4	2.65
72	Dp N 1/82 045	1274.99	(kOPS)	sandstone	+		3.69	3.57			0.97	26.3	2.62
73	Dp N 1/82 046	1281.35	(kOPS)	sandstone					3.54	3.38	0.96	21.7	2.66
74	Dp N 1/82 047	1281.66	(kOPS)	sandstone					4.21	4.14	0.98	27.2	2.67
75	Dp N 1/82 048	1281.77	(kOPS)	sandstone	+		3.30					25.2	2.87
76	Dp N 1/82 049	1286.55	(kOPS)	siltstone					2.02			11.6	2.62
77	Dp N 1/82 050	1125.13	(jusi)	siltstone					2.54	3.41	1.34	16.6	2.66
78	Dp N 1/82 051	1134.55	(jusi)	sandstone	+		3.18					28.4	2.53
79	Dp N 1/82 052	1135.96	(jusi)	sandstone	+		3.16	3.16			1.00	28.2	2.59
80	Dp N 1/82 053	1139.25	(jusi)	sandstone			3.57					20.6	2.68
81	Dp N 1/82 055	1145.95	(juhe)	sandstone			3.24					28.7	2.58
82	Dp N 1/82 057	1173.33	(juhe)	siltstone			3.84					26.0	2.68
83	Dp N 1/82 058	1185.26	(juhe)	sandstone			3.94					26.4	2.62
84	Dp N 3/86 001	1120.50	(juhe)	sandstone	+	++	3.31	3.56			1.08	22.4	2.50
85	Dp N 3/86 002	1122.58	(juhe)	sandstone	+	++	3.59	3.41			0.95	24.8	2.61
86	Dp N 3/86 003	1124.25	(juhe)	sandstone	+	++	3.47	3.23			0.93	21.1	2.51
87	Dp N 3/86 004	1125.66	(juhe)	sandstone	+	++	4.02	4.06			1.01	16.5	2.20
88	Dp N 3/86 005	1135.30	(juhe)	claystone		0			1.80	2.82	1.57	14.7	2.62
89	Dp N 3/86 006	1136.00	(juhe)	claystone		0			1.81			14.0	2.61
90	Dp N 3/86 007	1139.21	(juhe)	sand-siltstone		0			3.04	3.36	1.10	15.7	2.58
91	Dp N 3/86 008	1141.41	(juhe)	claystone		0			1.91	2.09	1.09	13.6	2.56
92	Dp N 3/86 009	1144.22	(juhe)	sandstone	+	++	3.02	3.15			1.04	32.4	2.63
93	Dp N 3/86 010	1145.91	(juhe)	sandstone	+	++	3.40	3.21			0.95	26.9	2.54
94	Dp N 3/86 011	1150.70	(juhe)	sandstone	+	++	3.22	3.29			1.02	27.4	2.57
95	Dp N 3/86 012	1153.05	(juhe)	sandstone	+	++	3.31	3.27			0.99	31.5	2.61
96	Dp N 3/86 013	1154.02	(juhe)	sandstone	+	++	3.23	3.20			0.99	25.7	2.41
97	Dp N 3/86 014	1157.53	(juhe)	sandstone	+	++	3.27	3.29			1.01	26.7	2.51
98	Dp N 3/86 015	1159.27	(juhe)	sandstone	+	++	3.29					29.6	2.60
99	Dp N 3/86 017	1164.18	(juhe)	sandstone		++	3.17	3.36			1.06	26.3	2.51
100	Dp N 3/86 018	1168.00	(juhe)	sandstone		++	3.29	3.29			1.00	25.4	2.41
101	Dp N 3/86 019	1169.18	(juhe)	claystone		0			3.37	3.54	1.05	11.4	2.63
102	Dp N 3/86 020	1177.60	(juhe)	sand-siltstone		+			2.72	2.84	1.05	24.3	2.62
103	Dp N 3/86 021	1183.15	(juhe)	sand-siltstone		+			3.13	3.36	1.07	27.4	2.61
104	Dp N 3/86 022	1189.07	(juhe)	claystone		0			2.30	2.22	0.96	7.5	2.94
105	Dp N 3/86 023	1220.21	(kOPS)	claystone		0			3.06	2.16	0.71	12.0	2.76
106	Dp N 3/86 024	1222.56	(kOPS)	claystone		0			2.02	2.24	1.11	14.0	3.06
107	Dp N 3/86 025	1230.50	(kOPS)	sandstone		+	3.29	3.38			1.03	30.6	2.63
108	Dp N 3/86 026	1231.95	(kOPS)	sandstone		+	3.62	3.29			0.91	28.9	2.62
109	Dp N 3/86 027	1233.43	(kOPS)	sandstone		+	3.41	3.24			0.95	19.8	2.32
110	Dp N 3/86 028	1235.27	(kOPS)	sandstone		+	3.23	3.37			1.04	28.8	2.63
111	Dp N 3/86 029	1237.70	(kOPS)	sandstone		++	3.57	3.31			0.93	30.7	2.59
112	Dp N 3/86 030	1239.05	(kOPS)	sandstone		++			5.93	5.62	0.95	30.2	1.81
113	Dp N 3/86 032	1256.97	(kOPS)	sandstone		++				3.58		27.4	1.87
114	Gt S 5/87 001	2055.42	(kTs)	claystone		0	3.60	3.98			1.11	2.2	2.77
115	Gt S 5/87 002	2058.09	(kTs)	claystone		0			3.46	3.96	1.15	9.3	1.86
116	Gt S 5/87 003	2061.30	(kTs)	siltstone		0			2.40	2.99	1.25	20.7	1.80
117	Gt S 5/87 004	2063.15	(kTs)	sandstone	+	0	4.03	3.80			0.94	25.5	2.65
118	Gt S 5/87 005	2072.10	(kCs)	sandstone	+	0	4.20	4.08			0.97	22.8	2.65
119	Gt S 5/87 006	2072.70	(kCs)	sandstone	+	+	4.08	4.06			1.00	23.7	2.65
120	Gt S 5/87 007	2072.93	(kCs)	sandstone	+	0	4.45	3.97			0.89	20.0	2.65
121	Gt S 5/87 008	2109.45	(kCs)	sandstone	+	0	4.39	4.06			0.93	20.1	2.66
122	Gt S 5/87 009	2110.53	(kCs)	sandstone	+	0	4.24	3.92			0.92	20.5	2.64
123	Gt S 5/87 010	2112.36	(kCs)	sandstone	+	0	3.68	3.63			0.99	22.3	2.66
124	Gt S 5/87 011	2113.12	(kCs)	sandstone	+	0	4.02	3.94			0.98	18.8	2.64
125	Gt S 5/87 012	2114.23	(kCs)	sandstone	+	0	4.24	4.17			0.98	23.0	2.65
126	Gt S 5/87 013	2115.23	(kCs)	sandstone	+	0	4.15	4.08			0.98	22.6	2.64
127	Gt S 5/87 014	2117.30	(kCs)	sand-siltstone		0			4.10	4.16	1.02	20.7	2.59
128	Gt S 5/87 015	2136.46	(kOPS)	sandstone	+	0	4.51	4.28			0.95	22.0	2.64
129	Gt S 5/87 016	2136.87	(kOPS)	sandstone	+	0	4.08	4.19			1.03	22.1	2.61
130	Gt S 5/87 017	2137.87	(kOPS)	sandstone		0	4.24	4.45			1.05	28.3	3.69
131	Gt S 5/87 018	2139.64	(kOPS)	siltstone		0			3.96	4.06	1.02	7.0	2.67
132	Gt S 5/87 019	2169.33	(kOPS)	sandstone		0	4.43	4.19			0.95	22.6	2.64

	Sample	Depth	Stratigraphy	Petrography	Table 2-1	Lime content	Measured bulk TC		Calculated bulk TC[1]		Aniso-tropy	Effective porosity	Matrix density
							TC⊥	TC ||	TC⊥	TC ||			
		m					W/(m·K)	W/(m·K)	W/(m·K)	W/(m·K)	-	%	g/cm³
133	Gt S 5/87 020	2169.82	(kOPS)	sandstone		0	4.08	4.13			1.01	25.7	2.65
134	Gt S 5/87 021	2170.20	(kOPS)	sandstone		0			4.90	5.07	1.03	22.7	2.66
135	Gt S 5/87 022	2172.35	(kOPS)	sandstone		0			4.79	4.45	0.93	23.0	2.51
136	Gt S 5/87 023	2173.08	(kOPS)	dolomite		+			2.07	2.04	0.99	7.2	2.66
137	Gt S 5/87 024	2173.58	(kOPS)	dolomite		0			3.23	3.80	1.18	3.0	2.52
138	Gt S 5/87 025	2179.50	(kOPS)	siltstone		0			3.18	3.32	1.04	12.4	2.66
139	Gt S 3/87 001	2040.37	(jmal)	sandstone		++	5.11	4.46			0.87	21.2	2.64
140	Gt S 3/87 002	2040.84	(jmal)	sandstone		++	4.24	3.98			0.94	25.1	2.65
141	Gt S 3/87 003	2045.02	(jmal)	sandstone		++	4.69	4.57			0.98	23.1	2.65
142	Gt S 3/87 004	2048.98	(jmal)	claystone		0	2.15					7.5	2.63
143	Gt S 3/87 006	2072.32	(jmal)	sandstone		+	4.29	4.25			0.99	24.6	2.72
144	Gt S 3/87 007	2076.30	(jmal)	sandstone		+	4.31	4.05			0.94	27.3	2.65
145	Gt S 3/87 008	2077.05	(jmal)	sandstone		+	3.84	3.74			0.97	26.6	2.66
146	Gt S 3/87 009	2077.48	(jmal)	sandstone		+	4.61	4.32			0.94	24.8	2.65
147	Gt S 3/87 010	2080.29	(jmal)	sand-siltstone		0	4.42	4.30			0.97	17.5	2.63
148	Gt S 3/87 011	2081.53	(jmal)	sandstone		+	4.11	4.13			1.00	26.2	2.65
149	Gt S 3/87 012	2081.76	(jmal)	sandstone		+	4.53	4.24			0.94	26.3	2.65
150	Gt S 3/87 013	2082.86	(jmal)	sandstone		++	4.10	4.19			1.02	26.6	2.65
151	Gt S 3/87 014	2084.70	(jmal)	sandstone		+	4.32	4.32			1.00	25.3	2.65
152	Gt S 3/87 015	2089.57	(jmal)	sandstone		+	4.52	4.28			0.95	22.0	2.67
153	Gt S 3/87 016	2090.96	(jmal)	sandstone		+	4.60	4.07			0.89	25.8	2.66
154	Gt S 3/87 017	2091.96	(jmal)	sandstone		0	3.94	4.45			1.13	25.7	2.64
155	Gt S 3/87 018	2095.40	(jmal)	claystone		0			2.50			10.6	2.56

[1] *Calculation of water-saturated bulk TC from isooctane-saturated bulk TC and porosity using the geometric-mean model. Depths are measured depths. All measurements are performed as described in Section 2.3.*

List of Figures

DOI: 10.2312/GFZ.b103-13111

List of Tables

List of Abbreviations

Ba	-	Barth (location)
BMBF		Federal Ministry of Education and Research
Bulk TC	W/(m·K)	Bulk thermal conductivity
CI	-	Color interval
Ed.	-	Editor
Fig.	-	Figure
Fm.		Formation
GE	-	Gamma-Einheiten (gamma units)
GeoEN	-	Verbundvorhaben GeoEnergieforschung
GFZ Potsdam	-	GeoForschungsZentrum Potsdam
GR	API	Gamma-ray
gradT	°C/km	Temperature gradient
Gt	-	Geothermie
GTN	-	Geothermie Neubrandenburg
jmbj	-	Bajocian
jmal	-	Aalenian
jmbt	-	Bathonian
joK	-	Korallenoolith
juhe	-	Hettangian
jupl	-	Pliensbachian
jusi	-	Sinemurian
kmS	-	Stuttgart Formation (Schilfsandstein)
kOPS	-	Postera
kCs	-	Contorta
krv	-	Valangin
LBGR	-	Landesamt für Bergbau, Geologie und Rohstoffe Brandenburg, Germany
LIAG	-	Leibniz-Institut für Angewandte Geophysik
LUNG	-	Landesamt für Umwelt, Naturschutz und Geologie Mecklenburg Vorpommern, Germany
Matrix TC	W/(m·K)	Matrix thermal conductivity
N	-	Neubrandenburg (location)
NEGB	-	Northeast German Basin
NGB	-	North German Basin

DOI: 10.2312/GFZ.b103-13111

NWGB	-	Northwest German Basin
q	mW/m²	Heat flow (means: heat-flow density)
Q	W	Heat-source power
qs	mW/m²	Surface heat flow
S	-	Schwerin (location)
Sam	-	Samtens (location)
sm	-	Middle Buntsandstein
smD	-	Detfurth
smH	-	Hardegsen
smS	-	Solling
smV	-	Volpriehausen
Ss	-	Stralsund (location)
SD	-	Standard deviation
T	°C	Temperature
TC	W/(m·K)	Thermal conductivity
TD	m²/s	Thermal diffusivity
gradT	°C/km	Temperature gradient
Wa	-	Waren (location)
Wd	-	Wealden
XRD	-	X-ray diffraction

λ	W/(m·K)	Thermal conductivity
λ_{matrix}	W/(m·K)	Matrix thermal conductivity
λ_{pore}	W/(m·K)	Thermal conductivity of the pore filling
λ_{dryM}	W/(m·K)	Dry measured thermal conductivity
λ_{satM}	W/(m·K)	Saturated measured thermal conductivity
λ_{water}	W/(m·K)	Thermal conductivity of water
$\lambda_{\perp}$	W/(m·K)	TC measured perpendicular to the bedding
$\lambda_{\|\|}$	W/(m·K)	TC measured parallel to the bedding
Θ	°K	Maximum temperature rise
Θ_S	°K	Temperature rise of reference standard
Φ	p.u.	Effective porosity

DOI: 10.2312/GFZ.b103-13111

Curriculum Vitae

Personal Details

Name:	Sven Fuchs
Date of Birth:	May 25, 1981
Place of Birth:	Berlin, Germany

Education and professional qualification

Apr 09 – Aug 13	**Research assistant** at GFZ German Research Centre for Geosciences Potsdam (Germany), Section 4.1: Reservoir Technologies, cluster: exploration geology
Sep 07 – Mar 09	**Project engineer** at Groundwater Consulting Engineering Company (GCI, Grundwasser Consulting Ingenieurgesellschaft)
Oct 01 – Aug 07	**Graduated engineer** Hydrogeology (Diplom-Ingenieur Hydrogeologie) at the Technical University of Berlin (Germany), Study of 'Applied Earth Engineering Sciences'
Nov 00 – Aug 01	Basic military service at the armored infantry
Jul 00	University entrance qualifications (Abitur) at the Raoul-Wallenberg-Oberschule in Berlin (Germany)

DOI: 10.2312/GFZ.b103-13111

Selbstständigkeitserklärung

Hiermit erkläre ich, dass diese Dissertation – abgesehen von den angegebenen Mitarbeiten und Co-Autoren der einzelnen Manuskripte – nach Inhalt und Form meine eigene Arbeit ist. Ich erkläre, dass die wörtlichen oder dem Sinne nach anderen Veröffentlichungen entnommenen Stellen von mir kenntlich gemacht wurden. Die Arbeit ist weder ganz noch zum Teil einer anderen Stelle im Rahmen eines Prüfungsverfahrens vorgelegt worden und unter Einhaltung der Regeln guter wissenschaftlicher Praxis entstanden. Die Bedeutung der eidesstattlichen Versicherung und die strafrechtlichen Folgen einer unrichtigen oder unvollständigen eidesstattlichen Versicherung sind mir bekannt. Ich versichere an Eides statt, dass ich nach bestem Wissen die reine Wahrheit erklärt und nichts verschwiegen habe.

Declaration of authenticity and originality

This dissertation is an original and authentic piece of work by myself. I have fully acknowledged and referenced all material incorporated form secondary sources and I have truthfully documented all methods and operational procedures. All assistance I have received in the performance of this study is duly cited, according to the accepted standards and practices of the scientific community, in the acknowledgments and reference section of this work.

.....

Sven Fuchs

Potsdam, 30.04.2013

ISSN 1610-0956